Polytechnic University of Marche

RATIONAL DESIGN OF FUNCTIONALIZED LIPIDS WITH ANTIOXIDANT AND SCAVENGING ACTIVITY AS COMPONENTS OF INNOVATIVE ARTIFICIAL TEARS

PhD course "Biomolecular Sciences"

XV cycle

Academic tutor:
Dott. Roberta Galeazzi

Aziendal tutor:
Dott. Dario Rusciano

PhD Eureka course in collaboration with SOOFT Italia company

PhD Laudadio Emiliano

INDEX

1. OBJECTIVE OF RESEARCH

The main aim of my PhD research work is the *in silico* design and the development of new drugs able to efficiently deal with free radicals at the target tissue or organ, more in particular for the eye. Such objective is of great interest in the pharmaceutical field because free radicals are responsible for the processes of aging and cell death of the animal tissues, and therefore also of at the ocular level. Our aim is to create an innovative product that could be used as drug delivery nanovector in ocular drops. In fact, it is known that the formulations based on nanoparticles such as micelles, microemulsions and monolaminar liposomes exploit the fact that a high surface/volume ratio leads to a significant increase in pharmacological activity. The nanoparticle can carry the drug to the specific site, releasing it in a controlled manner and at the same time protect it from premature degradation. However, the innovation of our project involves the design of the liposome binding the new antioxidant molecule directly to a lipid molecule that thus becomes itself a constituent of the liposomal nanovector and not only incorporated inside. This strategy is aimed at improving the functionality of transport and of resistance to degradation. In fact, the new molecule synthesized will remain longer in the tear film, and will be active for a greater period. This aspect is very important because the eye in contact with light uses a large amount of ATP, and this generates the free radicals. They are molecules that possess an unpaired electron on electric orbital and this makes them highly unstable and highly reactive. Free radicals react easily with anyone molecule is in their proximity damaging and often compromising its function. Also, by reacting with other molecules, have the ability to disseminate themselves transforming their targets in free radicals and thereby causing a chain reaction that can cause extensive damage in the cell.

More in detail, during my PhD period, we explored two different strategies: (i) functionalization of known antioxidant molecules in order to insert them deeply into the bilayers; (ii) improving encapsulation of known antioxidant molecules. The final object will produce liposomal antioxidant systems for ophthalmic use that will be stable and efficient. Moreover, the antioxidant molecules will be retained on lacrimal film, and thus they will use their antioxidant activity against the free radicals generated outside the eye. For this reason, the functionalization has to improve lipophilicity on antioxidant molecules but it must not influence the proper antioxidant activity of the chosen molecules. Only in this way, we can obtain an efficient ocular drug delivery system. To reach all these goals efficiently and fast, we settled out an *in silico* molecular modeling protocol based on atomistic molecular dynamics simulation of lipid bilayer systems as liposomal models. Indeed, thanks to the improvement of both Molecular Modeling Software Packages and hardware resources, it is nowadays possible to get new insights on complex molecular aggregates. Extensive structural

analysis and accurate inter-molecular interactions previsions via computational methods arise today as a key part of laboratories protocols in many scientific fields such as chemistry, drug design, biology and materials science. To highlight the latest results attainable with computational chemistry tools, we will describe how we successfully recreated a realistic model for inhomogeneous systems such as lipid membranes. We describe our extensive analysis on particular membrane bilayers containing functionalized lipids with antioxidant activity. Molecular Dynamics (MD) simulations were implemented on the basis of our tested laboratory protocol, to better understand the behaviors of antioxidant molecules in their lipophilic carriers.

In this work, I discuss the innovation perspectives offered by an *in silico* analysis, both in terms of "better understanding" and "suggesting": the first as a complementation of experimental data, the latter as a novel way to plan the experiment itself.

2. INTRODUCTION AND STATE OF ART

2.1 TEAR FLUID LIPID LAYER

Human tear film comprising lipids, proteins, metabolites, and water protects the eye from dryness and injury. The tear film have a unique structure that enables it to perform many functions, composed by lipid, aqueous, and mucous components. There is also a mucin containing glycocalyx interface that extends from the apical membranes of the corneal and conjunctival epithelia which acts as an integral part of the tear film. The seven major functions of the tear film are:

- Maintaining a smooth surface for light refraction. The tears form the first refractive surface encountered by light on its path to the retina. For clear vision, it is critical to maintain the transparency of the second refractive surface that rays of light encounter, i.e. the cornea.
- Lubricating the eyelids.
- Lubricating the conjunctiva and the cornea by providing a smooth and reflective surface, thus avoiding ocular surface mechanical damage from the surprisingly high pressures generated by each blink.
- Supplying the cornea with nutrients by transporting oxygen and a limited number of other nutrients to the avascular cornea, regulating the electrolyte composition and pH.
- Providing white blood cells with access to the cornea and conjunctiva.
- Removing foreign materials from the cornea and conjunctiva. The tear film protects the ocular surface from the external environment by responding dynamically to a wide range of external conditions and potentially damaging situations. These external stresses include desiccation,

bright light, cold, mechanical stimulation, physical injury, noxious chemicals, and bacterial, viral, and parasitic infection.

- Defending the ocular surface from the pathogens via specific and nonspecific antibacterial substances [1].

In humans, tear film is composed by three distinct parts: the innermost mucin-rich layer, an aqueous layer in the middle, and the outermost tear fluid lipid layer (TFLL). The latter is a lipid layer located at the water-air interface. The function of tear film is to protect the epithelium of the eye. Tear fluid fulfils this purpose in many ways. When blinking, tear fluid forms a lubricating film between the lid and ocular surface. It possesses antibacterial properties and flushes contaminants from the ocular surface. Tear fluid also acts as a nutrient for the corneal epithelium and improves the optical properties of the eye. Tear film has an ill-defined trilaminar and concentration gradient-dependent structure [2].

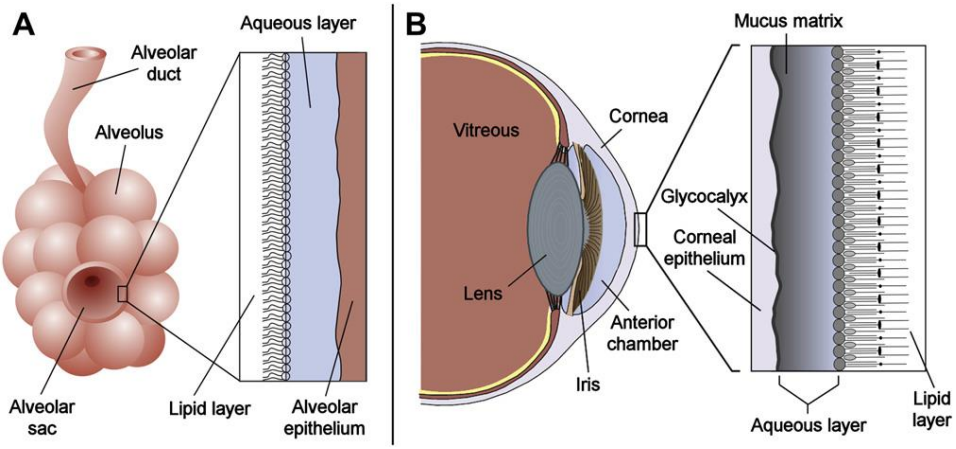

Figure 1A and 1B: Structure of lacrimal film

TFLL coats the aqueous phase and may also protect the ocular surface from evaporation, though the latter property has been questioned very recently. The lipid layer prevents evaporation of tears, the aqueous layer allows spread of tears over the ocular surface and mucin layer adheres the tear film to ocular surface. In an unstimulated human eye at a normal blink rate of 15–20 blinks/min, the tear volume on the ocular surface is about 6–8 ml and the basal tear turnover rate is approximately 16%/min of the total tear volume. The ability to retain water is due to the Van der Waals interactions among hydrophobic carbon chains. Furthermore, these incompressible lipid layers have very low free volumes, preventing diffusion of small molecules through the layers. An increase in surface pressure increases the retardation of evaporation by decreasing the chain tilt and, therefore, increasing the thickness of the layer. To a certain extent, evaporation-retardant lipids can be mixed with non-retardant lipids and still hold their ability to retard evaporation [3].

Very minute changes in molecular composition may disturb the delicate balance between healthy and unhealthy ocular surfaces, highlighting the importance of understanding the role of the TFLL (with

regard to its dynamics, composition, structure, and mechanical properties) in maintaining the sensitive balance of the ocular surface. Nonetheless, the current understanding of TFLL properties is quite limited. Perhaps the best known aspect is its lipid composition, as recent studies have revealed the most abundant lipids present in human TFLL to be phospholipids (PLs), free fatty acids (FFAs), cholesteryl esters (CEs), triglycerides (Tgs), and wax esters (Fig. 1). Further, the relatively high ratio of PLs in the mixture (more than 50%) supports the idea of a single lipid monolayer at the air-water interface, though one cannot rule out a possibility of a more complex structure either. Meanwhile, the organization and role of neutral lipids (e.g., CEs, TGs, and fatty acids) in the lipid layer is more intriguing [4].

The ocular tissue absorption of topically administered drugs is estimated to be less than 5%. Majority of drug loss is attributed to overspill. The capacity of the conjunctival sac when lower lid is pulled away is approximately 25 ml and reduces to approximately 10 ml when eyelid returns to its normal position. The pathological conditions affecting conjunctiva may further limit the holding capacity of conjunctival sac. Hence, instillation of eye drops in a volume larger than 25 ml results in drug loss due to overspill. The amount of drug retained in the conjunctival sac mixes with the precorneal tear film before it comes in direct contact with ocular surface. It has been observed that even if the drug loss due to drainage is compensated by sustained drug delivery through a solid delivery system, the ocular bioavailability reaches only up to 10% indicating the importance of barriers on the ocular surface. Not only the barrier functions of ocular surface tissue i.e. cornea, conjunctiva and sclera are now extensively studied; investigations have also revealed the importance of precorneal tear film as a significant barrier to drug absorption [5].

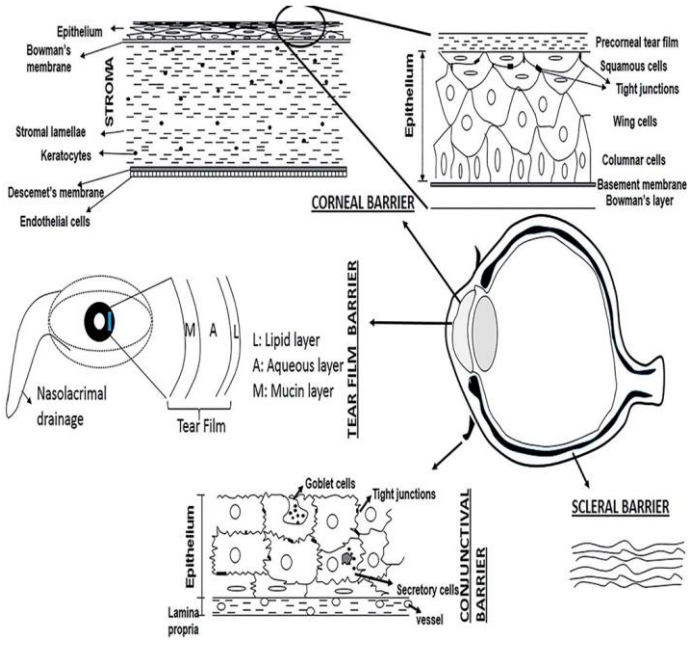

Figure 2: Structures of Corneal, Tear film and scleral barriers

An intact tear film is essential for a healthy ocular surface. However, as described above, for the penetration of drugs applied topically to ocular surface, tear film is a significant barrier. This tear turnover rate may increase significantly due to reflex tearing which may occur due to drug instillation resulting in accelerated washout of the drug. Tears are drained through the nasolacrimal duct into the nasal cavity. Blinking creates a pumping mechanism to facilitate flow of tears into the nasolacrimal duct. Drainage of the instilled drug into the nasolacrimal system along with tears is the main factor contributing to drug loss from pre-corneal tear film and reduction in the rate of tear drainage significantly increases the drugs' ocular bioavailability.

Considering the challenges in ocular drug delivery, ideal topical drug delivery system musts to have these characteristics:

- Should be able to resist pre-corneal clearance and provide prolonged corneal contact time.
- Should be delivered in a dosage form that provides adequate trans-corneal absorption (paracellular or transcellular).
- Should be of suitable viscosity that provides good corneal contact time but avoids reflex blinking, tearing and blurred vision.
- Should have a suitable pH that favors the absorbable form of drug molecule (non-ionized) but is non-irritant to ocular surface.
- Should cause minimal adverse effects.
- Should be easy to administer.
- Should require sufficiently low frequency of administration to ensure patient compliance.

2.2 LIPOSOMES

Liposomes are artificial vesicles consisting of outer covering of lipids that encloses the inner core. In the early twentieth century, liposomes were considered as artificial cells due to their lipid bilayer covering; after this, liposomes were recognized as important drug delivery systems and their potential uses in cancer chemotherapy were investigated. Since then, liposomes have undergone extensive investigation to develop them for targeted and sustained drug delivery.

The liposomal vesicles vary in size from 10 nm to 1 mm or greater. Structurally liposomes are classified into unilamellar vesicles (ULVs) and multilamellar vesicles (MLVs). Based on the size of vesicles, ULVs are further classified into small unilamellar vesicles (SUVs), giant unilamellar vesicles (GUVs), and large unilamellar vesicles (LUVs) (Figure 2). In ULVs, single lipid bilayer consisting of lecithin or phosphatidylglycerol encloses the aqueous core. MLVs consist of more than

one lipid bilayer, each separated by an aqueous compartment. Structure of liposomal vesicle allows them to serve as carrier for hydrophilic drugs that can be encapsulated into the aqueous core as well as hydrophobic and amphiphilic drugs that can be embedded in the lipid bilayer. Since the liposomes with multiple compartments have greater aqueous space, their capability to entrap hydrophilic drugs is higher than those with single compartments are. Lipids commonly used for the preparation of liposomes are phospholipids, which can be synthetic or naturally occurring (Fig. 3). The phospholipids that are commonly used include egg phosphatidylcholine, brain and synthetic phosphatidylserine, sphingomyelin, synthetic dipalmitoyl-DL-a-phosphatidylcholine, phosphatidylinositol andovolecithin. A nonionic or zwitterionic lipid is generally used as the basic lipid and to introduce surface charge other lipids are included such as stearylamine for positive charge and diacetylphosphate, phosphatidyl glycerol or phosphatidyl serine for negative charge. Incorporation of charged lipids leads to a greater overall volume for aqueous entrapment and the likelihood of aggregation reduces. However, stearylamine containing cationic liposomes have been shown to cause toxicity in rabbit [102]. Incorporation of cholesterol increases the stability, enhances the fluidity or microviscosity of the lipid bilayer and reduces the leakage of water-soluble molecules.

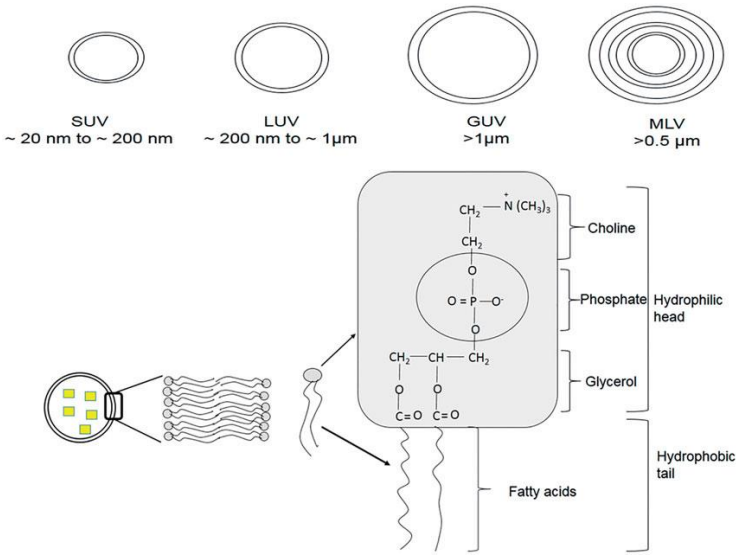

Figure 3: Structures of different liposomes

The mechanisms of interaction of liposomes with cell membranes that result into intracellular drug delivery have been studied extensively but are poorly understood. Due to highly complex nature of this interaction, the interpretation of experimental data is often difficult. The initial liposome-cell membrane interaction is the key process that leads to intracellular drug delivery. This liposome-cell membrane interaction may involve different receptors on different cell types or more than one receptor on a particular cell and is greatly affected by the lipid composition of liposomes [103]. Largely,

four mechanisms of intracellular drug delivery by liposomes are widely accepted and are as follows (Fig 4).

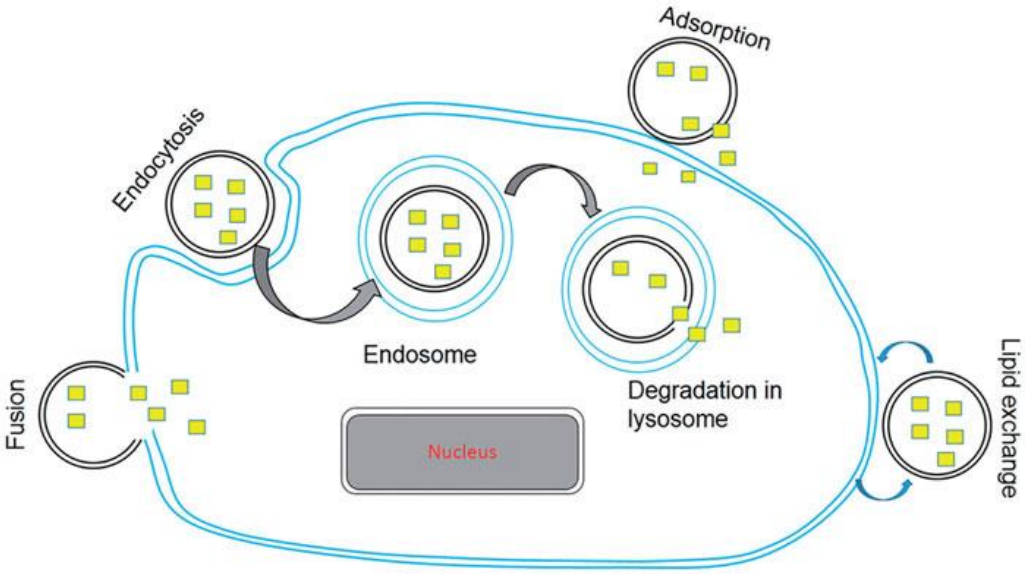

Figure 4: mechanisms of intracellular drug delivery using liposomes

Adsorption: Adsorption of liposomes to cell membrane is one of the important mechanisms of intracellular drug delivery. The adsorbed liposomes, in the presence of cell surface proteins, become leaky and release their contents in proximity of cell membrane. This results in a higher concentration of drug close to cell membrane and facilitates cellular uptake of drug by passive diffusion or transport [104].

Endocytosis: Adsorption of liposomes on the surface of cell membrane is followed by their engulfment and internalization into endosomes. Endosomes transport liposomes to lysosomes. Subsequently, lysosomal enzymes degrade the lipids and release the entrapped drug into the cytoplasm [105].

Fusion: Fusion of lipid bilayer of liposomes with cell membrane by intermixing and lateral diffusion of lipids results in direct delivery of liposomal contents into the cytoplasm.

Lipid exchange: Due to the similarity of liposomal membrane lipids with the cell membrane phospholipids, lipid transfer proteins in the cell membrane recognize liposomes and consequently cause lipid exchange. This results in the destabilization of liposomal membranes and intracellular release of drug molecules [106]. An understanding of the mechanisms of intracellular drug delivery by liposomes provides the basis for bringing about manipulations in the characteristics of liposomes to enhance their favorable interaction with cell membranes and hence the drug delivery.

Liposomes have the advantage of delivering both the lipophilic drugs that they can entrap in their lipid covering and hydrophilic drugs that are incorporated into their aqueous core. Studies have shown that liposomes are also efficient carriers of amphiphilic drugs. Liposomes enhance the corneal

permeability of lipophilic, hydrophilic as well as amphiphilic drugs due to their ability to come in close contact with cornea and conjunctiva and increase the extent of corneal uptake by prolonging the corneal contact time [107]. Additionally, liposomes are completely biodegradable and relatively nontoxic. Despite these advantages, some limitations of the liposome-based formulations have restricted their therapeutic uses in the past. Conventional liposomes do not differentiate the target cells from others and manipulation of the structure of liposomes in order to achieve targeted drug delivery is another important issue. Additionally, the requirement of prolonged sustained drug delivery also warrants manipulations of the liposome characteristics. Efficacy of liposomes as a drug carrier depends upon various factors such as charge, size, and lipid composition of the liposomal membrane, stability and corneal residence time. To circumvent the limitations of liposomes summarized above and to achieve the characteristics of an ideal drug carrier, several modifications particularly to the surface characteristics and lipid composition of the liposomes have been explored.

Modifications:

Charge: In general, charged liposomes resist aggregation and fusion better compared to uncharged liposomes and positively charged liposomes provide greater duration of action and higher drug delivery compared to negatively charged liposomes [107]. This is because positively charged liposomes intimately interact with negatively charged cornea leading to prolonged residence time [108]. It has also been suggested that cationic vehicle slows down the drug drainage with lacrimal fluid by increasing the viscosity and interaction with negative charges of the mucus [109]. The effect of surface charge of liposomes on ocular irritation has also been evaluated. Positively charged liposomes significantly increase the rabbit eye blinking rate compared to neutral liposomes, however, the mean total score on Draize test remains below ‘‘practically non-irritating level’’ and no corneal histological changes appeared.

Size: The size of the liposomes also affects their efficiency of drug delivery. MLV have prolonged retention compared to SUV of same lipid composition and the interaction of liposomes with cornea decreases in the order of $MLV^+ > SUV^+ > MLV^- > SUV^- > MLV$. However, in another study it was observed that inulin-loaded neutral MLV, despite lesser affinity for cornea, provide 100-times greater and sustained inulin concentration in the anterior segment of eye compared to positively charged MLV [110]. This effect was attributed to a two-fold faster disappearance rate of positively charged MLV from the tear pool. Other study also showed that MLV demonstrate prolonged drug delivery [111]. The increase in vesicle size restricts drainage from the inner canthal region, hence providing prolonged residence time [112].

Lipid composition: Lipid composition of the liposomal membrane determines its capacity to resist leakage of the entrapped drug. Tear-induced leakage of entrapped drug can be reduced by incorporating increasing amounts of cholesterol in the vesicle bilayers. The lipid composition of the liposomes needs to be optimized depending on the drug to be loaded. Similarly, drug to phospholipid ratio also affects the entrapment efficiency of the liposomes. The type of lipid used also determines the surface charge of liposomes [5].

Type and concentration of salt: Considering the biological relevance of salt, the most important ones include as anions Cl^- and as cations Na^+, K^+, Ca^{++}, and Mg^{++}. The binding of cations has been found to have a significant impact on the structural and dynamical properties of PC membranes: It leads to a drop in the area per lipid accompanied by an enhanced ordering of lipid acyl chains and the slowing down of lateral diffusion in the membrane plane. The effect of monovalent salt strongly depends on the type of lipids and cations. We can identify some computation studies results [7, 8], that developed a methology to include these ions into molecular dynamics simulations of bilayers (Table 1-2-3).

ions	σ (nm)[a]	ϵ (kJ/mol)[a]
Na^+	0.25752 (0.24299)	0.061774 (0.19629)
K^+	0.64541 (0.31426)	0.56651×10^{-4} (0.364001)
Cl^-	0.44480 (0.40447)	0.44559 (0.62760)

TABLE 1: Lennard-Jones Parameters of Ion

	lipids	salt[a]	$\langle A \rangle$ (nm^2)[b]	$\langle N_{coord}^{(cations)} \rangle$ [c]	$\langle \chi_{bound}^{(cations)} \rangle$ [d]	$\langle N_{coord}^{(anions)} \rangle$ [c]	$\langle \chi_{bound}^{(anions)} \rangle$ [d]	$\langle \phi_{PN} \rangle$ (deg)[e]
1	POPC		0.652					77.9
2	POPC	NaCl	0.604 (0.608)	3.09 (2.14)	0.87 (0.85)	1.30 (1.22)	0.30 (0.25)	71.3 (69.6)
3	POPC	KCl	0.648 (0.639)	1.17 (1.88)	0.07 (0.37)	1.15 (1.13)	0.17 (0.17)	77.3 (74.2)
4	POPE		0.519					92.8
5	POPE	NaCl	0.509 (0.511)	2.99 (2.38)	0.24 (0.34)	1.36 (1.11)	0.16 (0.15)	89.9 (88.6)
6	POPE	KCl	0.511 (0.509)	0.16 (1.66)	0.01 (0.06)	1.20 (0.94)	0.11 (0.08)	93.1 (93.6)

TABLE 2: Summary of MD Simulations of Phospholipid Membranes with Monovalent Salt

	lipids	salt	D_L (10^{-8}cm^2/s)[a]
1	POPC		5.68 ± 0.82
2	POPC	NaCl	3.11 ± 0.47 (3.20 ± 0.76)
3	POPC	KCl	6.36 ± 1.64 (4.97 ± 0.97)
4	POPE		1.16 ± 0.30
5	POPE	NaCl	0.98 ± 0.20 (1.01 ± 0.27)
6	POPE	KCl	0.71 ± 0.18 (0.84 ± 0.26)

TABLE 3: Lateral Diffusion Coefficients *D*L of POPC and POPE Membranes

For a salt-free POPC bilayer at 310 K the area per lipid was found to be 0.652 +/- 0.002 nm2. On the experimental side, values of 0.66 nm^2 (T = 310 K), 0.65 nm^2 (T = 298 K), 0.64 nm^2 (T = 298 K), and 0.63 nm^2 (T = 297 K) have been reported for the area per lipid for POPC bilayers. Therefore, calculated value for the area per lipid is in good agreement with available experimental data (as well as with previous MD studies), validating thereby the molecular model.

POPC under the Influence of NaCl. Addition of NaCl drastically changes the structural properties of a POPC lipid bilayer through the binding of cations to the lipid-water interface. Previous MD studies clearly demonstrated that ion binding is a rather slow process, which emphasizes the fact that system equilibration is one of the central issues in simulations of lipid bilayers with salt. The change of membrane parameters can modify functionality of the liposome; this is due to different solvation free energy and different size of every type of ion, so some ions can break the solvation shell and move itself near the polar heads of liposome, creating ionic interactions with the negative components phospholipids. The tight binding of Na+ ions to PC lipid bilayers leads to a notable decrease in the area per lipid accompanied by a more vertical orientation of PC head groups with respect to the membrane surface, by a considerable slowing down of the lateral lipid mobility, and by an increase in the potential difference across a monolayer**.**

As for potassium ions, their binding to PC membranes and, therefore, the overall salt induced effects are found to be much weaker compared to Na+. This is mostly due to the larger size of a K+ ion, which implies a smaller ionic surface charge and a less ordered first hydration shell **[6].**

The interaction between metal divalent cations and negative lipids plays an essential role in the structure and function of biological membranes. Aggregation and fusion processes seem to be intimately related to the ability of these cations to bind to phospholipid headgroups and form dehydrated intermembrane complexes. In this sense, the effectiveness of Ca^{++} and Mg^{++} in inducing membrane aggregation and fusion has been correlated to their respective binding constants. Recent studies showed that the different effect of Ca^{++} and Mg^{++} in membranes is more profound than a simple numerical difference in binding constants. Aggregates formed by Ca^{++} were branched structures, whereas dense structures were observed for PS_ clusters induced by Mg^{++}. These reported differences also suggest the possibility of different binding modes or binding sites for Ca^{++} and Mg^{++} with negative lipids. In a system with negative lipids, Ca^{++} seems to interact with PO_4^- group of a phopspholipid and COO^- group of another phospholipid, while Mg^{++} seems to interact with two PO_4^- groups or two COO^- groups of phospholipids, suggesting different modifications on membrane structure **[7]**.

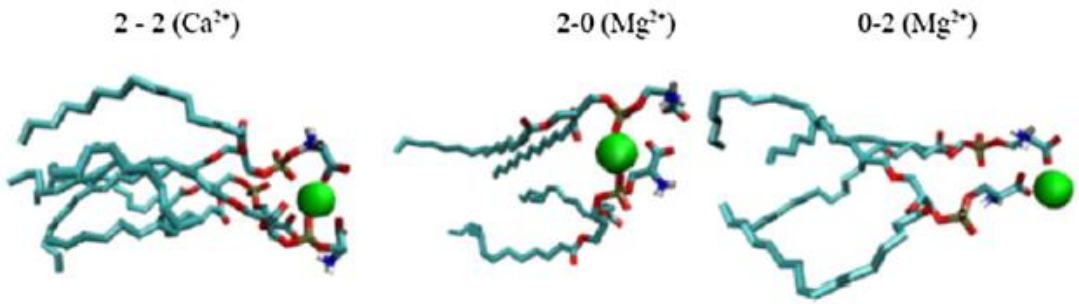

Figure 5: Different binding modes of Ca^{++} and Mg^{++} as observed in MD simulations. The snapshots were made with the use of the VMD program. Cations are shown as spheres and lipid molecules are shown in the bond representation of the VMD program

2.3 THERAPEUTIC APPLICATIONS OF LIPOSOMAL FORMULATIONS IN TOPICAL OCULAR DRUG DELIVERY

Antiviral drugs

Herpes Simplex virus (HSV) keratitis is a common cause of cornea related blindness worldwide. Global incidence of HSV keratitis is roughly 1.5 million, including 40 000 new cases of severe monocular visual impairment or blindness each year. Several antiviral drugs have been used in the treatment of HSV keratitis. Acyclovir, a nucleoside analog, has been shown to be effective against HSV. However, because of its limited water solubility, poor lipophilicity and low bioavailability following topical application, it has not shown effectiveness in the treatment of HSV keratitis. It has been compared the bioavailability of topically administered acyclovir with that of subconjunctival administration [113]. The corneal levels of acyclovir were 2.5 times lower and aqueous levels were 5 times lower with topical administration compared to subconjunctival. Systemic acyclovir has been shown to be more effective than topically applied ointment in terms of recurrence rate, functional improvement and graft survival in patients after keratoplasty. Prodrug strategy using more stable amino acid esters of acyclovir has been shown to have enhanced bioavailability. Use of liposomal formulations to enhance bioavailability of topically applied acyclovir has also been evaluated. In one of the studies, in vitro corneal penetration and in vivo corneal absorption of acyclovir containing liposomes was evaluated using rabbits. Liposomes were prepared by drug-lipid hydration method. Phosphatidylcholine and cholesterol were used as lipids, stearylamine as cationic charge inducing agent and dicetylphosphate as anionic charge inducing agent. The loading concentration of acyclovir in the liposome dispersion was 1.24 mg/ml. In vitro studies showed that the acyclovir in solution had fastest permeation through cornea while the corneal permeability of negatively charged liposomes was two times lower and that of positively charged 3.6 times lower than solution. Because of the slower permeation, negatively charged liposomes provided longer permeation time and the same was

even longer with positively charged liposomes. In vivo studies also showed that positively charged liposomes penetrate cornea slower than negatively charged liposomes and solution, however, due to prolonged corneal contact time, the extent of corneal penetration is highest with positively charged liposomes [108]. It has been studied acyclovir delivery by topical application using liposome [114]. 1, 2-Dipalmitoyl-sn-glycerol-3-phosphocholine (DPPC) and cholesterol were used as the lipids. Negative charge was introduced by adding 1, 2-dipalmitoyl-sn-glycerol-3-phosphatidic acid (DPPA) and positive charge by stearylamine or dimethyl-dioctadecyl glycerole bromide (DDAB). Liposomes were prepared following four different techniques; thin-layer evaporation, reverse phase evaporation, frozen and thawed, and dehydrated- rehydrated. Positively charged oligolamellar liposomes were shown to have most suitable bioadhesivity towards corneal epithelium. In vivo studies exhibited 42.3-folds increase in the acyclovir concentration in aqueous humor by acyclovir-loaded liposomes compared to free drug.

Antibacterial drugs

Several antibacterial agents have been formulated in liposomal forms to enhance the ocular bioavailability of these agents in the treatment of bacterial ocular infections. Ciprofloxacin, a fluoroquinolone antibiotic, is widely used in the treatment of ophthalmic infections; however, the efficacy is often limited due to poor ocular bioavailability of aqueous solutions. In other works, it has been prepared multilamellar liposomes containing ciprofloxacin by thin film hydration method using lecithin and a-L-dipalmithoylphosphatidylcholine (DPPC) [115]. Release profile of the liposomes was then studied in vitro. DPPC liposomes were found to significantly prolong the release half-time especially when 0.1% polymethacrylic acid was incorporated in the formulation as vehicle. Ciprofloxacin-loaded liposomes coated on soft contact lenses have also investigated for efficient drug delivery. The contact lenses with ciprofloxacin in liposomes inhibited both the Staphylococcus aureus and Pseudomonas aeruginosa on an agar plate and showed an enhanced antibacterial effect as determined by minimal inhibitory concentrations. The system was found to be nontoxic in in vitro experiment [116]. It has been studied in vitro and in vivo distribution of ciprofloxacin hydrochloride using liposomes coated with chitosan complex [117]. Liposomes were prepared by thin film hydration method. It was observed that positively charged liposomes entrapped high level of ciprofloxacin. However, when chitosan complex coating was added, even higher entrapment was seen with negatively charged liposomes. In vivo studies showed that negatively-charged chitosan-coated liposomes provide significantly higher level of ciprofloxacin in external eye tissues with prolonged duration of up to 8 h compared to non-coated positively-charged liposomes (4 h) and commercial eye

drop (2 h). In a recent study, it was reported that ciprofloxacin-loaded liposomes provide higher ocular bioavailability compared to commercially available drug [118].

Antifungal agents

Ocular fungal infections are often difficult to treat. Although, several antifungal agents are available for systemic use their ocular bioavailability after topical or systemic administration is poor and intraocular administration is associated with toxic effects. Amphotericin B is an important antifungal drug for the treatment of mycotic infections in eye, however, topical use of the drug causes irritation and ocular permeation is poor. Therefore, use of liposome encapsulated amphotericin B has been investigated. Application of one drop of amphotericin containing unilamellar liposomes to rabbit eyes provided very stable corneal amphotericin B level and had the benefit of lowered ocular toxicity. In a study involving 11 patients with culture positive Candida keratitis, the treatment was given as topical liposomal fluconazole (2 mg/ml) 3 times daily over a period of 30 d. Among all, eight patients showed complete improvement, one patient showed partial improvement while two patients had no improvement. Thus the fluconazole in liposomal form was found to be highly effective in treating Candida keratitis. Although topical fluconazole in liposomal form was found to be superior to solution form in the rabbit model of Candida keratitis, in Candida endophthalmitis model the intravitreal liposomal fluconazole showed lower efficacy than fluconazole in solution [119].

Anti-inflammatory and immunomodulatory agents

Several anti-inflammatory and immunomodulatory agents are widely used in the treatment of ocular inflammatory and immunological diseases. To enhance the ocular bioavailability and reduce the toxic effects following topical or intravitreal adminsitration, liposomal forms of many of these drugs have been evaluated. Cyclosporin is an anti-inflammatory and immunomodulatory drug and is used for the treatment of ophthalmic conditions like dry eye syndrome and in patients undergoing corneal transplant. It has been investigated the efficacy of cyclosporine encapsulated in liposomes in preventing the corneal graft rejection in rats that received allogenic graft [120]. When compared with cyclosporine in olive oil or empty liposomes, the group treated with cyclosporine-loaded liposomes showed increased mean survival time. The graft survival rate was 77% in liposome treated group compared to 45% in cyclosporine in olive oil or 36% in empty liposomes treated group. In another study cyclosporine loaded liposomes or olive oil containing equivalent amount of cyclosporine was applied topically to rabbit eyes at 15-min intervals within the first hour and then one hourly over a 6-h period. Additionally, collagen shields soaked for 30 min in the liposome preparation of cyclosporine were also tested in vitro and in vivo. It was observed that cyclosporine in liposomes applied topically

or in collagen shields delivered significantly higher drug levels to the cornea and sclera at 1 and 3 h compared to cyclosporine in olive oil. Similarly, the levels of cyclosporine in aqueous and vitreous humor were significantly higher in animals treated with liposomes topically or in collagen shields compared to cyclosporine in olive oil. The aqueous humor concentration of cyclosporine was also found to be higher after subconjunctival injection of cyclosporine containing liposomes in rabbits compared to subconjunctival injection of the same quantity of free cyclosporine. One of the recent studies in rabbits has demonstrated that topically applied fusogenic liposomes are safe and in some eyes may produce mild conjunctival injection.

Antiglaucoma agents

Several antiglaucoma agents are used topically to lower intraocular pressure for the treatment of glaucoma. However, topical use is associated with adverse effects and the reduction in intraocular pressure is often suboptimal. Use of these drugs in liposome form may enhance their efficacy by increasing the ocular bioavailability and on the other hand may reduce the adverse effect by slow drug release over prolonged period. Latanoprost, a prostaglandin analog, is one of the most effective drugs in lowering IOP. It is a lipophilic substance and is available as oil/water emulsion. Studies have been done to encapsulate latanoprost in liposomes and achieve long-term delivery for better patient compliance. In one of the studies, latanoprost-loaded large unilamellar liposomes were given subconjunctivally in rabbits as a single injection and reduction in intraocular pressure was monitored. A comparison was made with daily topical application of latanoprost in solution. It was observed that the liposomal formulation provided a greater sustained IOP lowering effect compared with daily administration of topical latanoprost beyond 90 d and no signs of inflammation were evident in the eyes. Liposome entrapped brimonidine tartrate and diltiazem hydrochloride also exhibit greater IOP lowering effects compared to corresponding free drug solutions.

Other potential uses

Use of liposomes for gene therapy is another potential application that has recently been investigated, and this study showed that N-(alpha-trimethylammonioacetyl)-didodecyl-D-glutamate (TMAG) liposomes can effectively transfer plasmid DNA to retinal ganglionic cells.

Antioxidants are finding application in several disease processes. Edaravone, a radical scavenger, was used in liposomal formulation to study its effect against light-induced retinal damage. The liposomal formulation of edaravone was shown to reduce the photic damage as well as apoptotic cell death of the retinal ganglion cells much more effectively compared to free drug formulation.

Many experimental studies suggested that liposome formulations are effective for transcorneal drug delivery of anticataract agents such as disulfiram. Other studies demonstrated that liposomal CoQ10 is a promising candidate for the topical application of CoQ10. In our experimental studies we demonstrated that liposomal formulations of magnesium taurate and tocotrienol delay the onset and progression of galactose-induced cataract in rats [5].

3. MATHERIALS AND METHODS

3.1 ENERGY AND SIMULATION OF LIPID BYLAYERS

Thanks to the improvement of both Molecular Modeling software and hardware resources, it is nowadays possible to get new insights on complex molecular aggregates. Extensive structural analysis and accurate inter-molecular interactions previsions *via* computational methods arise today as a key part of laboratories protocols in many scientific fields such as chemistry, drug design, biology and materials science. Among these tecniques, Molecular Dynamics (MD) allows a more accurate analysis of the whole system's kinetics and it is particularly suitable to describe dynamical behaviors.. In our study, the liposomial nanovectors were described throught MD simulations, carried out using a tested protocol developed in our laboratory, in order to get a realistic model of lipid components, and to point out the main differences arising as type of interactions of different antioxidant molecules tested. Indeed, computer simulations of lipid bilayers research has become prominent for the last couple of decades. As computational resources became more available to the scientific community, simulations play an increasingly important role in understanding the processes that take place in and across cell membranes. The scientific interest is strictly related to the biological importance of the Biomembranes, which act as barriers separating cell's internal environment from the external one. The membranes have a heterogeneous complex composition and they include many different lipids together with proteins, steroids, carbohydrates and other membrane-associated molecules. Each of these compounds are involved in a great number of cellular processes and thus, membranes exist as dynamic structures. In the last decades, molecular dynamics simulations have become one of the most useful tool in the *in silico* investigations of molecular structures; in fact, such computations provide structural dynamical information, which is essential and hardly obtained by experimental methods; furthermore, it furnishes a system real-time imaging at atomistic-level resolution.

Indeed, the spectacular growth of membrane simulations in the last 10-15 years had led to a better overall picture of lipid bilayers at atomic resolution, when the only employment of experimental methods is often insufficient. Thus, the usage of high-performance computing (HPC) allows

investigation of complex membrane molecular systems using powerful molecular modeling techniques such as molecular dynamics (MD). In particular, full atoms MD simulations reproduce the motions of each atom in the simulation, by using an empirical potential energy function and it provides molecular atomistic interactions and energetic details that are generally hard to obtain from experiments. Thus, it represents a critical additive information for the full comprehension of membrane macroscopic behavior. The timeline for the first attempts of computer simulations of model bilayers withatomistic resolution might begin in the 1980's with the early simulation of a solvent free decanoate lipid bilayers and with water between rigid lipid headgroups which was followed in the 1990's by simulations of fully hydrated bilayers formed by lipids generally found in biological membranes, with both phospholipids and water represented with atomic details. Later on, the development of HPC power has made feasible simulations of more huge complex systems, with increased size. At present, simulation of hundred hydrated lipids for a time length of 50-100 ns, is considered routinely and can be easily extended for a much longer simulation time (1 μs-1ms).

Scientists mede many efforts to develop new safe and efficient supramolecular vectors for transporting a pharmaceutical compound in the body to achieve the desired therapeutic effect (Drug Delivery). In fact, if a drug is not able to reach its site of action, it is essentially useless; moreover, its delivery is affected by its physico-chemical properties, and also by the interplay of these factors with binding, transport, and metabolism of the drug in the body. Thus, the choice of the delivery methods to efficiently transport *hard-to-deliver* compounds to the appropriate target sites, is of great importance.

The mixed lipid systems have a composition in line with the cell lipid composition and thus they represent a good choice to design safe and efficient nanovectors for Drug or Gene Delivery. In this point of view, the use of *in silico* models allows the lipid to target drug design allowing the saving of time and money, features that make the *in vitro* experiments very tiring. Computational models also allow a more detailed study of the interactions, which allows the development of vehicles for drugs even better directed towards their biological target.

3.1.1. CLASSICAL MOLECULAR MECHANICS APPROACH

With the aim of pursuing the full comprehension at atomistic level of biological and chemical systems, Molecular Modeling was developed as a computational theoretic technique, which allows scientists to mimic the behavior of real molecules in a virtual environment. This description at the atomistic level performed *in silico,* includes two possible treatment: the classical Molecular Mechanics (Classical mechanics/Newtonian mechanics) approach, or the Quantum Mechanics ones. As the Molecular Mechanics is the main approach suitable to study large biological systems, we will focus on a brief description of this method, to give a better comprehension of Classical Mechanics Model benefits and limits.

Molecular Mechanics calculations, also known as Force Field calculations, can be of considerable use in the qualitative/quantitative descriptions in these cases where we concentrate on the structural aspect and not on the electronic and/or spectroscopic properties. In essence, we describe the potential energy surface without invoking any quantum mechanical calculations or descriptions. The Born-Oppenheimer approximation, fundamental to gain a molecular description, states that the Schrödinger Equation for a molecule can be separated into a part describing the motions of the electrons and a part describing the motions of the nuclei and that these two motions can be studied independently. With Molecular Mechanics we focus on the motions of the nuclei while the electrons are not explicitly examined at all, but are assumed to find an optimal distribution about the nuclei. The Born-Oppenheimer PES (Potential Electrostatic surface) is then a multidimensional surface describing the energy of the molecule in terms of nuclear positions.

The common chemical representation of molecules as mechanical assemblies is made up of simple elements like balls (atoms), rods or sticks (bonds), and flexible joints (bond angles and torsion angles). The method then treats a molecule as a collection of particles held together by simple harmonic forces. These various types of forces are described in terms of individual potential functions that in sum constitute the overall molecular potential energy or steric energy of the molecule. In its simplest representation, the molecular mechanics equation is:

$$\boldsymbol{E = E_{bond} + E_{angle} + E_{dihedral} + E_{electrostatic} + E_{van\ der\ Waals}}$$

E is the molecular system's total potential energy in a given conformation and it is treated as a sum of individual energy terms [6, 7].

All these potential terms, together with the equilibrium bond, angle, and dihedral values, partial charge values, atomic masses and radii, and energy function definitions, are collectively known as a Force Field. Parameterization is typically done through agreement with experimental values and theoretical calculations results. The atoms of the calculated molecular system are classified as “atom

types" which really go further the element type definition and classification. In addition to atomic number (C,N,O, ecc), connectivity and nature of bonded atoms or group are considered.
Thus, the "atom types" could therefore be seen as identification codes that correlate every virtual atom we find in our model, with a set of specifics parameters for the real atom and its physico-chemical properties. Every set of parameters must be used for the proper force field. The main points to distinguish the chemical environment of an atom and assign the correct atom type, are as follows:

1. *Hybridization*
2. *Atom formal charge*
3. *Vicinal atoms which is linked to*

As an example, **AMBER** force field defines the following set for oxygen:

O *carbonyl oxygen*

OH *hydroxyl oxygen*

OS *eter or ester oxygen*

Each force field is parameterized to be internally consistent, but the parameters are generally not transferable from one force field to another. For all these reasons, a particular attention must be put on the use of a correct parametrization for the molecular systems that must be studied.

3.1.2 FORCE FIELD FOR LIPID BILAYER SIMULATIONS

A critical component for this aspect has been the development of a reliable force field (FF) potential energy function. A simulation cannot proceed without it, and the availability of the appropriate FF is among the first issues that a researcher must confront when considering a new system. Furthermore, proper parameterizations in the force field developed is necessary. This is a technical aspect, which needs continuous attention in molecular simulations since a force field is good if it provides agreement with all available experimental data, taking into account for the simulation and experimental uncertainty. It is true that experimental techniques are improving and thus, even if a force field have always provided satisfactory agreement with experimental data, it may later begin to show discrepancies. The only way to solve this problem is further and continuous improvements of the force field, which can lead to a better description of the molecular interactions and a better agreement with the experimental data. The three main force fields, which have been tested and used in recent years in lipid bilayers simulations, are GROMOS, AMBER and, in our case, CHARMM.

CHARMM force field describes all hydrogens explicitly and within this FF, a more detailed description of intramolecular interactions is provided. Thus, the Urey-Bradley term for covalent angles and a richer variety of parameters for dihedral angles are included. Concerning the force field (FF) parametrization, CHARMM parameters for lipids were introduced first by Feller *et al.* (Charmm22 parameter set or referred as C22) and then were updated in Charmm27 (c27) parameter set and in its extension C27r. The CHARMM force field was firstly born in the original CHARMM software, and it is originally present in NAMD simulation package. It is also implemented in a number of other simulation packages such as GROMACS. Successively, the CHARMM36 lipid force-field have been developed which have led to a quantitative accuracy for many membrane-protein properties predictions. The limit is the membrane dipole potential that is incorrectly predicted unless some form of polarization is included within the force-field. Indeed, non-polarizable FFs attempt to reproduce many-body polarization effects in an averaged way, using partial atomic charges that are invariant to their electrostatic environment. To solve this problem, recently there has been some efforts to introduce polarization for the common lipids found in cell membranes. However, there still remains only non-polarizable FFs for the treatment of other membrane molecules as sphingomyelin (SM) and Cholesterol (Chol).

AMBER Force Field

By the 1980s, enough experience had accumulated with earlier parameterizations for several groups to develop a new generation of force fields. At the first time, the tendency was not include all hydrogen atoms as explicit force centers. The importance of hydrogen bonding, however, led many investigators to adopt a compromise whereby polar hydrogens were represented but hydrogens bonded to carbon were combined into united atoms. A widely used force field at this level was developed in 1984 in the Kollman group [11]; this FF was incorporated into the Amber molecular mechanics package [12]. Charges were derived from quantum chemistry calculations at the Hartree-Fock STO-3G level. The van der Waals terms were adapted from fits to amide crystal data by Lifson's group [13] and from liquid-state simulations pioneered by Jorgensen [14]. Force constants and idealized bond lengths and angles were taken from crystal structures, and adapted to match normal mode frequencies. Finally, torsion force constants were adjusted to match torsional barriers extracted from experiment or from quantum chemistry calculations. But were born three problems with this ''polar hydrogen only'' approach, and for this reason, there were improvements in the speed of available computers, led many groups to move to an all-atom approach:

- aromatic rings have a quadrupolar charge distribution;

- the forces that affect the pseudo-rotation between conformations of five-member aliphatic rings [13] are difficult to describe when only the heavy atoms are available as force centers;
- it is difficult with united atom models to make comparisons between computed and vibrational frequencies.

In 1986 was published an extension of the 1984 force field to an all-atom model. The continued increase in the speed of computers led the Kollman's group to conclude in 1990 that a new round of force-field development was warranted; this labeled the ''Cornell et al.'' or ff94 force field [16].
In addition to improvements in the parameters, a more serious attempt was made to explicitly describe the algorithm by which the parameters were derived, so that consistent extensions could be made to molecules other than proteins. The use of fitted charges at the HF/6-31G* level appeared to offer a general procedure for quickly developing charges for all 20 amino acids in a way that would be roughly consistent with the water models that were expected to be used. The actual implementation of this scheme for developing charges had to deal with two complications:

- effective charges of the more buried atoms are often underdetermined, and second the resulting charges depend on molecular conformation, often in significant ways. A method to overwhelm this problem called RESP (for restrained electrostatic potential fit) and weakly favors solutions with smaller charges for buried atoms, yielding fairly consistent charge sets with little degradation in the quality of the fit to the electrostatic potential outside the molecule.
- The resulting charges depend on molecular conformation, often in significant ways. This is a manifestation of electronic polarizability, which can only be described in anaveraged way if fixed atomic charges are to be used.

Once the charges and the ''stiff'' internal parameters for bonds and angles were available, reference to densities and heats of vaporization in liquid-state simulations. Only a small number of sets of 6-12 parameters were necessary to achieve reasonable agreement with experiment. A key expansion from earlier work was the notion that parameters for hydrogens should depend in an important way on the electronegativity of the atoms they are bonded to. The question of how best to partition torsional barriers into ''bonded'' versus ''nonbonded'' interactions is a thorny one, and many developers of force fields have adopted a strictly empirical approach, fitting k_φ, n, and δ so that the total profile (including the nonbonded terms) matches some target extracted from quantum mechanics or from experiment. Some account of the longer-range effects was provided in subsequent parameterizations, referred to as ff96 [17] and ff99 [18], in which the potentials were fit to tetrapeptide as well as dipeptide quantum mechanical conformational energies. In recent years, it has become computationally feasible

to test protein potentials (and especially their backbone torsion angle behavior) by carrying out converged or nearly converged simulations on short peptides and comparing the resulting conformational populations to those derived from experiment [19]. The experimental estimates, obtained mainly from circular dichroism or from NMR, are often only qualitative, but this can be enough to identify obvious errors in computed ensembles [20].

Many groups have noticed that ff99 (and ff94 as well) do not provide a good energy balance between helical and extended regions of peptide and protein backbones. Another problem is that ff94 variants had incorrect treatment of glycine backbone parameters; in fact, it was one of the latest attempt to improve this behavior, and was developed in the Simmerling group. It presents a careful re-parametrization of the backbone torsion terms in ff99 and achieves much better balance of four basic secondary structure elements. Dihedral term parameters were obtained through fitting the energies of multiple conformations of glycine and alanine tetrapeptides to high-level ab initio QM calculations. This force field provides much improved proportions of helical versus extended structures. In addition, it corrected the glycine sampling and should also perform well for β-turn structures, two things which were especially problematic with most previous Amber force field variants [21]. AMBER now has implements a wider range of parameters: ff10 consists of the ff99SB amino acid parameters, the BSC0 DNA parameters, the Cheatham et al. updated the ion parameters, and modifications to RNA. There is also a new fixed-charge protein force field, ff12SB, provided with AMBER v12 along with enhanced support for polarizable potentials as well as the CHARMM force fields via an auxiliary program called Chamber [22].

AMBER has been implemented to treat at best lipid systems only in recent years. The release of Amber 14 [23] includes Lipid14 [22], a lipid force field suitable for the dynamics of phospholipids. Lipid14 derives directly from Lipid 11 which was originally developed to be fully compatible with the other pairwise additive AMBER-based force fields. Currently, it includes parameters from the General Amber Force Field (GAFF), a novel charge derivation, as well as ongoing refinements of parameters for phospholipids. Furthermore, in this implementation within the AMBER MD package, it allows tensionless simulation of a wide number of lipid types. In addition, the modular nature of this force field provides a large number of combinations of head and tail groups to create different lipid types, permitting in this way the easy insertion of new lipid species. It is completely compatible with the standard AMBER force fields built for protein, nucleic acid, carbohydrate, thus it enables simulation of hybrid molecular systems

CHARMM Force Field

Empirical force fields (FF) have become integral tools in the study of complex phenomena in numerous fields such as materials science and biomolecular simulations. The first protein molecular dynamics (MD) simulation was performed in 1970 on a system of 458 atoms over a length of 9.2 ps on an IBM 370, a top-of-the-line computer at the time, using precursor versions of the program CHARMM and CHARMM force field [25]. From its initial conception in the late 1970s to the present time, CHARMM and the associated force field have evolved to allow MD simulation studies to be performed on a host of systems of different sizes, functions, and complexity. The current version of the CHARMM program, which has been extensively reviewed by Brooks et al [26], is compatible with and has been optimized for multiple types of computer platforms capable of running either in serial or in parallel ranging from single processors PCs to clusters of multi-core processor machines to shared-memory supercomputer installations. The molecular mechanics approach was originally pioneered by Alder and Wainwright in the late 1950's [27]. It consists of using a "balls-on-springs" scheme to represent molecules where each ball corresponds to an atom and each spring a covalent bond. This representation allows to model molecules through Newtonian mechanics. Calculation of the forces and integration of the Newton's equation of motion allows the time evolution of a given system to be calculated, thus giving birth to the field of MD simulations. In molecular mechanics (MM) the potential energy of a system of particles is determined using a defined functional form and associated parameter set, the combination of which is called a force field. In MM force fields the properties of a system of particles are defined by the elasticity of the covalent bonds, the suppleness of two or three adjacent bonds (valence and dihedral angles), as well as the interactions that arise between non-bonded atoms (van der Waals "vdW" and electrostatic interactions). These elements represent the individual contributions to the energy of the system, which are ultimately combined allowing for the energy and forces of a system to be calculated as a function of geometry.

In addition, parametrization of the CHARMM force field consists of obtaining appropriate intramolecular (bond, angle, dihedral, Urey-Bradley and improper, or "out-of-plane", terms), vdW, and electrostatic parameters that adequately reproduce the selected target data. Determination of the electrostatic parameters differs between the additive and the Drude polarizable force fields in that the polarizabilities and Thole factors need to be optimized in addition to the point charges in the additive force field. Here, we describe the strategies behind the various steps depicted in figure 6 that are involved in parameter optimization for the additive and Drude polarizable force fields.

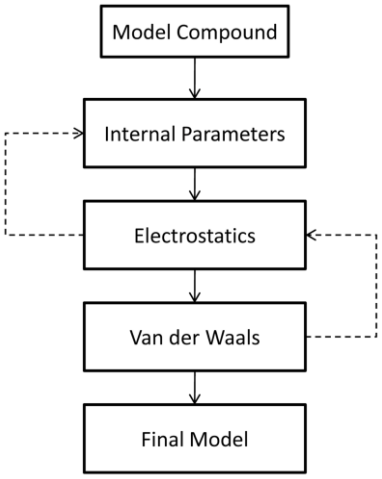

Figure 6: simplified parametrization flow chart.

As was suggested earlier, parametrization is a tedious process that directly affects the outcome of subsequent usage. It is therefore a requirement that this task be performed in a careful and consistent fashion. The development of an accurate electrostatic model is one of the more tedious steps in the parametrization workflow, laying the foundation for the model to reproduce the proper electronic response as a function of environment. In the additive CHARMM force field optimization of point charges is based on a supramolecular approach where the charges are adjusted to reproduce QM HF/6-31G(d) interaction energies and geometries of the model compound with, typically, individual water molecules as illustrated in figure 7

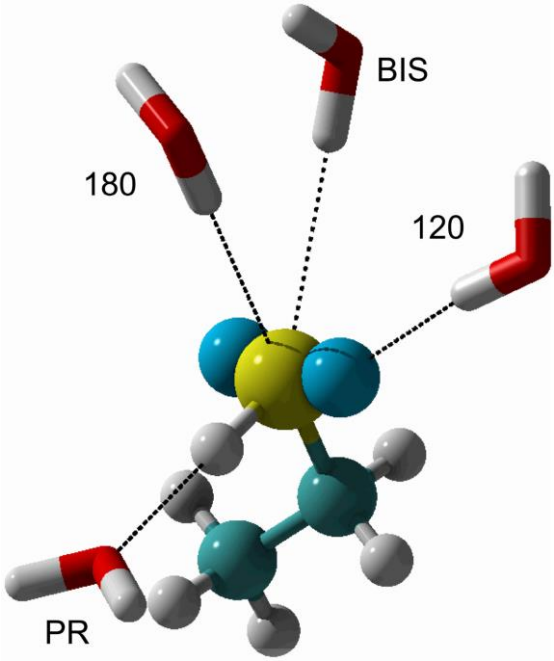

Figure 7 Orientation of test water molecules around the polarizable atom of interest exemplified through ethanethiol. Carbon is in cyan, sulfur in yellow and LP in blue. “120” is probing for interactions along the S-LP axis. “180” is oriented towards the C–S bond. “BIS” water points at the bisection of the C-S-H valence angle. “PR” is pointed directly at the sulfur proton and along the S–H bond.

Placement of water molecules at different orientations around the molecule has the distinct advantage of implicitly accounting for local electronic polarization, a desirable feature for accurate reproduction

of condensed phase properties. In addition, interactions with water are often supplemented with dimers of the model compounds and with dipole moments of the models, with the dipole moments overestimated to account for condensed phase effects [28] [29].

The CHARMM27r [30] lipid force field has been used for the study of biological systems involving the lipid bilayer. Recent publications include, for example, elucidation of the free energy profile and barriers for cholesterol flip-flops in three different types of lipid environments [31], simulation of a peptide in lipid bilayers [32] ,to better understand the dynamics of peptides as a function of membrane type and thickness, and exploration of the mechanism behind which a serine protease is anchored to a bilayer [33]. Success of these studies is associated, in part, with revisions of the original CHARMM27 force field. In the revision parameters for the aliphatic tails were optimized using high level QM calculations as target data to yield better agreements with NMR order parameters for the aliphatic tails. However, one major flaw exists in the CHARMM27r version where positive surface tension of the bilayer results in shrinking of the membrane to a gel-phase state well above the transition temperature. This flaw has been recently addressed by Klauda et al. [34] where headgroup torsions parameters and LJ and partial atomic charges of the ester linkage were re-optimized to yield the CHARMM36 lipid force field. This version reproduces experimental surface areas for saturated and unsaturated lipid bilayers, which prevents unwarranted shrinking of the lipid bilayer. One issue that remains to be addressed is that of the treatment of long-range LJ interactions, which, as discussed by the authors of the CHARMM36 article, is different for monolayers with respect to bilayers, the latter being correctly treated with standard truncation methods common to all simulation programs. Accordingly, the CHARMM36 version of the lipid force field is suitable for the majority of the current research interests involving lipids including heterogeneous systems involving bilayers.

An important utility of empirical force fields is to aid in the design and development of new therapeutic agents. Because of the extent of structural and chemical diversity in drug molecules, parameters geared towards transferability across a wide range of compounds are required from the computational scientific communities. Fulfilling this purpose are specialized force field parameters including MMFF [35], AMBER GAFF [36], CVFF [37], COMPASS [38], and the commercial version of CHARMm [39]. These force fields are appropriate, for example, for methods that identify biologically active or “lead” compounds from a large database of small molecules as well as computer-based de novo molecular design of drug-like molecules. However, it should be emphasized that reliable calculations such as those required for target-based structure optimization of lead compounds require the use of a well-balanced force field that properly treats both the drug and target (e.g. protein) molecules. In addition, to accurately capture the subtle differences across a series of test compounds it is generally necessary that at least some level of parameter optimization of the

molecules of interest be performed, due to the inherent limited transferability of parameters within a force field. With sufficient optimization, a force field can provide superior accuracy in conformational sampling and energy evaluations, leading to improved results from a variety of techniques such as 4D-QSAR [40], conformationally sampled pharmacophore (CSP) [41] and related methods, as well as free energy perturbation calculations [42]. The increasing need for computational analysis of drug-like molecules was the driving force behind the development of the CHARMM General Force field (CGenFF). Over 100 common and medicinally useful molecular scaffolds and linkers have been formally added to the existing collection of model compounds in the CHARMM force field. From this pool of model compounds, researchers can intuitively assemble compounds of interest, followed by evaluation of the quality of the resulting model and optimization of selected parameters to improve the accuracy of the treatment of the molecule of interest. Typically, one would only need to optimize the linker regions between ring systems. A summary of the steps involved in creating a new molecule is shown in Figure 8.

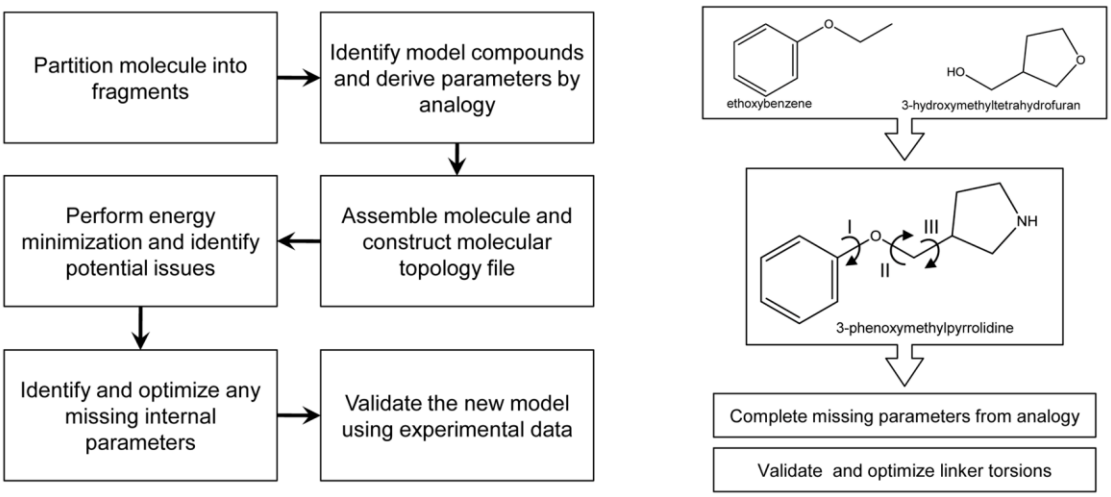

Figure 8: Flowchart for the determination of parameters for drug-like molecules as described in reference 16. 3-phenoxymethylpyrrolidine is assembled from two of its constituents, ethoxybenzene and 3-hydroxymethyltetrahydrofuran, available from the CGenFF. Parameters were identified for the pyrrolidine group by analogy. Optimization of the dihedrals I, II, and III is required to produce an accurate computational model for this molecule.

CGenFF was conceived using a methodology consistent with the parametrization philosophy behind the biological CHARMM additive force field. As a result, CGenFF is fully compatible with the biological portions of the force field, which makes possible simulations of heterogeneous systems such as protein-ligand interactions. This concept is similar to the philosophy used in OPLS [43] [44]. For complex systems or cases where a large number of molecules need to be studied, scripts that generate initial guesses of the atom type and parameters are available on the MacKerell group web

page (http://mackerell.umaryland.edu/) and efforts are ongoing with respect to the development of a web server that automatically assigns atom types, charges and parameters (https://www.paramchem.org/). The ultimate goal of that server will be the ability to validate and optimize selected parameters, a capability that is anticipated to facilitate the expansion of CGenFF to cover a larger range of chemical space. The availability of CGenFF will likely spur additional interest in computer-aided drug design using the CHARMM force field.

3.2 ATOMISTIC MOLECULAR DYNAMICS SIMULATION OF BILAYER SYSTEMS

Over the last few decades, among the other computational techniques that have emerged in Science, the atomistic Molecular Dynamics (MD) simulation have been extensively implemented and used from scientists all over the globe to obtain insight with atomic detail of steady and dynamic properties of lipid bilayers based supramolecular systems. In this regard, a critical aspect that must be identified in all the MD simulations is related to the time and length scale of process observed, the ensamble used, the pressure and temperature control. However, the amount of works on simulations of lipid membranes has achieved higher accuracy and prediction capabilities; the scale of systems that can be studied continues to increase with the increasing of the computer power and with the improvement of the MD simulation software. At present it can be identified a general limit on simulations which can be up to 5000 lipids in full atoms MD simulations and up to 50000 in coarse grained models. Concerning simulation time length, it must be pointed out that the equilibrium motions in lipid bilayers range from picosecond time scales (rattling of individual lipid hydrocarbon tails) to over many microseconds (collective motion of all lipids, m size dimension). Those motions can be investigated experimentally by means of spectroscopy methods (the former) and microscopy (the latter). Actually, hundreds of ns have become routinely for full atoms MD in bilayers, but if a further extension of the simulation time lengths is required, it must be necessary to refer to the coarse grained approach (up to ms-s time length). Usually, periodic boundary conditions (PBC) are able to avoid strong artifacts from presence of boundary planes, and this way a stack of bilayers with infinite dimension is simulated. Finally, a particular attention in simulations must be taken to identify the equilibration time to reach a steady state. To this purpose, Porasso *et al.* studied lipid bilayers with different composition in their liquid crystalline phase in order to establish a general criterion to identify the reaching of such a state. In particular they studies the dynamical temporal evolution of some lipids properties (*i.e.* area per lipid, the deuterium order parameter, the lipid hydration and lipid salt coordination) and they observed that the time required depends strictly on the single property studied. It has been found out the following order from faster equilibration property to slower:

coordination of ions = deuterium order parameter > area per lipid=hydration. Therefore, when the mean area per lipid or hydration of lipids are stable, we can ensure that the lipid membrane has equilibrated to the steady state.

Live cell membranes contains possibly by thousands of unique lipid species, and the complete *in silico* reproduction of such complex systems is quite impossible. For this purpose, *ad hoc* model systems have been built to gain a deep insight into the way the lipids mix and these kind of simulations have developed in parallel with the study of Cholesterol containing bilayers. At the start, such simulations explored interactions between steroids and other lipids, in particular local interactions often reproduced in terms of highly stylized umbrella or other models. More systematic studies,which may be extended to a length scale where domains might form, have been out of reach until recently. Besides, the condensing effect of Cholesterol on phospholipid bilayers can be reproduced both with all-atoms and Coarse Grained models. However, atomistic simulations have not been the primary choice to directly observe lipid domain formation in membranes, due to its intrinsic computational constraints. In fact, the dimension of a small domain is considered around 10 nm in diameter and this still represents a rather large simulation by today's standards [10].

As we previously discussed, starting from an equilibrium conformation (a minimum point on the energy potential surface) is the key step to perform the correct evaluation of non-equilibrium ensembles. The need for non-equilibrium states analysis is justified by the fact that the knowledge of a single structure, even if it is the structure of the global energy minimum, cannot represent the molecular behavior in function of time. Biological structures undergo a series of conformational changes that can be studied only implementing molecular dynamics simulation protocols. Through MD simulations what do we obtain is not only a single shot of the (macro)molecular conformation, but a more complex cluster of conformation, a trajectory of the system evolution in time, under simulated experimental conditions. The conformational search performed with MD simulations, can also pushes the macromolecule across his energy barrier (e.g. increasing the kinetic energy of the system) allowing a better evaluation of the potential energy surface itself.

In the sections below, we will describe the basic equation to give an overview of Molecular Dynamics methods, specifically referring to GROMACS algorithms, because this was the software package most used in this work.

3.2.1. THE NEWTON EQUATION OF MOTION

Molecular Dynamics solves the simple Newton equation of motion:

$$F_i(t) = m_i a_i(t)$$

Where: $\mathbf{F_i}$ is the force acting on atom **i**

$\mathbf{m_i}$ is the mass of atom **i**

$\mathbf{a_i(t)}$ is the acceleration of atom **i**

The force acting on atom i could be derived by calculating the potential energy derivative with respect to its coordinates r_i:

$$-\left(\frac{dE}{dr_i}\right) = m_i\left(\frac{d^2 r_i}{dt^2}\right)$$

The classical equation of motion is deterministic, so that, knowing the coordinates and velocities at t_0, the two variables can be calculated for $\mathbf{T_1}$ (trajectory). The standard method to solve the equation of motion is to calculate velocities and positions at time ($\mathbf{t + \Delta t}$).

Whether choosing or not a particular $\mathbf{\Delta t}$ (*time step*), depends on the integrator method to be used. A good integrator must be:

- rapid
- not so demanding in terms of computer memory
- capable to handle long simulation time and long simulation step Δt
- show a good energy conservation and its time-reversible
- Only one calculation of forces per time step especially for complex potential energy functions.

The most used integrator algorithms are will be better discussed in section 2.4.6.
The best choice of integrator depends on several factors, and quoting Herman J.C. Berendsen *"How accurate a simulation has to be in order to provide reliable statistical results is still a matter of debate. The purpose is never to produce reliable trajectories. Whatever accuracy the forces and the algorithms have, significant deviations from the exact solution will inevitably occur. Also in the real physical world individual trajectories have no meaning: in a quantum mechanical sense they do not exist and even classically they become unpredictable in the long run due to the non-isolated character of any real system. So what counts are statistical averages. It seems that very little systematic*

evaluation of algorithm has been done with this in mind. We have the impression that a noise as high as 10% ofthe kinetic energy fluctuation is still acceptable, although the accuracy of fluctuations may not be sufficient to obtain thermodynamic data from them. With such a level of inaccuracy the Verlet or leap frog algorithm is always to be preferred."

3.2.2. ENSEMBLES

Solving the equation of motion, generates a sequence of points in phase space as a function of time. We call phase space, the multidimensional space where the atomic positions q and the momenta p (which define the microscopic state of a system) can be considered the coordinates of the phase space itself. A single point in phase space, generated by the simulation, describes the state of the system. An ensemble is a collection of points in phase space satisfying the conditions of a particular thermodynamic state. These points belong to the same ensemble, and they correspond to the different conformations of the system and their respective momenta. There are four ensembles that are commonly used in molecular simulations, described by the three thermodynamic quantities that are kept constant. The ensembles are:

- the constant-NVE or microcanonical ensemble,
- the constant-NVT or canonical ensemble,
- the constant-NPT or isothermal-isobaric ensemble,
- the constant-μVT or grand canonical ensemble.

Another possible ensemble is the constant-μPT ensemble.
When MD is performed using Newton's equations of motion, the total energy is conserved resulting in a microcanonical ensemble (NVE). As our need is to obtain a different ensemble, the equations of motion need to be modified. A way of doing this is the extended system approach: to obtain a canonical ensemble (NVT), the Temperature coupling control can be added, as well as the Pressure coupling for the isothermal-isobaric ensemble (NPT).

3.2.3. PERIODIC BOUNDARY CONDITIONS

In computational simulations, **periodic boundary conditions** (PBC) are a set of boundary conditions often used to simulate large systems by modelling a small part that is far from its edge. A *unit cell* or *simulation box* of a geometry suitable for perfect three-dimensional tiling is defined, and when an

object passes through one face of the unit cell, it reappears on the opposite face with the same velocity. The size of the simulation box must also be large enough to prevent periodic artifacts from occurring due to the unphysical topology of the simulation. In a box that is too small, a macromolecule may interact with its own image in a neighboring box, which is functionally equivalent to a molecule's "head" interacting with its own "tail". This produces highly unphysical dynamics in most macromolecules, although the appropriate box size relative to the size of the macromolecules depends on the intended length of the simulation, the desired accuracy, and dynamics. For example, simulations of protein folding that begin from the native state may undergo smaller fluctuations, and therefore may not require as large a box, as simulations that begin from a random coil conformation.

Thus, before starting the simulation, the box size, the coordinates and velocities of all particles are required. The box size and shape is determined by three vectors (nine numbers) $\mathbf{b}_1$; $\mathbf{b}_2$; $\mathbf{b}_3$, which represent the three basis vectors of the periodic box.

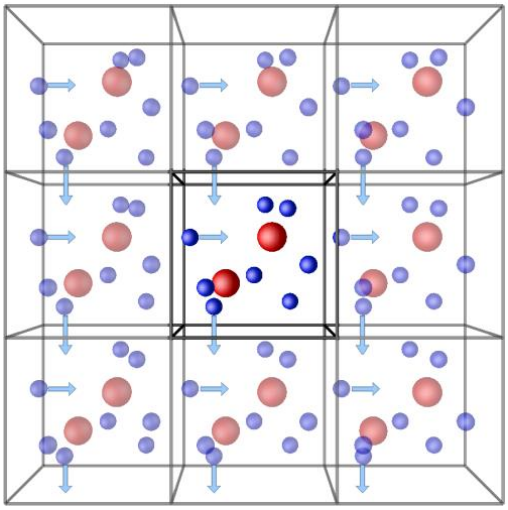

Fig 9. Periodic Boundary Conditions at the central box.

The box we define is periodic in all three dimensions x,y,z (even if “wall simulation” or “bidimensional simulation” is possible, as we cut the periodicity in the z dimension). This means that the central box contains the system we are simulating, while the surrounding boxes contain periodic images of all atoms in the central box. We refer to this method as periodic boundary conditions. Periodic images follow the same pathway as the reference atoms do, so that they can enter the central box as the reference atoms move away.

There are several possible shapes for space-filling unit cells. Some, like the rhombic dodecahedron and the truncated octahedron are closer to being a sphere than a cube is, and are therefore better suited

to the study of an approximately spherical macromolecule in solution, since fewer solvent molecules are required to fill the box given a minimum distance between macromolecular images.
GROMACS uses periodic boundary conditions, combined with the *minimum image convention*: only one – the nearest – image of each particle is considered for short-range non-bonded interaction terms. For long-range electrostatic interactions this is not always accurate enough, and GROMACS therefore also incorporates lattice sum methods such as Ewald Sum, PME and PPPM.
The Particle Mesh Ewald (PME) method calculates direct-space interactions within a finite distance using a modification of Coulomb's Law, and in reciprocal space using a Fourier transform to build a "mesh" of charges, interpolated onto a grid. It is from this charge interpolation that long-range forces can be calculated and incorporated into the non-bonded interactions in a simulated system.

3.2.4 OPTIMIZATION OF THE STARTING MOLECULAR STRCUTURES FOR MOELCULAR DYNAMICS SIMULATIONS

Molecular Dynamics simulations is the best approach for the generation of non-equilibrium ensembles and for the analysis of dynamic events, since it can represent the real PES (Potential Energy Surface) of the molecular systems.
Even if our interest is focused on non-equilibrium properties, we must take into account for the initial equilibrium state of the system, because if a starting conformational geometry is very far from equilibrium, the forces may be excessively large and the MD simulation may fail. That is the main reason for applying a robust energy minimization to the system, before simulating.
It is well known that the potential energy function of a molecular system as a very complex hypersurface in a large number of dimensions. This surface has one deepest minimum point, the global minimum conformation, and a number of local minima, where all derivatives of the potential energy function with respect to the coordinates are zero and all second derivatives are non-negative.
If (x_i, y_i, z_i) are the Cartesian coordinates of atom i, the derivative (gradient) of potential energy for atom i, with respect to its coordinates, is:

$$\nabla E = \left(\partial E / \partial x_i , \partial E / \partial y_i , \partial E / \partial z_i \right)$$

For multidimensional energy potential surfaces it is convenient to use the RMS as a measure of gradient vector, as it represents the root mean square of the squares of the gradient along the Cartesian axes:

$$RMS(gradient) = \sqrt{\sum_{i=1}^{N} \frac{\left(\frac{\partial E}{\partial x_i}\right)^2 + \left(\frac{\partial E}{\partial y_i}\right)^2 + \left(\frac{\partial E}{\partial z_i}\right)^2}{3N}}$$

Energy minimization is therefore the method to compute the equilibrium state of a molecule that correspond to global and local minima on its PES. Starting from a non-equilibrium molecular geometry, energy minimization employs the mathematical procedure of optimization to move atoms in order to reduce the net forces (the gradients of potential energy) on the atoms until they become negligible. The main used and tested downhill methods algorithms to locate energy minima: Steepest Descent and Conjugate Gradient.

Although **Steepest Descent** is not the most efficient algorithm for searching, it is robust and easy to implement. The search for energy minimum proceeds along one direction (line search) that is opposite to gradient (g). Once it will locate the minimum along the line search, a new line search will be created, opposite to the gradient in that point. Minimization is converging as the derivative approximates to zero.

In this case every line search creates a new vector that is perpendicular to the previous one so that the all approach assumes an oscillatory pathway, and becomes very inefficient as the algorithm reach the minimum. The algorithm stops when, either a user-specified number of force evaluations has been performed, or when the maximum of the absolute values of the force (gradient) components is smaller than a chosen value. Minimization is fast as the geometry is far from the minimum, but it slows down as the conformation comes to an optimum.

Conjugate gradient method, instead, is slower than Steepest Descent in the early stages of the minimization, but becomes more efficient closer to the energy minimum.
This method improves the gradient calculation by using information from the previous step. The gradients of the current geometry are first computed, and then the direction of the largest gradient is determined after the previous calculation. The geometry is minimized along this one direction (line search), and subsequently minimized along a direction orthogonal to the first one (conjugate search).

3.2.5. KYNETIC ENERGY AND TEMPERATURE

The temperature is given by the total kinetic energy of the N-particle system:

$$E_{kin} = \frac{1}{2}\sum_{i=1}^{N} m_i v_i^2$$

From this the absolute temperature T can be computed using:

$$\frac{1}{2}N_{df}kT = E_{kin}$$

where *k* is Boltzmann's constant and N_{df} is the number of degrees of freedom which can be computed from:

$$N_{df} = 3N - N_c - N_{com}$$

Here N_c is the number of *constraints* imposed on the system. When performing molecular dynamics N_{com} = 3 additional degrees of freedom must be removed, because the three center-of-mass velocities are constants of the motion, which are usually set to zero. When more than one temperature-coupling group is used, the number of degrees of freedom for group *i* is:

$$N_{df}^i = (3N^i - N_c^i)\frac{3N - N_c - N_{com}}{3N - N_c}$$

If the run starts at t = t_0, the coordinates at t = t_0 must be known, by the *leap frog* algorithm (the default algorithm in GROMACS for integration of equation of motion) as well as the velocities at

$$t = t_0 - \frac{1}{2}\Delta t$$

If velocities are not available, the program can generate initial atomic velocities v_i, i= 1…3N with a Maxwell-Boltzmann velocity distribution, generated from random numbers, at a given absolute temperature T.

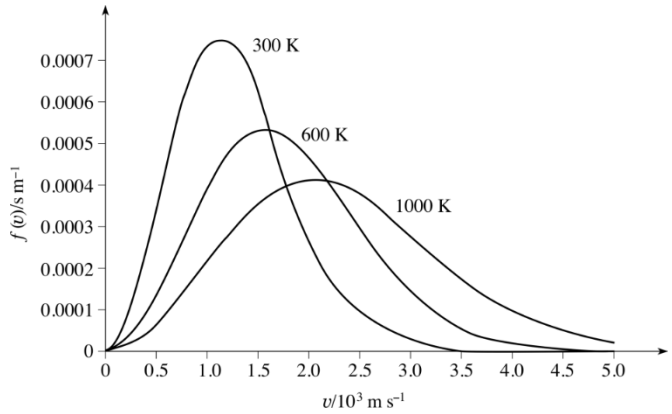

3.2.6 INTEGRATOR ALGORITHMS

The potential energy is a function of the atomic positions (3N) of all the atoms in the system. Due to the complicated nature of this function, there is no analytical solution to the equations of motion; they must be solved numerically.
Numerous numerical algorithms have been developed for integrating the equations of motion:

- Verlet algorithm
- Leap-frog algorithm
- Velocity Verlet
- Beeman's algorithm

Below we will analyze the two implemented in GROMACS: the Leap-frog and Velocity Verlet.

- **LEAP-FROG**

  The default MD integrator in GROMACS is the so-called leap-frog algorithm[43] for the integration of the equations of motion. The leap-frog algorithm uses positions r at time t and velocities v at time $t - \frac{1}{2}\Delta t;$ it updates positions and velocities using the forces F(t) determined by the positions at time t using these relations:

$$\begin{aligned} \boldsymbol{v}(t+\frac{1}{2}\Delta t) &= \boldsymbol{v}(t-\frac{1}{2}\Delta t) + \frac{\Delta t}{m}\boldsymbol{F}(t) \\ \boldsymbol{r}(t+\Delta t) &= \boldsymbol{r}(t) + \Delta t \boldsymbol{v}(t+\frac{1}{2}\Delta t) \end{aligned}$$

The algorithm can be visualized as follows:

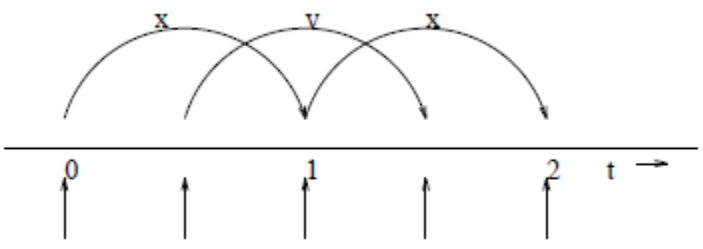

It produces trajectories that are identical to the Verlet algorithm, whose position-update relation is

$$\boldsymbol{r}(t+\Delta t) \;=\; 2\boldsymbol{r}(t) - \boldsymbol{r}(t-\Delta t) + \frac{1}{m}\boldsymbol{F}(t)\Delta t^2 + O(\Delta t^4)$$

The algorithm is of third order in r and is time-reversible.

- **VELOCITY VERLET**

The velocity Verlet algorithm is also implemented in GROMACS, though it is not yet fully integrated with all sets of options. In Velocity Verlet, positions **r** and velocities **v** at time t are used

$$\begin{aligned}
\boldsymbol{v}(t+\frac{1}{2}\Delta t) &= \boldsymbol{v}(t) + \frac{\Delta t}{2m}\boldsymbol{F}(t) \\
\boldsymbol{r}(t+\Delta t) &= \boldsymbol{r}(t) + \Delta t\, \boldsymbol{v}(t+\frac{1}{2}\Delta t) \\
\boldsymbol{v}(t+\Delta t) &= \boldsymbol{v}(t+\frac{1}{2}\Delta t) + \frac{\Delta t}{2m}\boldsymbol{F}(t+\Delta t)
\end{aligned}$$

or, equivalently,

$$\begin{aligned}
\boldsymbol{r}(t+\Delta t) &= \boldsymbol{r}(t) + \Delta t\, \boldsymbol{v} + \frac{\Delta t^2}{2m}\boldsymbol{F}(t) \\
\boldsymbol{v}(t+\Delta t) &= \boldsymbol{v}(t) + \frac{\Delta t}{2m}\left[\boldsymbol{F}(t) + \boldsymbol{F}(t+\Delta t)\right]
\end{aligned}$$

With no temperature or pressure coupling, and with corresponding starting points, Leap-Frog and Velocity Verlet will generate identical trajectories, as can easily be verified by hand from the equations above. Given a single starting file with the same starting point x(0) and v(0), Leap-Frog

and Velocity Verlet will not give identical trajectories, as the first will interpret the velocities as corresponding to $t = -\frac{1}{2}\Delta t$, while the latter will interpret them as corresponding to the time point t = 0.

For temperature- and pressure-control schemes, however, Velocity Verlet with half-step-averaged kinetic energies and Leap-Frog will be different.

3.2.7. TEMPERATURE COUPLING

GROMACS can use either the weak-coupling scheme of Berendsen [46], the extended ensemble Nosé-Hoover scheme [47, 48], or a velocity-rescaling scheme [49] to simulate constant temperature, with advantages of each of the schemes laid out below.

- The Berendsen algorithm mimics weak coupling with first-order kinetics to an external heat bath with given temperature T_0.Theeffect of this algorithm is that a deviation of the system temperature from T_0 is slowly corrected according to: $\frac{dT}{dt} = \frac{T_0 - T}{\tau}$

  which means that a temperature deviation decays exponentially with a time constant τ . This method of coupling has the advantage that the strength of the coupling can be varied and adapted to the user requirement: for equilibration purposes the coupling time can be taken quite short (e.g. 0.01 ps), but for reliable equilibrium runs it can be taken much longer (e.g. 0.5 ps) in which case it hardly influences the conservative dynamics. The Berendsen thermostat suppresses the fluctuations of the kinetic energy. This means that one does not generate a proper canonical ensemble, so rigorously, the sampling will indeed be incorrect.

- The velocity-rescaling thermostat [49] is essentially a Berendsen thermostat (see above) with an additional stochastic term that ensures a correct kinetic energy distribution by modifying it according to:

$$dK = (K_0 - K)\frac{dt}{\tau_T} + 2\sqrt{\frac{KK_0}{N_f}}\frac{dW}{\sqrt{\tau_T}},$$

where K is the kinetic energy, N_f the number of degrees of freedom and dW a Wiener process. There are no additional parameters, except for a random seed. This thermostat produces a correct canonical ensemble and still has the advantage of the Berendsen thermostat: first order decay of temperature deviations and no oscillations. When an NVT ensemble is used, the conserved energy quantity is written to the energy and log file.

- The Nosé-Hoover thermostat enablescanonical ensemble simulations. It is an extension of approach first proposed by Nosé [45] and later modified by Hoover [48]. The system Hamiltonianis extended by introducing a thermal reservoir and a friction term in the equations of motion. Thefriction force is proportional to the product of each particle's velocity and a friction parameter, ξ.This friction parameter (or "heat bath" variable) is a fully dynamic quantity with its own momentum(p_ξ) and equation of motion; the time derivative is calculated from the difference between thecurrent kinetic energy and the reference temperature. In this formulation, the particles' equations of motion

$$\frac{\mathrm{d}^2 \boldsymbol{r}_i}{\mathrm{d}t^2} = \frac{\boldsymbol{F}_i}{m_i}$$

are replaced by:

$$\frac{\mathrm{d}^2 \boldsymbol{r}_i}{\mathrm{d}t^2} = \frac{\boldsymbol{F}_i}{m_i} - \frac{p_\xi}{Q}\frac{\mathrm{d}\boldsymbol{r}_i}{\mathrm{d}t},$$

where the equation of motion for the heat bath parameter ξ is:

$$\frac{\mathrm{d}p_\xi}{\mathrm{d}t} = (T - T_0)$$

The reference temperature is denoted T_0, while T is the current instantaneous temperature of the system. The strength of the coupling is determined by the constant Q (usually called the "mass parameter" of the reservoir) in combination with the reference temperature.

It is however important to keep the difference between the weak-coupling scheme and the Nosé-Hoover algorithm in mind: using weak coupling you get a strongly damped exponential relaxation, while the Nosé-Hoover approach produces an oscillatory relaxation.

The weak temperature coupling scheme (Berendsen or V-rescale) are commonly used for the first step of the dynamics, when the system is far from equilibrium. Subsequently is better shifting to Nosé-Hoover to obtain the desired thermodynamic ensemble.

3.2.8 PRESSURE COUPLING

In the same spirit as the temperature coupling, the system can also be coupled to a "pressure bath." GROMACS supports both the Berendsen algorithm [46] that scales coordinates and box vectors every step, the extended-ensemble Parrinello-Rahman approach [50, 51].

- The Berendsen algorithm rescales the coordinates and box vectors every step, or every n_{PC} steps, with a matrix μ, which has the effect of a first-order kinetic relaxation of the pressure towards agiven reference pressure P_0 according to

$$\frac{\mathrm{d}\mathbf{P}}{\mathrm{d}t} = \frac{\mathbf{P}_0 - \mathbf{P}}{\tau_p}$$

The scaling matrix μ is given by

$$\mu_{ij} = \delta_{ij} - \frac{n_{PC}\Delta t}{3\,\tau_p}\beta_{ij}\{P_{0ij} - P_{ij}(t)\}.$$

Here, β is the isothermal compressibility of the system. In most cases this will be a diagonal matrix, with equal elements on the diagonal, the value of β which is generally not known. It suffices to take a rough estimate because the value of only influences the non-critical time constant of the pressure relaxation without affecting the average pressure itself.

Scaling can be done isotropically, anisotropically or semi-isotropically. In case of semi-isotropically scaling, the x=y-directions are scaled isotropically and the z direction is scaled independently. The compressibility in the x=y or z-direction can be set to zero, to scale only in the other direction(s). It is important to note that although the Berendsen pressure control algorithm yields a simulation with the correct average pressure, it does not yield the exact NPT ensemble.

- the Parrinello-Rahman approach, which is similar to the Nosé-Hoover temperature coupling, is capable to give the true NPT ensemble. With the Parrinello-Rahmanbarostat, the box vectors as represented by the matrix *b*obey the matrix equation of motion[2]

$$\frac{\mathrm{d}b^2}{\mathrm{d}t^2} = V\boldsymbol{W}^{-1}b'^{-1}\left(\boldsymbol{P}-\boldsymbol{P}_{ref}\right)$$

The volume of the box is denoted V , and$W$ is a matrix parameter that determines the strength ofthe coupling. The matrices P and P_{ref} are the current and reference pressures, respectively. The equations of motion for the particles are also changed, just as for the Nosé-Hoover coupling. In most cases you would combine the Parrinello-Rahmanbarostat with the Nosé-Hoover thermostat.

Just as for the Nosé-Hoover thermostat, the Parrinello-Rahman time constant is not equivalent to the relaxation time used in the Berendsen pressure coupling algorithm. In most cases you will need to use a 4–5 times larger time constant with Parrinello-Rahman coupling.

As for the coupling of temperature, If the pressure is very far from equilibrium, the Parrinello-Rahman coupling may result in very large box oscillations that could even crash your run. In that case is better using the weak-coupling scheme to reach the target pressure, and then switch to Parrinello-Rahman coupling once the system is in equilibrium.

3.3 SOLVENT WATER MODELS

Our need to simulate the correct solvation environment for the (macro) molecule, is correlated with the search for the best explicit water model to be use. The electrostatic interaction is modeled using Coulomb's law and the dispersion and repulsion forces using the Lennard-Jones potential. The potential for models such as TIP3P and TIP4P is represented by:

$$E_{ab} = \sum_{i}^{\text{on } a}\sum_{j}^{\text{on } b}\frac{k_C q_i q_j}{r_{ij}} + \frac{A}{r_{\mathrm{OO}}^{12}} - \frac{B}{r_{\mathrm{OO}}^{6}}$$

where k_C, the electrostatic constant, has a value of 332.1 Å·kcal/mol in the units commonly used in the field of computational chemistry; q_i are the partial charges relative to the charge of the electron;

r_{ij} is the distance between two atoms or charged sites; and A and B are the Lennard-Jones parameters. The charged sites may be on the atoms or on dummy sites (such as lone pairs). In most water models, the Lennard-Jones term applies only to the interaction between the oxygen atoms.

The figure below shows the general shape of the 3- to 6-site water models. The exact geometric parameters (the OH distance and the HOH angle) vary depending on the model.

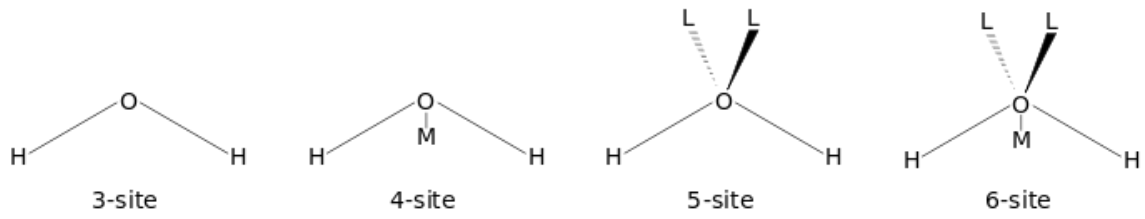

Figure 10: Water Models

3-site models (TIP3P, SPC) are widely use as the best compromise between accuracy and computational cost. Three-site models have three interaction sites, corresponding to the three atoms of the water molecule. A point charge is assignedto each atom, and the oxygen atom also gets the Lennard-Jones parameters.

4-site, 5-site and 6-site models give us an increasingly improvement in solvation, but, because of the high computational costs, they're usually implemented in small biochemical and chemical system, to study for example, the radial distribution of water around the solute or the property of ice.

4. DESIGN OF THE LIPOSOMIAL NANOVECTOR

4.1 CELL MEMBRANE COMPOSITION

The 'cell membrane' (also known as the plasma membrane or cytoplasmic membrane) is a biological membrane that separates the interior of all cells from the outside environment. The cell membrane is selectively permeable to ions and organic molecules and controls the movement of substances in and out of cells. The basic function of the cell membrane is to protect the cell from its surroundings. It consists of the phospholipid bilayer with embedded proteins. Cell membranes are involved in a variety of cellular processes such as cell adhesion, ion conductivity and cell signaling and serve as the attachment surface for several extracellular structures, including the cell wall, glycocalyx, and

intracellular cytoskeleton. Cell membranes can be artificially reassembled [52][53]. Lipid bilayers form through the process of self-assembly. The cell membrane consists primarily of a thin layer of amphipathic phospholipids which spontaneously arrange so that the hydrophobic "tail" regions are isolated from the surrounding polar fluid, causing the more hydrophilic "head" regions to associate with the intracellular (cytosolic) and extracellular faces of the resulting bilayer. This forms a continuous, spherical lipid bilayer. Forces such as van der Waals, electrostatic, hydrogen bonds, and non-covalent interactions all contribute to the formation of the lipid bilayer. Overall, hydrophobic interactions are the major driving force in the formation of lipid bilayers.

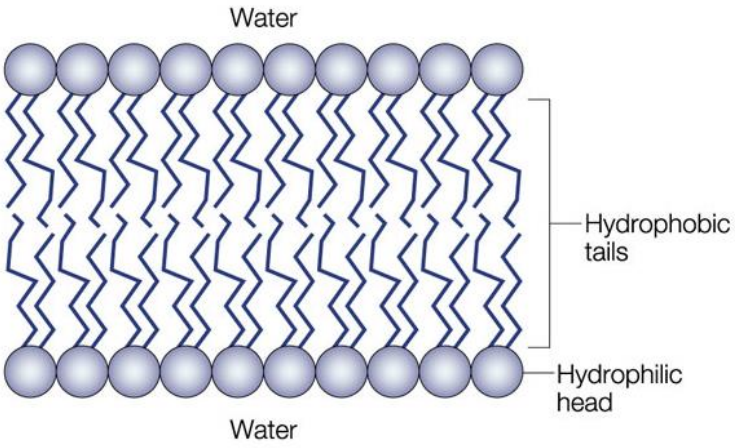

Figure 11: Bilayer structure.

The cell membrane consists of three classes of amphipathic lipids: phospholipids, glycolipids, and sterols. The amount of each depends upon the type of cell, but in the majority of cases phospholipids are the most abundant [52]. Among them, phosphatidylcholine, phosphatidylethanolamine, phosphatidylserine, and sphingomyelin, together account for more than half of the lipid in most membranes. These phospholipids are asymmetrically distributed between the two halves of the membrane bilayer. The outer leaflet of the plasma membrane consists mainly of phosphatidylcholine and sphingomyelin, whereas phosphatidylethanolamine and phosphatidylserine are the predominant phospholipids of the inner leaflet. A fifth phospholipid, phosphatidylinositol, is also localized to the inner half of the plasma membrane. Two naturally present lipids are the most relevant in this study, POPC and DOPC, because they were taken as a model for the simulation *in silico* of mixed bilayers. POPC (1-palmitoyl-2-oleoyl-sn-glycero-3-phosphocholine), the main phosphatidylcholine representative, is naturally present in eukaryotic cell membranes and is also available via synthetic pathways. It is an important lipid for biophysical experiments and has been used to study various subjects such as lipid rafts.

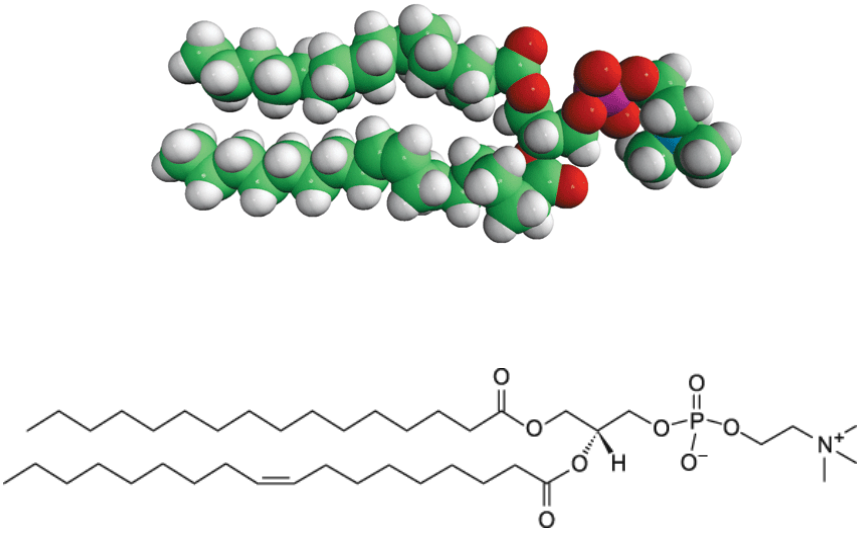

Fig 12: POPC in VdW sphere (upper) and structural formula (lower).

4.2 LIPOSOMIAL NANOVECTORS: STRUCTURE AND COMPOSITION

Liposomes are colloidal, vescicular structures composed of one or more lipid bilayers surrounding an equal numbers of aqueous compartments. The sphere, like a shell, encapsulates a liquid interior phase which contains substances such as peptides and proteins, hormones, enzymes, antibiotic, antifungal and anticancer agents. A free drug injected in blood stream typically achieves therapeutic level for short duration due to metabolism and excretion. As cell membranes do, liposomes act as shells, protecting drugs and allowing for a longer lasting duration, before it can be released from metabolism and excretion mechanisms.

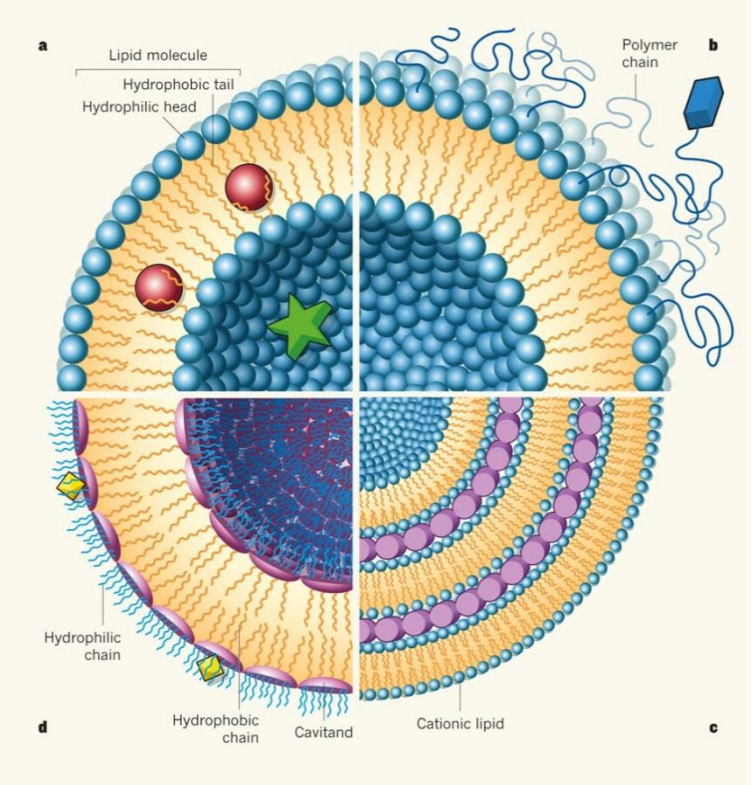

Figure 13: Different types of liposome structures: unilamellar with drugs encapsulated (a); unilamellar with functionalized lipids head (b); multilamellar with DNA encapsulated (c); inverse micelle (d)

Advantages of liposomes encapsulation can be resumed as follows:

- Liposomes are suitable for delivery of hydrophobic, amphipathic and hydrophilic drugs
- Protect the encapsulated drug from external environment
- Reduced toxicity and increased stability as well as therapeutic activity, can be improved for chemotherapeutic agents. This reduces deleterious effects that are observed at concentrations similar to or lower than those required for maximum therapeutic activity.
- Reduce exposure of sensitive tissue to toxic drugs.

Disadvantages especially concern:

- High production costs
- Leakage and fusion of encapsulated drug/molecules
- Short half life

We can distinguish different types of liposomes on the basis of:

A. STRUCTURAL PARAMETERS

1) Unilamellar vescicles:

- Small unilamellar vescicles: size range from 20-40 nm

- Medium unilamellar vescicles: size range from 40-80 nm
- Large unilamellar vescicles: size range from 100-1000 nm

2) Oligolamellar vescicles: These are made up of 2-10 bilayers of lipids surrounding a large internal volume.
3) Multilamellarvescicles: They present several bilayers and can compartimentalize the aqueous volumein an infinitenumber of ways. They differ according on their preparation

B. METHOD OF PREPARATION

1) REV: Single or oligolamellarvescicles made by Reverse-Phase Evaporation Method.
2) MLV-REV: Multilamellarvescicles made by Reverse-Phase Evaporation Method.
3) SPLV: Stable Plurilamellarvescicles.
4) FATMLV: Frozen and Thawed MLV.
5) VET: vescicles prepared by extrusion technique.
6) DRV: Dehydration-rehydration method.

C. C0MPOSITION AND APPLICATION

1) CL – Conventional Liposomes: Neutral or negatively charged phospholipids and Cholesterol.
2) RSVE – Fusogenic Liposomes: Reconstruited Sendai virusenvelopes
3) pH sensitive Liposomes: Phospholipids such as PE or DOPE with either CHEMS or OA.
4) Cationic Liposomes: Cationic lipids with DOPE.
5) LCL – Long Circulatory Liposomes: with polyethylene glycol derivatives attached to their surface to decrease their detection by phagocyte system.
6) Immuno-Liposomes: CL or LCL with attached monoclonal antibody or recognition sequence [43].

4.3 SETTING AND TUNING THE MOLECULAR DYNAMICS MEMBRANE SIMULATIONS PROTOCOL FOR MIXED COMPOSITION BILAYERS

The main strategy of this research work is to simulate the behavior of mixed lipid membranes that contains the active compound directly incorporated inside the bilayer. For this reason, the first part of my thesis work has been the tuning of our computational protocol able to reproduce the main chemical-physical properties of the built liposomes. Thus, we first started our studies on two simulated lipophilic molecules, developed to create liposomes able to act as Gene Delivery nanovectors. This strategy consist to insert functionalized lipid molecules in the bilayer as part of liposomal membrane. Thus, the molecules must not destabilize the membrane, since the liposomal carriers have to retain their fluidity. More in details, these liposomal systems showed to interact with DNA by bridge-type interaction between the polar headgroups of the functionalized molecules, divalent metal ions and the phosphate groups of DNA.

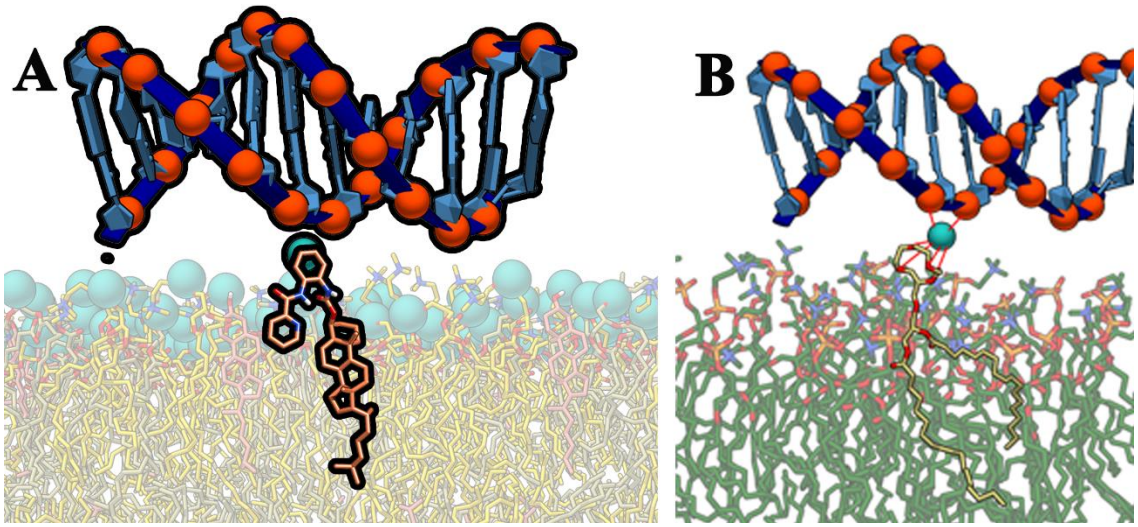

Figure 14: Gene Delivery systems. 14A shows CHOLp molecule, 14B shows crown ether molecule. In both cases, we observe direct interactions with divalent cations.

4.3.1 FUNCTIONALIZED COMPOUND FOR GENE DELIVERY:

4.3.1.1 CHOLP MOLECULES

Cholesteryl-2-(picolinamido)-phenylcarbamate (CHOLp) is a cholesteryl derivative containing an N-aryl picolinamide group as chelating agent linked to the steroid structure via a carbamate moiety. Thus, hydrophobic sterol molecule should be interact with cations, and first we tested to retain in liposomal medium and to coordinate metal divalent ions, we tested the stability of CHOLp compounds in mixed composition bilayer.

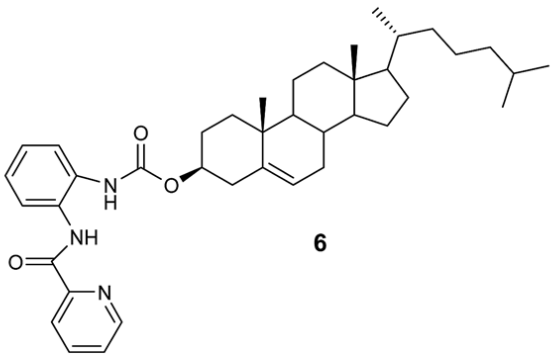

Fig 15: CHOLp molecule structural formula

Beside we investigated the phase behavior of mixtures of the functionalized cholesterol (CHOLp) and dioleoyl-phosphatidylcholine (DOPC) by means of X-ray diffraction. In order to compare our *in silico* results with the experimental findings, we carried out atomistic molecular dynamics simulations of DOPC/CHOLp bilayers as a function of CHOLp molar fractions to investigate the specific effects of the polar steroid on the structural and dynamic properties of these zwitterionic bilayers. In according with the protocol discussion in section 3.2, we performed the molecular modelling studies in absence and in presence of bivalent cations salts, in order to assess the CHOLp ability to interact with metal ions (figure 16). Before introducing the sterol compounds in the bilayer, we performed a conformational search and we found that the optimized lowest energy conformer for CHOLp shows high stability and is perfectly suitable to insert itself into a mixed composition bilayer. Indeed, from the MD results, even upon first analysis, the CHOLp molecule clearly appears well inserted into the lipid bilayer, a behavior that we can ascribe, as already suggested, to its physical chemical properties including shape and conformation. Furthermore, its aromatic polar head orients itself outside the leaflet and almost parallel to the DOPC polar head. This feature immediately places CHOLp in a good light with respect to an eventual metal ion interaction. The bilayer dynamical and structural properties arising from the collected MD trajectories, clearly point out that the CHOLp molecules strongly influence each other throughout all the simulations. This feature is particularly evident in absence of salt, while in the presence of $MgCl_2$ and $CaCl_2$ the intermolecular interactions between the steroids are competing with those between CHOLp and cations **[56]**.

In pure water, the CHOLp intermolecular interactions are smooth at low concentration (X_{CHOLp} = 0.05 molar fraction) but increasing CHOLp molar fraction (X_{CHOLp} = 0.15, 0.25), we found an aggregation of the functionalized polar cholesterol molecules.

In presence of magnesium chloride, CHOLp intermolecular interactions are evident even at low concentration (XCHOLp = 0.05) and well organized at higher concentrations. The steroid polar head

is kept outside the hydrophobic lipid environment, being able in this way to directly interact also with the metal ions through their aromatic moieties. Furthermore, the starting "closed" conformation of CHOLp opens becoming more suitable for a greater number of stabilizing interactions with metal ions.

In presence of calcium chloride, we can observe the existence of two different competing mechanisms of interactions: the first is calcium coordination through a cation–π interaction with the aromatic moieties of CHOLp; the second is the steroid aggregation. Increasing the CHOLp concentration, the first mechanism overcomes the second one, and the steroid assumes once again an extended conformation, which puts the polar head close to metal ion in the water phase. Overall CHOLp shows high propensity to coordinate the calcium cation regardless its concentration.

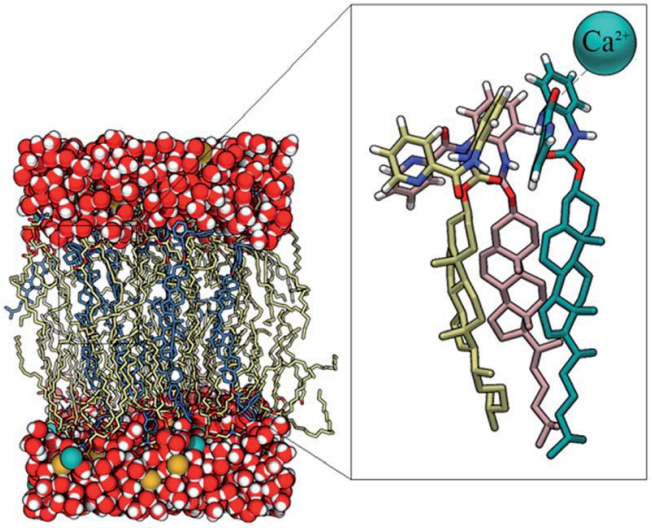

Figure 16: CHOLp cation–π and π–π stacking interactions at XCHOLp =0.25 in $CaCl_2$; calcium ions are represented in cyan while chlorine ions are represented in orange.

4.3.1.2 CROWN ETHER LIPIDS

Crown ether belong to the family of polycyclic ethers whose fundamental unit is the -OCH_2-CH_2- cyclic moiety. The crown compound allow the formation of a crown/ion complex, where the last lies in the crown's cavity. Below we show the structure of the new synthetized lipids:

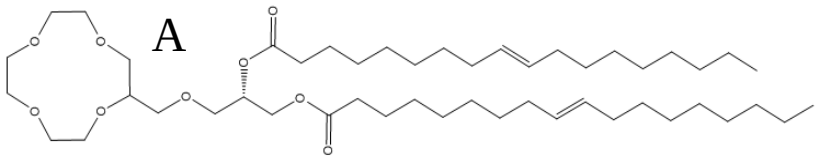

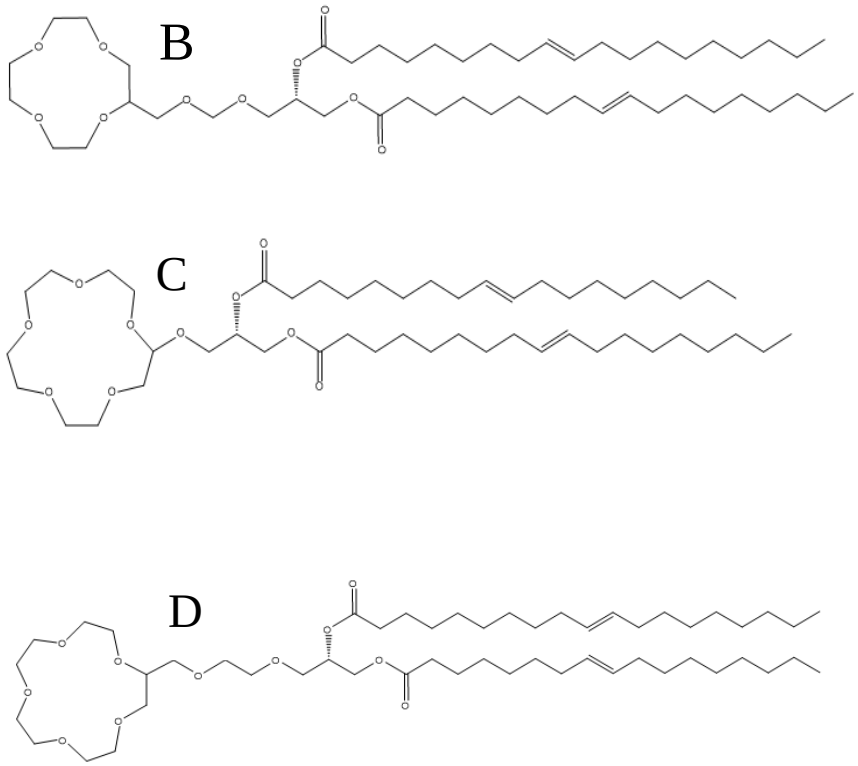

Figure 17: Crown ether lipids structural formula. **17A)** 12C4L'; **17B)** 12C4L; **17C)** 15C5L'; **17D)** 15C5L;

Like previous systems containing CHOLp molecules, we wanted to create efficient liposomal vectors used for the Gene Delivery strategy.

All compounds considered in this study (15C5L, 15C5L', 12C4L and 12C4L') show a stable insertion into the lipid bilayers after dynamical stabilization as can be well seen from the RMSD graphs. The dynamical and structural properties of the bilayers arising from the collected MD trajectories, clearly point out that the crown ether molecules strongly influence each other throughout all the simulations and that each specific crown-lipid assumes a different asset and conformation into the bilayers leaflets which depends strongly on the crown-ether structure and on the nature of the salt. In the following section, we will discuss the results obtained in details, observing more closely the specific effects of different salts on the simulated bilayer systems. We report the results for the same crown ether lipid in presence of three different salts.

As a common feature, all the functionalized lipids (15C5L, 15C5L', 12C4L and 12C4L') at the end of the 100 ns MD runs show a stable insertion into the lipid bilayers as can be well seen from the RMSD fluctuations through all the trajectories (Figure 19). Moreover, the dynamical and structural properties of the MD stabilized bilayers clearly point out that the each considered crown-ether lipid assumes a different asset and conformation in the bilayer leaflets that depends strongly on their structure and on the nature of the salt (Figure 18). Above, we refer more closely to the specific effects of different salts on the simulated bilayer systems.

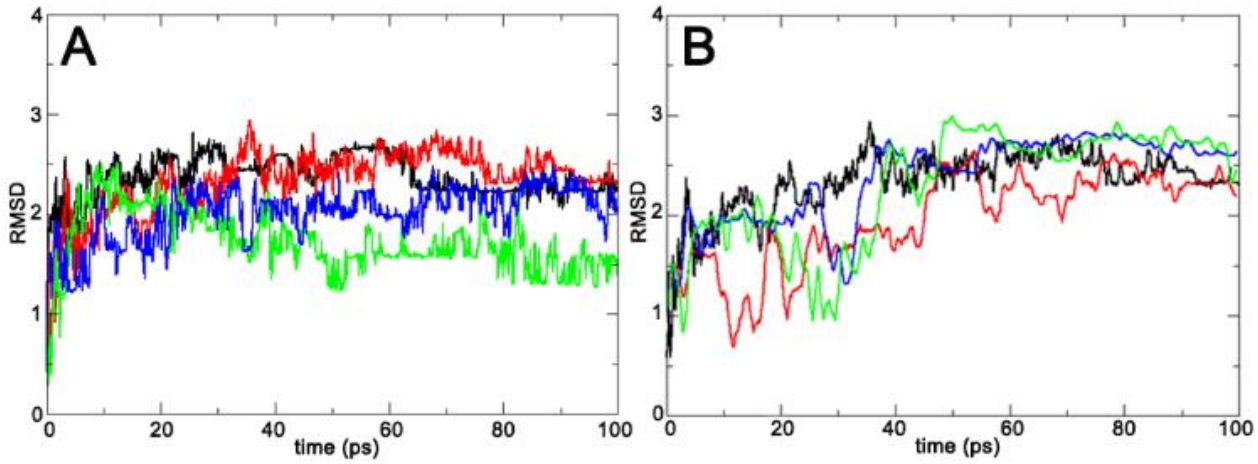

Figure 18. A) root-mean square deviation (RMSD) values of 12C4L in the systems without salts (black), with $CaCl_2$ (red), $MgCl_2$ (green)and with $MnCl_2$ (blue); **B)** root-mean square deviation (RMSD) values of 12C4L (black), 12C4L' (red), 15C5L (green) and 15C5L' (blue) in presence of $CaCl_2$.

*Crown-ether **15C5L***

The simulation was carried out in pure water, and at low concentration ($[X_{15C5L}] = 0.05M$), this crown-ether preferably dispose itself in a folded conformation that put the crown ring inside the hydrophobic core of the leaflet. Increasing 15C5L concentration ($[X_{15C5L}] = 0.25M$), the overall system appear more disordered. In fact, we can observe the crown-ether in a mixture of folded and extended conformations oriented towards the bilayer along axis (Z). Indeed, this behavior is due to the flexibility of the linker connecting the lipid skeleton with the ether-head. In fact, thanks to this 15C5L torsional freedom, switching between the folded and extended conformation, the crown-heads can lie to a proper distance minimizing their high steric hindrance. As a result, the bilayers loss its order. (Figure 19A)

The presence of the salts, indeed, strongly influences the behavior of the crown ether compound. More in details, through all the MD simulations carried out in presence of $MgCl_2$, Mg^{2+} ions are kept perfectly solvated by water, and we do not observe any peculiar interactions between the ether and the cations. In addition, the 15C5L behavior is very close to that in the model obtained in pure water, at low concentration. Increasing it, 15C5L tends to extend itself more toward the lipid matrix, and this confers a greater order degree to the bilayers than that observed in the model with no salt (Figure 19B).

Beside, we can observe for some molecules, electrostatic interactions between the crown heads (bearing negative electrostatic potential) with the choline moiety of POPC lipids (bearing positive electrostatic potential).

We found a different organization in presence of $MnCl_2$: the Mn^{2+} ions have a lower value of hydration enthalpy, because of their greater size respect to Mg^{2+}; as consequence, they are less solvated. At 15C5L low concentrations, the crown-ether molecules are totally fold inside the bilayer, so the corresponding *area per lipid* value is shift to much higher values than the $MgCl_2$ models. Increasing concentration (($[X_{15C5L}]$ =0.25M), we observe an increasing of the bilayer order since 15C5L assumes exclusively an extended conformation stretching along bilayers major axis (z) (Figure 20 C). In this case, we did not observe any coordination between crown-ether heads and manganese, but as for the corresponding model with $MgCl_2$, we report interactions between the crown ether and the choline moieties of POPC lipids.

Finally, in the presence of $CaCl_2$, we do not observe coordination with the ions Ca^{2+} at 15C5L low concentrations. The average *area per lipid* values are very close to those observed in models with $MnCl_2$ (Table 1 – *area per lipid*). However, during the simulation, the calcium ions move more closely to the bilayer surface and it is due to the lower value of solvation enthalpy of Ca^{2+} with respect to magnesium and manganese cations. As consequence, calcium have a strong tendency to break out the shell of solvation to promote other electrostatic interactions. Thus, increasing the crown-ether lipid concentration, we definitively can assist to an evident coordination between the crown-head and calcium ions (Figure 20 D).

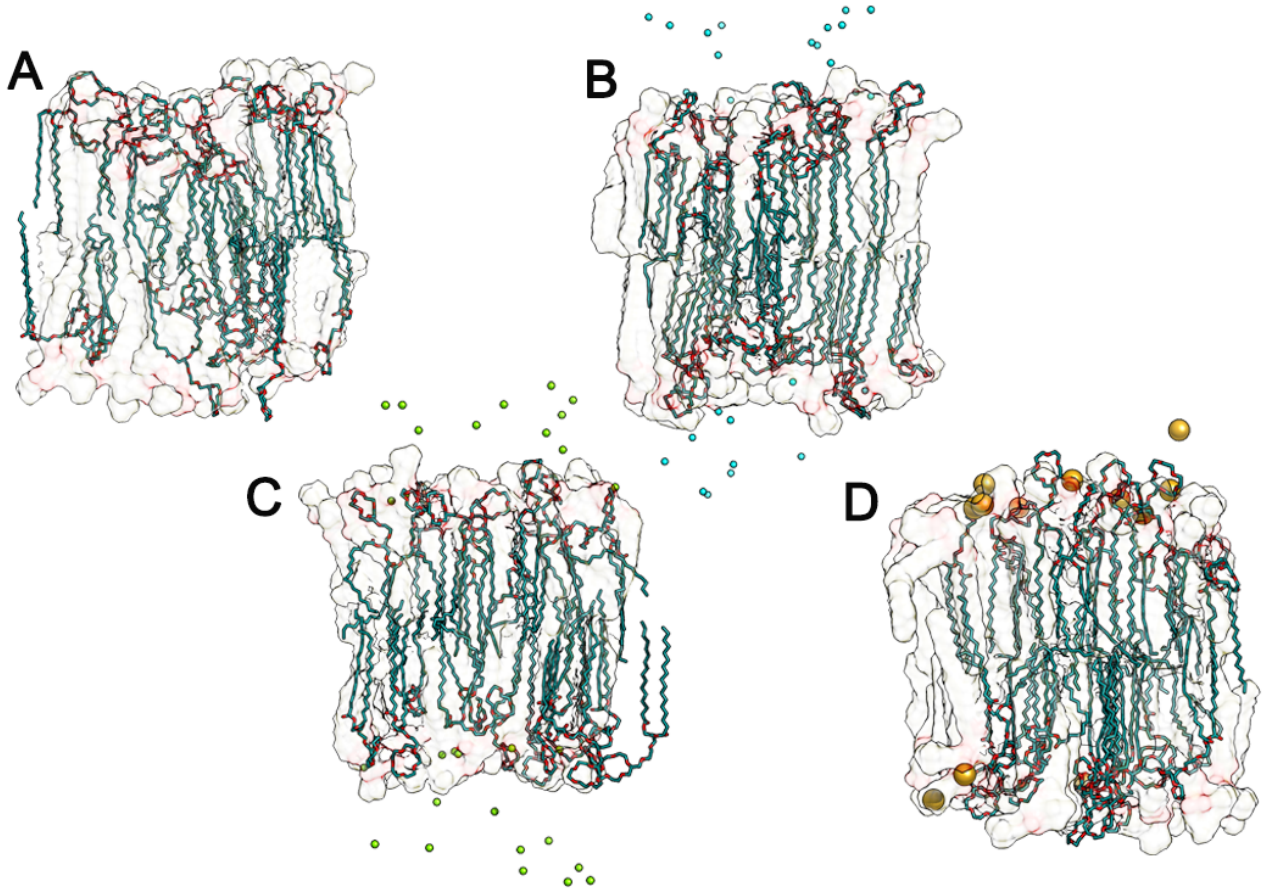

Figure 19: representative structures of steady states of 15C5L-POPC molecular model. A) shows the bilayer system simulations in pure water, B) with $MgCl_2$, C) with $MnCl_2$ and D) with $CaCl_2$

Crown-ether **15C5L'**

Crown ether 15C5L' is structurally related to 15C5L, since it bears the same crown-ether head but a different linker connecting it to the lipid backbone, but in this case, it is shorter and less flexible.

In pure water and at low crown-ether concentrations ($[X_{15C5L'}]$ =0.05 M), we can observe a strong tendency to expose the crown-head to the aqueous portion of the leaflet assuming an extended conformation. In addition, we find once again electrostatic interactions between the ammonium groups of POPC and the 15C5L' crown-heads. The increase of the 15C5L' concentration ($[X_{15C5L'}]$ =0.25M), does not affect the overall disposition and it keeps on to expose the crown-ether-head to the aqueous phase.

In presence of $MgCl_2$, instead, despite the high solvation degree of the Mg^{2+} ions, we observe at low concentrations coordination between the magnesium cations and the crown-lipid heads. This different behavior can be ascribed to the 15C5L' high propensity to assume an extended conformation that leave ether-head inside the aqueous phase, thus facilitating the formation of interactions with cations. Increasing concentration (($[X_{15C5L'}]$ =0.25M), the number of heads exposed to the solvent is kept high but the negative polar heads of 15C5L' interacts more strongly with the ammonium groups of the POPC molecules thus preventing Magnesium coordination.

Beside**,** Mn^{2+} ions are more able to break their hydration shell respect to magnesium (lower salvation enthalpy), and then in presence of $MnCl_2$, we find that manganese ions closer to the surface of lipid compared to the same model in presence of Mg^{2+} ions. Also in this case, the 15C5L' expose the heads to the aqueous phase, and a partial coordination with Mn^{2+} cations is observed at low concentrations. Increasing the concentration, once again, as already observed for the corresponding models with magnesium, we observe only a slight coordination with manganese ions despite the fact that all 15C5L' molecules kept the extended conformation; rather we can see consistent electrostatic interactions between the POPC NH^{3+} groups and the 15C5L'ether heads.

Finally, in presence of $CaCl_2$, we can observe strong and evident calcium-crown coordination both at low and high concentration of 15C5L' (($[X_{15C5L'}]$ =0.05M, 0.25 M). This different behavior is due both the calcium ions capability to break the shell of solvation, and to the fact that the crown lipid is more likely to expose the large polar heads in contact with the solvent. Moreover, the evident coordination does not seem to affect too much the parameters of the membrane, since them *area per lipid* and a membrane thickness values of the membrane in the models with calcium are comparable with the values calculated for models containing the other salts.

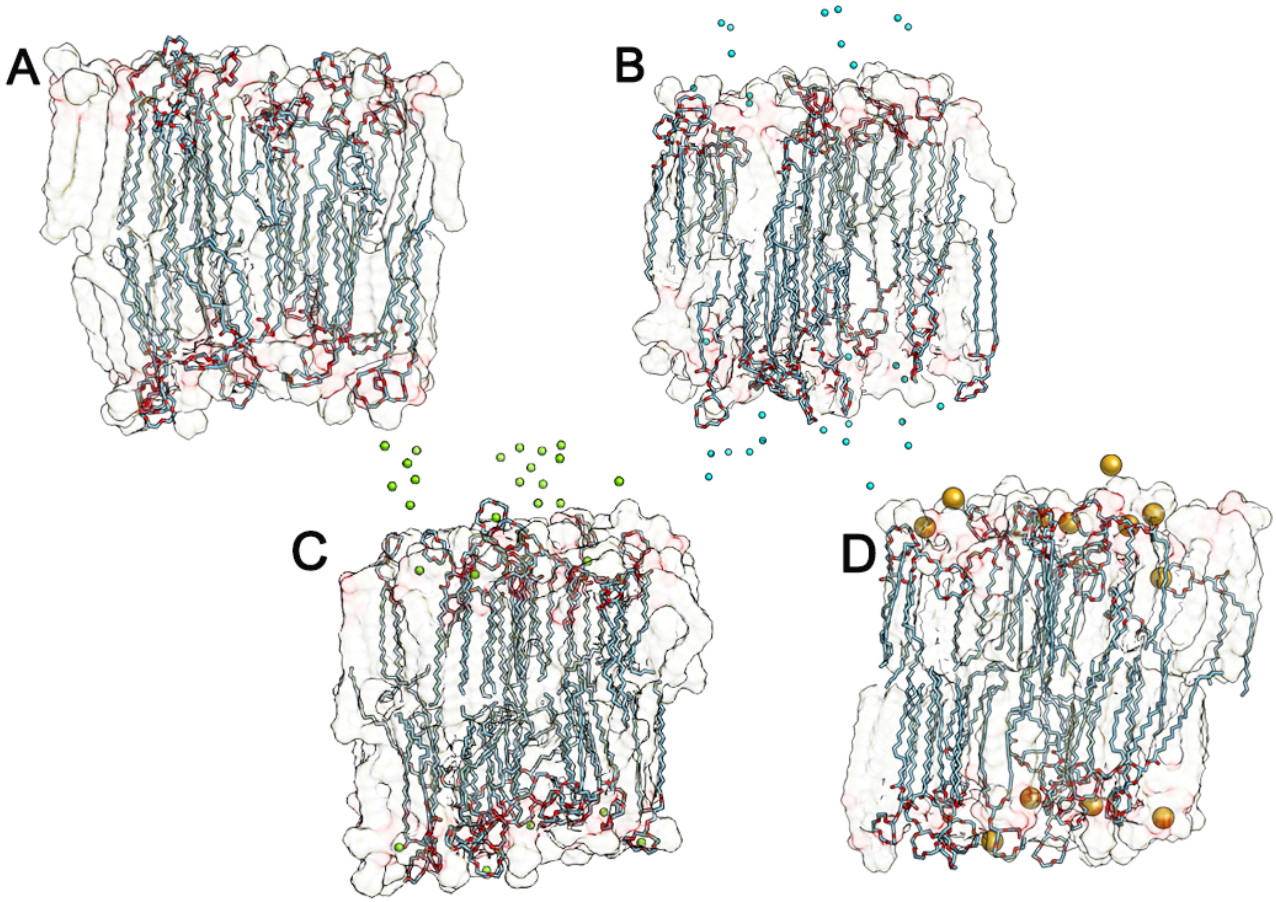

Figure 20: representative structures of steady states of 15C5L'-POPC molecular model. A) shows the bilayer system simulations in pure water, B) with $MgCl_2$, C) with $MnCl_2$ and D) with $CaCl_2$

Crown-ether **12C4L**

12C4L has a flexible linker and a four-oxygen atoms crown-head and this structure gives to the molecules an intrinsic flexibility (Figure 22).

At low concentration ($[X_{12C4L}]$ =0.05M) without salts, the overall system is rigid, with chains stretched, and such behavior influences the 12C4L arrangement, since its chains are kept rigid and straight, while the heads are folded towards inside the bilayer thanks the presence of the flexible linker. Increasing concentration ($[X_{12C4L}]$ =0.25M), we confirm the already observed effect of lipid matrix. Thus, in POPC models we found a more rigid structure, and 12C4L molecules presents both extended and folded conformations (Figure 22).

In presence of $MgCl_2$, there are no substantial differences with the pure water one both at low and high 12C4L concentration ($[X_{12C4L}]$ =0.05 and 0.25 M).

In the presence of $MnCl_2$, we do not find great changes; indeed, it appears to be a slight electrostatic effect of the salts, for this reason, the overall system has a greater order. We do not observe any coordination between Mn^{2+} ions and the heads of 12C4L molecules.

In the $CaCl_2$ model, instead, is evident the ability of cations to break the shell of solvation and move close to the leaflets. However, also in this case, we can observe any coordination between the Ca^{2+} ions and the polar heads of the 12C4L molecules. The increasing of 12C4L concentration ($[X_{12C4L}]$ =0.25M) does not seem to promote coordination. This behavior can be strongly relate to the small dimension of the crown rings.

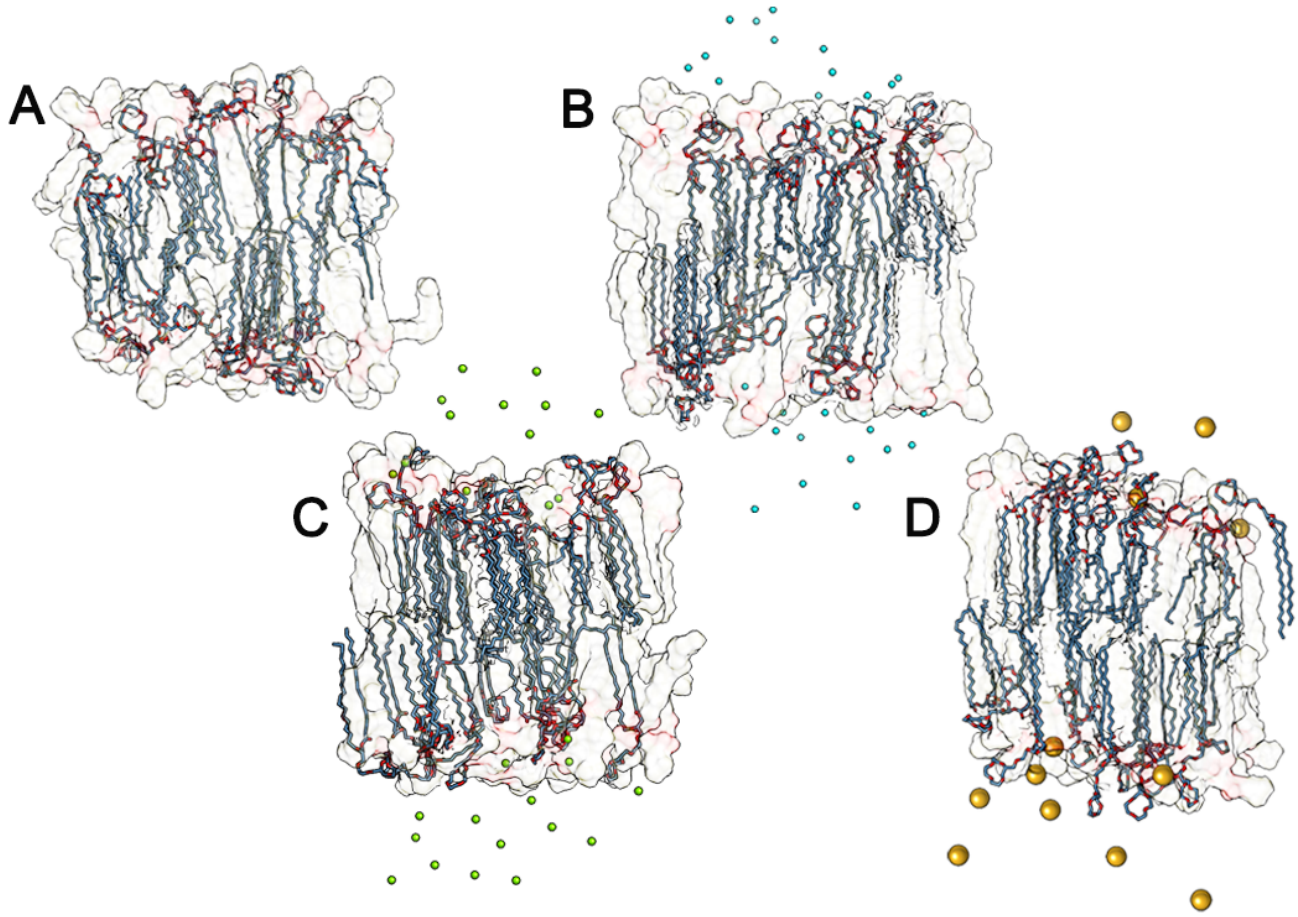

Figure 21: representative structures of steady states of 12C4L-POPCmolecular model. A) shows the bilayer system simulations in pure water, B) with $MgCl_2$, C) with $MnCl_2$ and D) with $CaCl_2$

Crown-ether **12C4L'**

In 12C4L', the crown ring is smaller respect the 15C5L and 15C5L' compounds, bearing four oxygen atoms but the same short linker as 15CL' is present. Consequently, it has overall a smaller structure. In pure water and low concentration ($[X_{12C4L'}]$ =0.05M), the molecules are strongly folded inside the bilayer. Increasing the concentration ($[X_{12C4L'}]$ =0.25M) of the crown ether, we do not observe

significant differences: in fact, the molecules are rigidly fold in the middle lipids' leaflets and shows a prevalence of hydrophobic interactions.

In presence of $MgCl_2$, we note different behavior. At low concentration ($[X_{12C4L'}]$ =0.05M), although the molecules keep their heads inside lipid core, some 12C4L' molecules interact with the Mg^{2+} ions, even if the cation still remains strongly solvated in the aqueous phase. As consequence, the crown ether assumes an extended conformation allowing exposure of the heads. The overall resulting structure is very order, as can be seen in Figure 23. Increasing the concentration, the coordination disappears and we observe instead the onset of hydrophobic interactions between the molecule chains, which prevent the molecules to expose the heads due to rigidity of the structure.

Changing the salt with $MnCl_2$, at lower concentration ($[X_{12C4L'}]$ =0.05M) we observe once again the prevalence of hydrophobic interactions between the crown lipid and POPC: Mn^{2+} ions are keep far from the crown-heads. Increasing concentration ($[X_{12C4L'}]$ =0.25M), we find a major exposure to the solvent of the crown heads but still we cannot observe any coordination with cations (Figure 23).

Finally, in the presence of $CaCl_2$, despite the tendency of calcium ions to approach the surface of the leaflet, we find no coordination with 12C4L'; increasing the concentration ($[X_{12C4L'}]$ = 0.25M) of the crown ether, no particular changes are observed, even if 12C4L' lipids expose their polar heads in the aqueous bilayers phase.

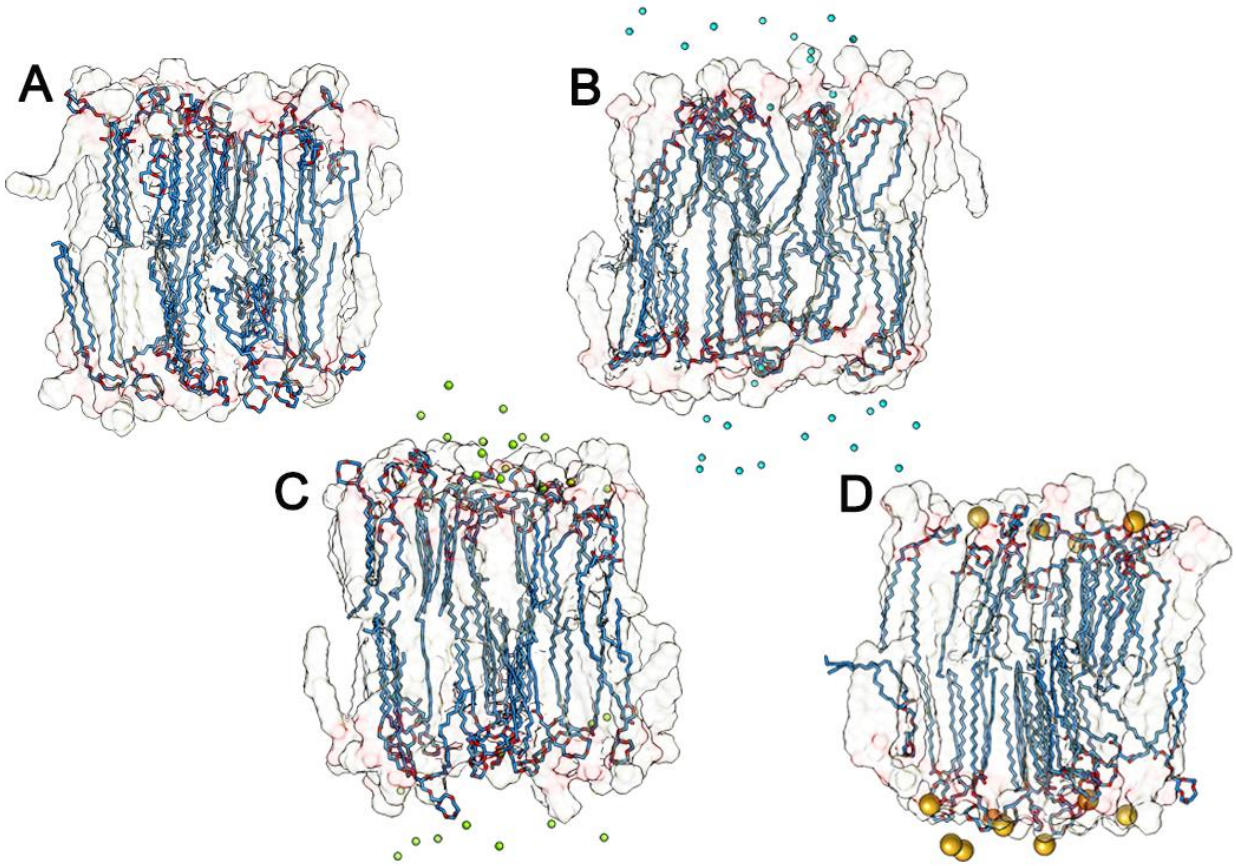

Figure 22: representative structures of steady states of 12C4L'-POPC molecular model. A) shows the bilayer system simulations in pure water, B) with $MgCl_2$, C) with $MnCl_2$ and D) with $CaCl_2$

Components	**12C4L**	**12C4L'**	**15C5L**	**15CL'**
Pure water	0.67 nm^2	0.64 nm^2	0.64 nm^2	0.63 nm^2
$CaCl_2$	0.60 nm^2	0.60 nm^2	0.61 nm^2	0.60 nm^2
$MgCl_2$	0.62 nm^2	0.63 nm^2	0.62 nm^2	0.62 nm^2
$MnCl_2$	0.63 nm^2	0.64 nm^2	0.63 nm^2	0.64 nm^2

Figure 23. Average computed *area per lipid* values (in nm^2) of all studied models

4.3.2 MD PROTOCOL VALIDATION: ANTIOXIDANT SYNTHETIC NITROXIDES (NOX)

Nitroxide radicals are known to have protective activity against oxidative processes in different media and under different stress conditions. In the overall strategy to incorporate the antioxidant compound inside the liposome, we synthesized five compounds (NOXs) having a pyrroline nitroxide linked to a cholesterol unit (chol-no) or to glycerol esterified with one (og-NO and og-l-NO) or two oleoyl moieties (dog-NO and dog-l-NO). Two of the NOXs have a polar spacer group between nitroxide moiety and the non polar lipophilic region (og-l-NO and dog-l-NO). We investigated *in silico* the conformational and dynamic structural behavior of these five liponitroxides in lipid bilayers, and we compared the calculated results with experimental EPR studies aimed to point out the depth of insertion of each nitroxide mojety.

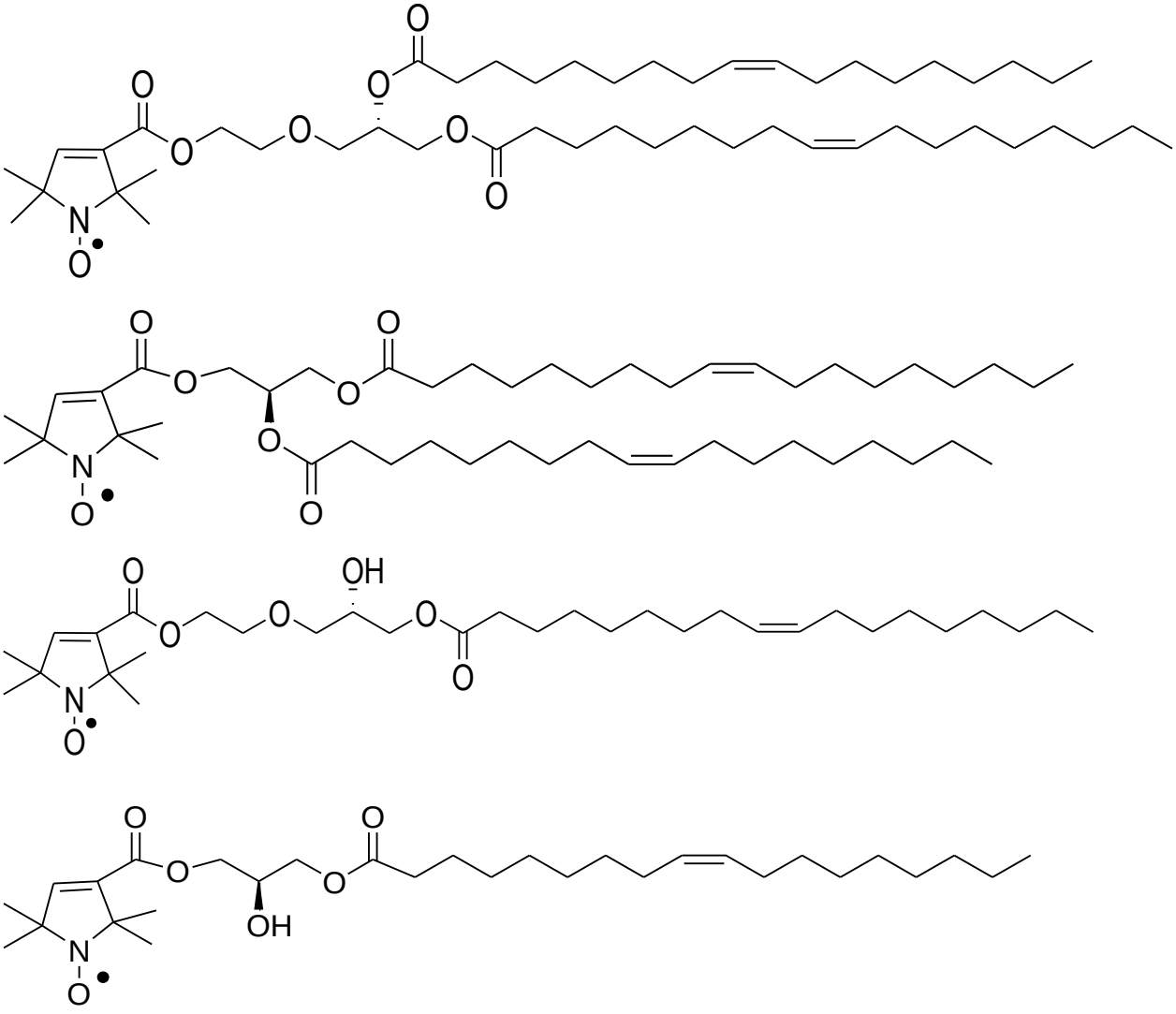

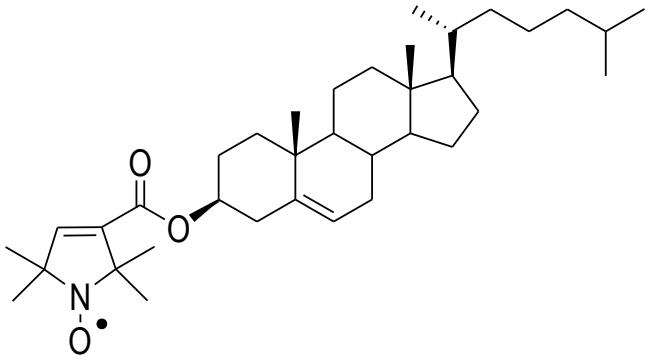

Figure 24: liponotroxides structural formula.
24A) Dog-l-NO, **24B)** Dg-NO, **24C)** Og-l-NO, **24D)** Og-NO **24E)** Chol-NO

The model membrane bilayer consists of 128 fully hydrated lipids in mixed composition; more in detail the model contains phosphatidylcholine lipids (98%) and liponitroxides (2%) that we have inserted by substituting randomly the pre-equilibrated PC molecules. We have appropriately hydrated the simulation models by adding water (TIP3P model) and NaCl (2 mM). We extended the AMBER force-field parameters to provide an accurate description of large and flexible nitroxide free-radicals, including new atom types fitted based on geometries, vibrational frequencies and potential energy surfaces computed at the DFT level [100]. These systems underwent a 100 ns atomistic MD simulation using GROMACS 5.0 in NPT ensemble at 310 K. As a result, the liponitroxide depth inside the bilayer have been determined.

Our settled out protocol, that include also novel compound parametrization, showed a very good correlation with the experimental structural study, and confirms definitively the accuracy of the employed methodology. In details, we find that each liponitroxide locates the nitro moiety at different depths inside lipid membrane, because of the different chemical structures, and we found a correlation between their penetration depth within bilayer and their antioxidant activity.

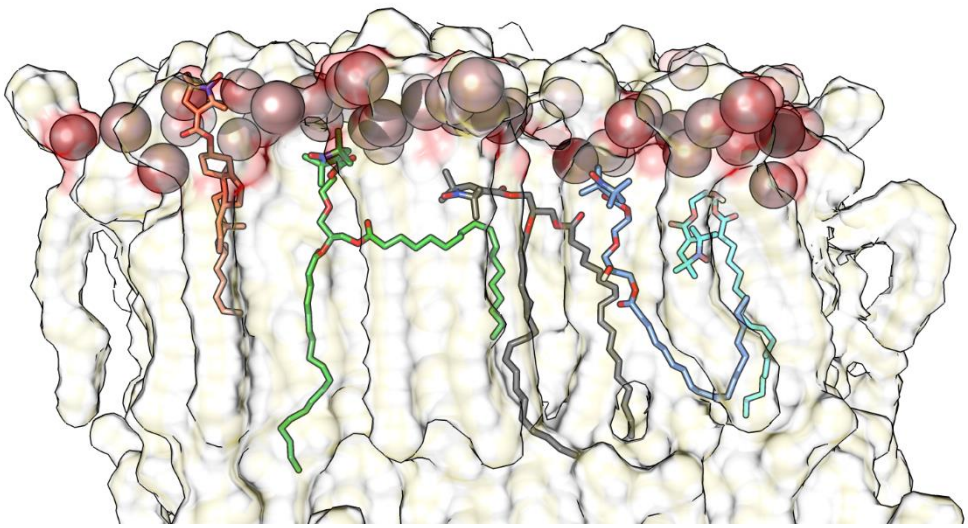

Figure 25: Average steady state structure of liponitroxides (NOXs) in membrane. We highlighted

Col-NO (orange), Dog-l-NO (green), Dog-NO (black), Og-l-NO (blue), Og-NO (light blue)

Overall, we observe rearrangement of NOXs (liponitroxides) in lipid medium through MD simulations, monitoring the position of the nitro group of each NOX studied. We also report the mass density profiles of each compound, and we note that the depth of insertion that we obtain with EPR studies and those observed with MD trajectories are very close between them.

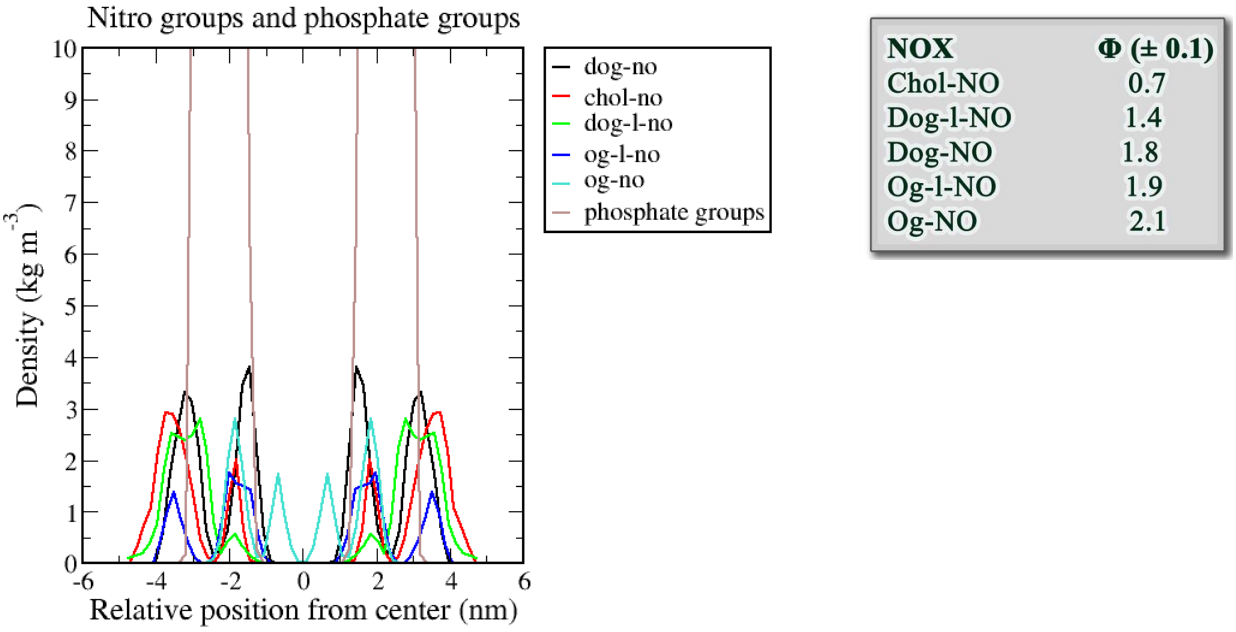

Figure 26: Mass density profile of nitro groups (left) and depth of insertion determined by EPR study (right)

5. DESIGN AND DEVELOPMENT OF LIPOSOMAL NANOVECTORS WITH ANTIOXIDANT ACTIVITY

The real aim of this thesis work is to create a liposomal vector able to deliver efficiently an antioxidant molecule in the eye. Following the previous described strategy (aimed to the direct incorporation of antioxidant compound inside the bilayer, we simulated a lipid derivative of a chosen antioxidant molecule. Is very important that the functionalization does not influence the antioxidant properties of active compound in liposomes. In this way, we will create an efficient system for drug delivery, able to retain the antioxidant activity of the active principle and to increase the bioavailability of molecule in its target site without inducing toxicity processes.

5.1 ANTIOXIDANT COMPOUND: EDARAVONE DERIVATIVE

Edaravone (3-methyl-1-(pyridin-2-yl)-5-pyrazolone) is a nootropic and neuroprotective agent; it's used for the purpose of aiding neurological recovery following acute brain ischemia and subsequent cerebral infarction [57]. It acts as a potent antioxidant and strongly scavenges free radicals, protecting against oxidative stress and neuronal apoptosis [59][60][61].

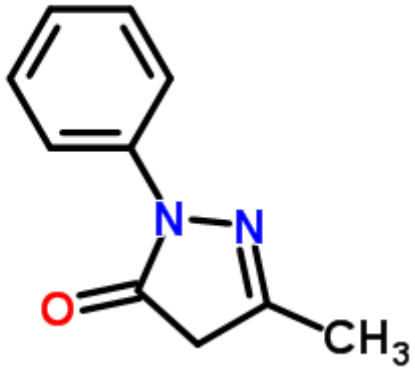

Figure 27: Edaravone structure

Edaravone (EDR) has been shown to attenuate methamphetamine- and 6-OHDA-induced dopaminergic neurotoxicity in the striatum and *substantia nigra*, and does not affect methamphetamine-induced dopamine release or hyperthermia[62][63]. It has also been demonstrated to protect against MPTP-mediated dopaminergic neurotoxicity to the *substantia nigra*, though notably not to the striatum[64][65][66].

Edaravone (EDR) is an efficient antioxidant already used in many application fields; through its enol form, EDR interacts with the peroxyl radical (LOO·) and hydroxyl (·OH), leading to formation of OPB, that is a stable oxidation product (2-oxo-3phenilidrazon-butanoic acid), through a radical intermediate [67].

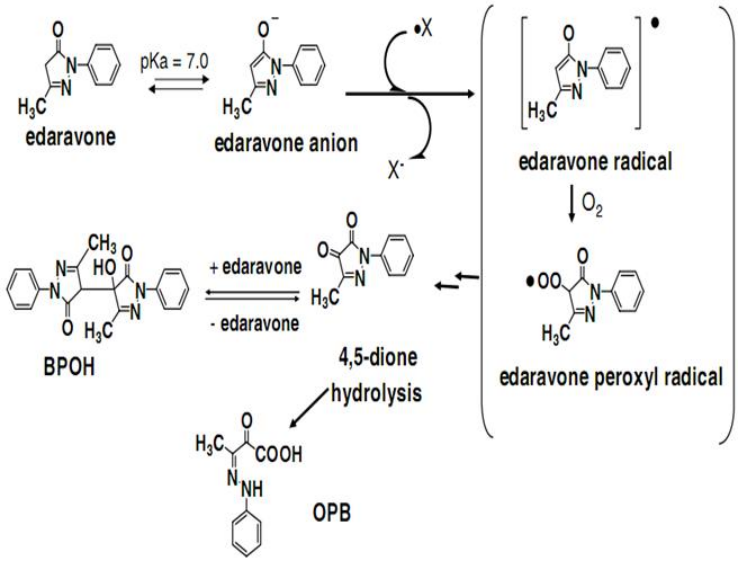

Figure 28: antioxidant mechanism of Edaravone

The amount of the EDR anionic form at equilibrium is important for the scavenging activity. This deprotonated form should be the one active for scavenging of free radicals through an electron transfer mechanism (SET Single Electron Transfer). Studies on oxidation of EDR with AMVN show an increase of the oxidation speed at pH variations.

Indeed, electron density of the pyrazolone ring plays an important role in a monoelectronic oxidation mechanism. Electron-donor substituents can lower the oxidation potential, but at the same time decrease the amount of the anionic form since it stabilize the protonated form due to the increase of the partial negative charge. Conversely, electron-withdrawing substituents can increase the population of the anionic form but also increase oxidation potential. The Edaravone structure seems to allow an optimal balance between oxidation potential and amount of anionic form.

We considered previous DFT studies carried out at B3LYP / 6-31G* level in order to synthesize an EDR derivative that retains its high antioxidant properties, but at same time is more lipophilic to be incorporated into the lipid matrix **[101]**. This approach allow us to work on development of relations SAR (structure-activity relationship) and on prediction the antioxidant activity of EDR and its derivatives. In particular, energy (E), ionization potential (IP), bond dissociation energy (BDE) and stabilization energies (ΔE (iso) have been evaluated.

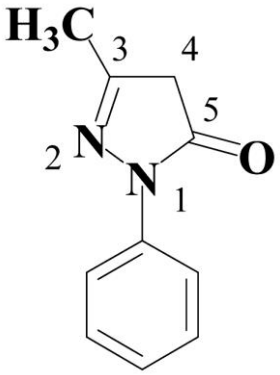

Figure 23: numbering of EDR functionalization sites

As results, the electron abstraction is favored by electron-donating groups at position 3, since they decrease the ionization potential when compared to substitution at position 4. The hydrogen abstraction is favored by electron-withdrawing groups at position 4, since they decrease the bound dissociation energy (BDE) when compared to other substitutions, resulting in a better antioxidant activity. In addition, other studies show that the best strategy is a functionalization [65, 101].

Analyzing the results obtained in these studies, we chose to introduce in 4 position a lipophilic group containing a C18 moiety (namely EDR-C18). Since this derivate could be suitable to be incorporated in liposomal carrier.

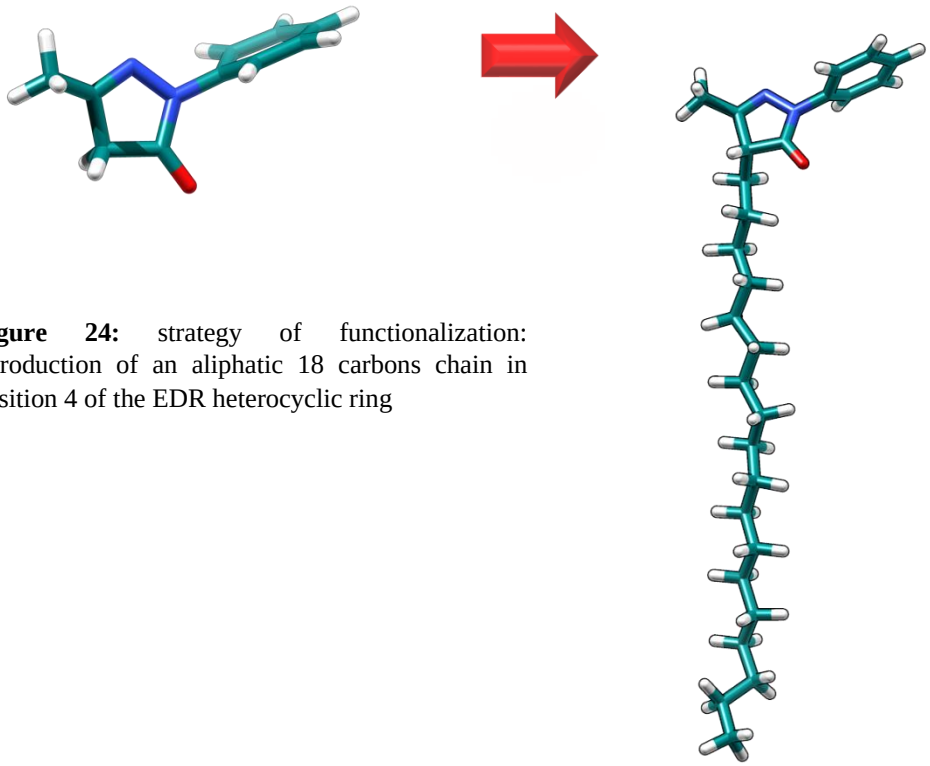

Figure 24: strategy of functionalization: introduction of an aliphatic 18 carbons chain in position 4 of the EDR heterocyclic ring

5.2 MODELING OF THE MIXED MEMBRANE SYSTEMS

We use Macromodel suite implemented in Maestro Molecular Modeling software package to build the tridimensional model of EDR-C18. The representative structures underwent a rigid conformational search through Replica Exchange Molecular Dynamics: the method consists in running N copies of the system, randomly initialized, at different temperatures. Then, based on the Metropolis criterion, it exchanges configurations at different temperatures. It results in a very robust ensemble, which is able to sample both lowest and highest energy configurations. In this way, thermo-dynamical properties such as the specific heat, which is not generally well compute in the canonical ensemble, can be compute with great precision. With the purpose of inserting the representative structures in lipid bilayers, we prepared and properly equilibrated with a model membrane containing EDR-C18 in a POPC matrix. POPC, EDR-C18 following the Klauda procedure: the membrane pure POPC (128 lipids) was equilibrated under NPT condition at a temperature of 303.00 K for a total run time of 50 ns; Randomly POPC molecules were then substituted with EDR-C18 taking into account for the experimental concentration of the synthetic lipids. We built lipid bilayer models in pure water and in presence of salts that are commonly use in ophthalmic formulations (NaCl, $MgCl_2$, KCl and $CaCl_2$) in order to evaluate the eventual salt effect in stabilization of the bilayer structures.
Then, for each system, we carried out MD 100 ns trajectories under the same conditions that we previously described (see Chapter 4).

5.3 MD SIMULATION ANALYSIS

We deeply analyzed the MD trajectories and calculated the three main parameters for assessing the bilayer and specific neo-synthetized lipids equilibration: RMSD, *Area per lipid* and membrane thickness. We observed that each simulated model reaches easily the steady state and in particular the RMSD (RMSF) fluctuations are very slight in the last 30 ns.
The root-mean-square deviation (RMSD) is the measure of the average distance between two or more equal atoms of superimposed structures. In MD simulations, this calculation is applied to a trajectory of (usually) thousands of frames, so RMSD becomes RMSF (root-mean-square fluctuation). In this study, we calculated the RMSD for all heavy atoms of synthetic lipids (EDR-C18). The parameter A (*Area per lipid*) reported is the average calculation on the last 10 ns of simulation, the so called "collection phase", and describes the bilayer microstructure with regard to molecular packing. It is the average interfacial *area per lipid* defined in reference to the average hydrocarbon thickness and the hydrocarbon chain volume **[63]**. It is reported in $Å^2$ according to the following equation:

*Area per Lipid= (Box X Lenght) * (Box Y Lenght) / (number of phospholipid per layer)*

The membrane thickness is a measure of the distance between the seats on the two phosphate groups of membrane leaflets. For homogeneous lipid composition systems, the membrane thickness values are determined experimentally and depends on the type of phospholipid and the temperature [64]. In fact, the determination of the membrane thickness can be useful to derive the phase transition temperature; only above this value, the efficiency of the liposomal carrier is sure. In our case, we determine this membrane parameter to evaluate the possibility that the presence of synthetized lipids could modify physical and chemical structure of vector liposomal medium.

POPC-EDR-C18 in water

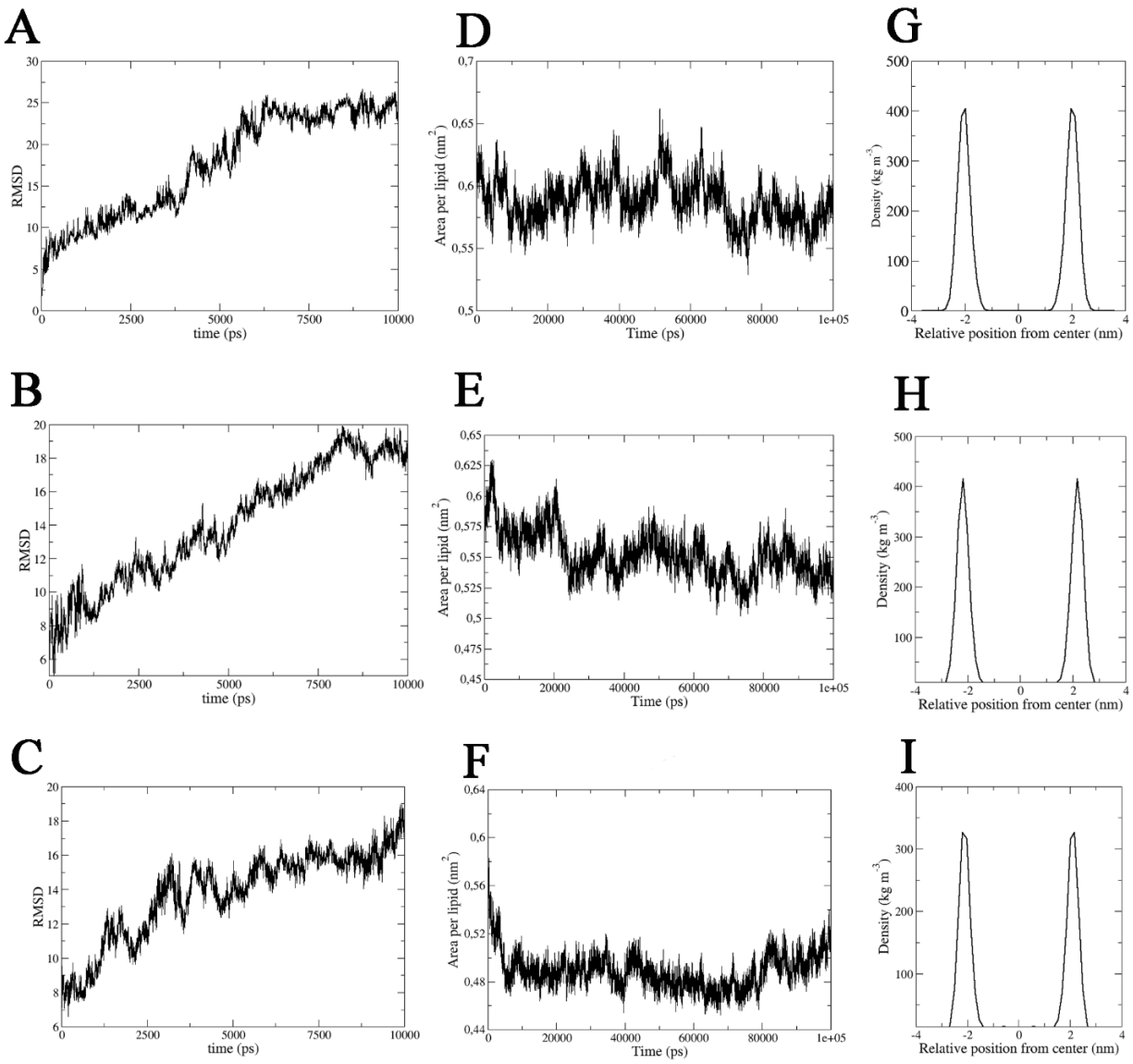

Figure 31: POPC-EDR-C18 in pure water. Tables **A)** EDR-C18 10 %; **B)** EDR-C18 20%; **C)** EDR-C18 40%, show RMSD fluctuation calculated on all heavy atoms of EDR-C18 or the whole 100 ns. Tables **D)** EDR-C18 10 %; **E)** EDR-C18 20%; **F)** EDR-C18 40%, show the *Area per lipid* fluctuation in $Å^2$ on the all MD 100 ns. Tables **G)** EDR-C18 10 %; **H)** EDR-C18 20%; **I)** EDR-C18 40%, show the thickness membrane calculated on the phosphate groups of POPC on the last 20 ns.

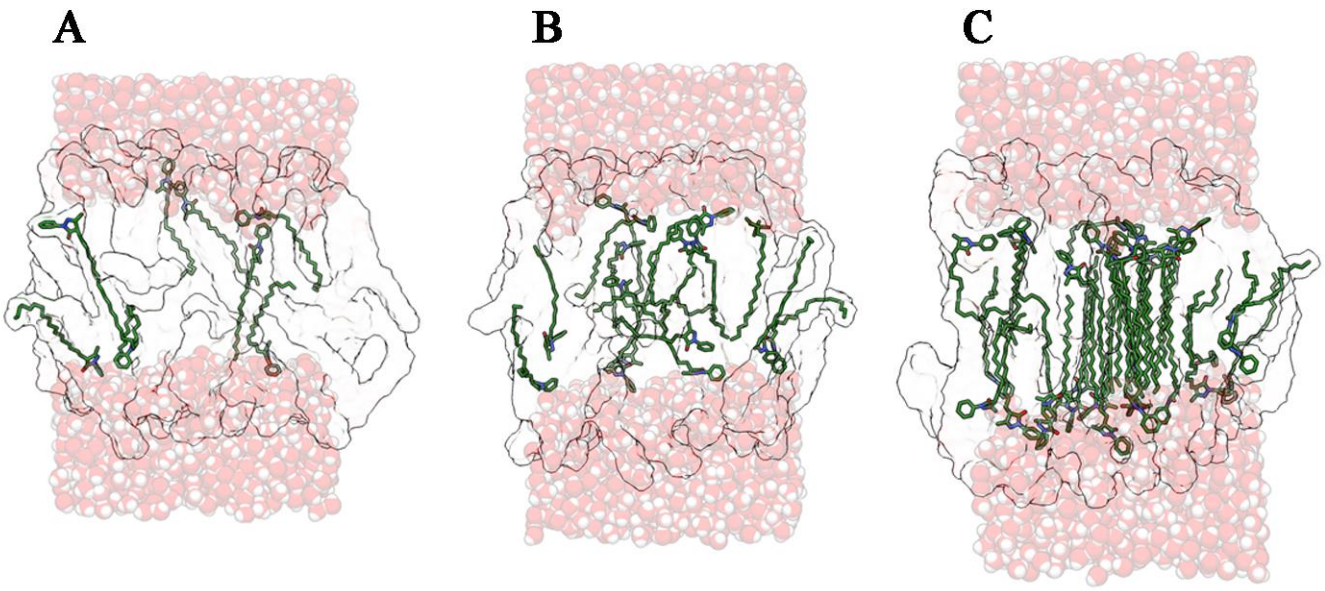

Figure 32: POPC-EDR-C18 in water. **A)** EDR-C18 10% ;**B)** EDR-C18 20%; **C)** EDR-C18 40%; Highlighted in green EDR-C18 carbon atoms, in blue Nitrogen atoms and red Oxygen atoms of EDR-C18 molecules. In transparence, we highlighted water molecules.

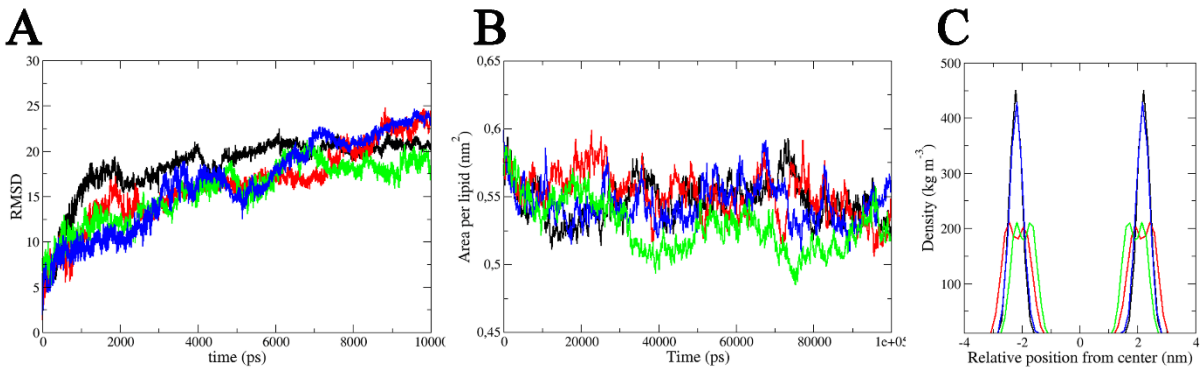

Figure 33: POPC-EDR-C18 at 20% with salts. Tables **A)** show RMSD fluctuation calculated on all heavy atoms of EDR-C18 or the whole 100 ns. Tables **B)** show the Area per lipid fluctuation in $Å^2$ on the all MD 100 ns. Tables **C)** show the mass density membrane calculated on the phosphate groups of POPC on the last 20 ns. In every table we reported in black model with 0.25 M NaCl, in red model with 0.25 M $MgCl_2$, blue model with 0.25 M KCl, in green model with 0.25 M $CaCl_2$

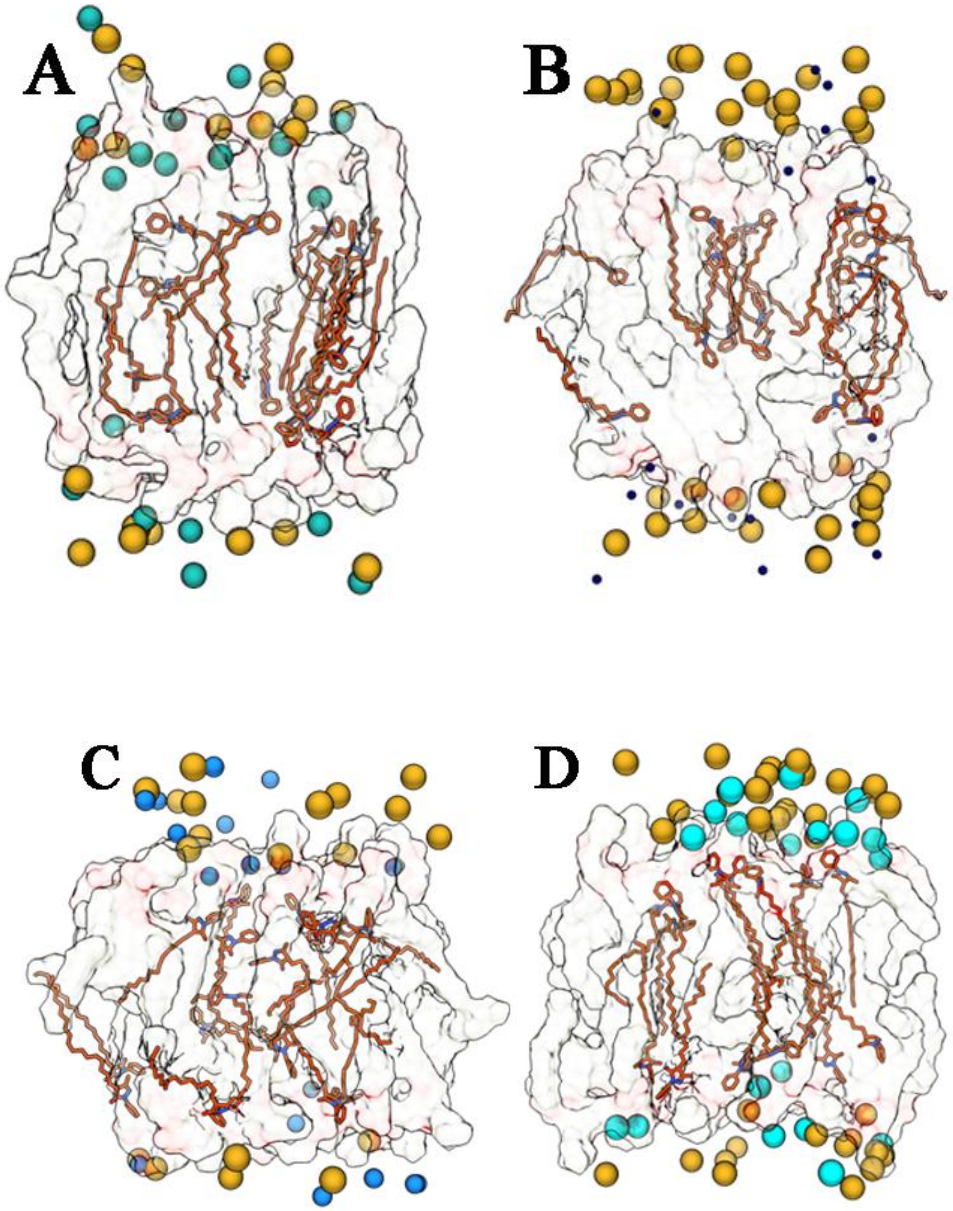

Figure 34: POPC-EDR-C18 in salt solutions. A) with 0.15 M NaCl, B) with 0.15 M $MgCl_2$, C) with 0.15 M KCl, D) with 0.15 M $CaCl_2$. Highlighted in sphere the Na^+ (A in green), Mg^{2+} (B in blue), K^+ (C in light blue), Ca^{2+} (D in cyan) and Cl^- (A, B, C, D in yellow) ions.

5.4 DISCUSSIONS AND CONCLUSIONS

For all models with water in solution, the RMSD data analysis on simulation clearly show that the EDR-C18 molecules reach stability in membrane, but it depends strictly to the synthetic lipid concentration. In particular, we note that in model with 10% of EDR-C18 concentration, the molecules show a great freedom of movement in lipid medium; in fact, some of them operate the *flip flop* phenomena during MD simulations. The *Area per lipid* and membrane thickness values

calculated on last 10 ns (steady state) are respectively 0.58 nm^2 and 4.04 nm. The *Area per lipid* calculation show a little decrease comparing by POPC pure system, and this is due to the EDR-C18 presence. The membrane thickness table shows that the picks are very tight and defined; this means a define dispositions of the phosphate groups, that are all in very orderly way at a determined distance from the center of box.

At 20% of EDR-C18 concentration, we again observe a massive fluidity of EDR derivatives in POPC membrane, with a major trend to expose aromatic heads towards the solvent. This is very important, because the heads of EDR-C18 are responsible of antioxidant activity of molecules. At 10% of concentration, the high movement degree allows a consistent protection against lipid peroxidation. At 20% of concentration, this trend is confirm and a major exposition degree of aromatic heads through solvent is very important for a protection strategy of lacrimal film. *Area per lipid* and membrane thickness values (respectively 0.54 nm^2 and 4.06 nm) confirm that increasing EDR-C18 concentration, we have no substantial modifications on physical-chemical properties of the liposome, that preserve its fluidity, thus confirming the possibility to use this system for EDR-C18 delivery.

Increasing again antioxidant molecules concentration in lipid membrane (40 % of molar ratio), we observe many differences. Analyzing the reported structures, that are representative of the reached steady state, we note an increased rigidity degree. This fact can be ascribed to EDR-C18 high concentration: the resulting overcrowding present in POPC matrix prevents to maintain the fluidity of system. For this reason, we discard this model for our strategy. The *Area per lipid* value is 0.51 nm^2, and membrane thickness is very similar to the first two models, but in this case, the peak is less tight and defined, because the phosphate groups are disposed in a more disordered manner respect to first two studied systems. This means that membrane order and parameters are strongly influence by excess of the EDR-C18 molecules.

From the overall obtained results, we identify the model bilayer containing 20% of EDR-C18 as the most suitable system for going further in our studies. Starting from this model, we create other four molecular systems, introducing in each model 0.25 M of saline concentration. The salts that we chose are NaCl, $MgCl_2$, KCl and $CaCl_2$, because they are already used for ophthalmic formulations **[68, 69]**, and our aim is to test the possible salt effects on EDR-C18 disposition.

After the 100 ns of MD simulations carried out for all models, we token representative structures of the steady states and we studied the salt influence in the bilayer disposition. In fact, is known the salt effect on lipid systems **[7]**, and by our results, we find many influences of salts on the EDR-C18 behavior in lipid medium.

For the system with NaCl, we observe a major order degree of antioxidant molecules respect to the models without salts. We have no relevant variations on lipid membranes, and this salt does not seem

to interact directly with EDR-C18 molecules. In fact, Na^{++} ions lie in solution, but they influence electrostatically the EDR-C18 behavior in membrane increasing the order degree along major axis of membrane model (Fig 34A).

When we add 0.25 M of $MgCl_2$, we observe different situation. In this case, membrane thickness varies so much, because phosphate groups dispose themselves on two different distance planes with respect the center of box (Fig 34B). This can be due to Mg^{++} ions that strongly interact with the phosphate of POPC molecules. As result, the bilayer stretches along the long axis of membrane (z), thus influencing membrane parameters. Even if we do not find direct interactions between cations and EDR-C18 molecules, it results a stretching of membrane, and this indirectly allow the antioxidant compounds to make clusters in the lipid matrix. These results show that the choice of $MgCl_2$ does not improve the tendency to expose aromatic heads of EDR-C18 toward the solvent. On the contrary, the molecules seem to be very blocked, decreasing their fluidity degree.

Adding 0.25 M KCl, we do not find substantial differences respect to starting models without salts; in fact, the EDR-C18 molecules dispose themselves in a very disordered manner. More, *area per lipid* value and membrane thickness did not vary respect to the starting model, and K^+ lies in solution without interaction with EDR-C18 molecules. For all these reasons, the KCl salt seems to be the worst choice for our strategy (Fig 34C).

When we use 0.25 M $CaCl_2$, we obtain very interesting results. Membrane thickness profile shows that we have direct interactions between phosphate groups and Ca^{++} ions, as we seen for model with $MgCl_2$. The *Area per lipid* value decreases respect all models studied before, and observing representative structure of steady state, we noted that EDR-C18 molecules expose clearly the aromatic heads through solvent. This means that area per lipid value decrease due to a major order degree, because antioxidant molecules are disposed along major axis of lipid system. More, this model is the only one in which we observed a direct interaction between Ca^{++} ions and EDR-C18 compounds. Analyzing structure figure we note that metal ions are arrange very close to leaflets, because they are able to broke the solvation shell and move themselves near the polar groups of lipid medium, as confirmed by literature data **[68]**. This means that Calcium ions are able to make direct interactions (cation-π) with EDR-C18 and ionic interactions with phosphate groups of POPC (Fig 34D). Antioxidant compounds compete with phospholipid molecules to interact with Ca^{++} ions, for this reason, our functionalized lipid molecules expose the heads. This is very important for our strategy, because the head of EDR-C18 is the component that solve antioxidant activity. Adding 0.25 M $CaCl_2$, we obtain a stable system that facilitates the exposure of antioxidant heads, favoring an opportune shield activity for lacrimal film.

The subsequent step has been the evaluation of EDR-C18 liposomes antioxidant activity. We started for EDR-C18 derivative and we found that this compound does not lose its antioxidant activity after functionalization, and that this molecule is very stable in liposomal system.

To this purpose, in our laboratories it has been carried out studies to determine the EDR-C18 scavenging ability. More, we compared scavenging activity of Edaravone derivative with vitamin E, Trolox and Edaravone, and we observed that EDR-C18 not only retains an high scavenging activity but it is more scavenger than vitamin E, thus confirming that this compound is a good choice for the development of an efficient antioxidant liposomal carrier.

$$\text{Scavenging ability} = \frac{\text{A in absence of compound} - \text{A in presence of compound}}{\text{A in absence of compound}} \text{ x}$$

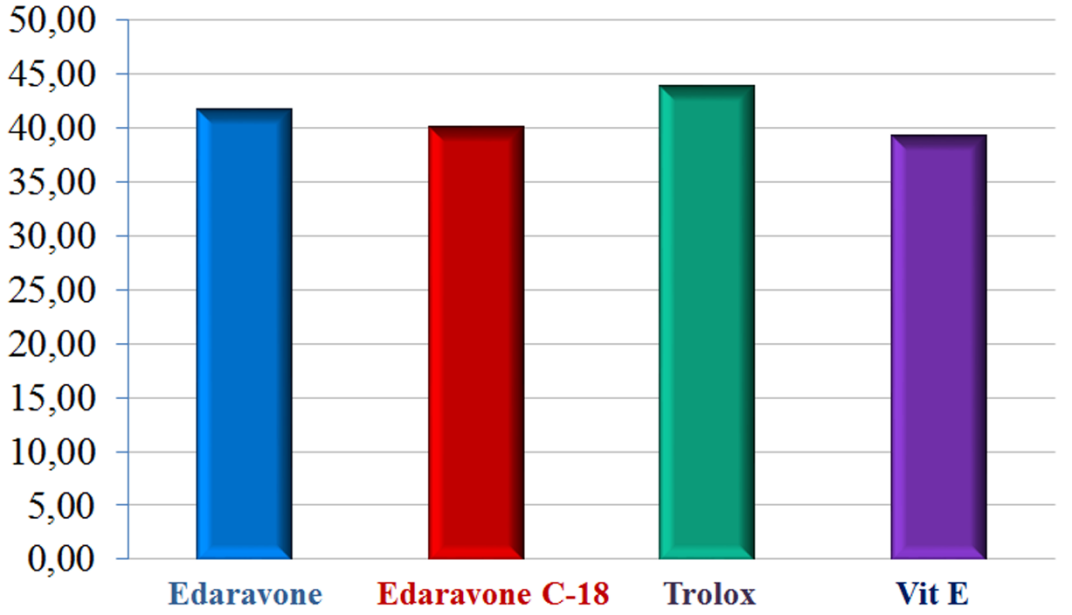

Figure 35: scavenging activity of Edaravone, Edaravone C-18, Trolox and E vitamin

Finally, we studied the salt effect to verify the possibility to modify the natural behavior of this functionalized lipid in membrane. Other studies are underway to determine the toxicity of these systems on retinal and corneal cellular lines.

6. OTHER ANTIOXIDANT NANOVECTORS: PHYTOSOMES

Following our purpose of creating an efficient ophthalmic liposomal vector with a strong antioxidant activity, we focalized our attention to another strong natural antioxidant: Epigallocatechin3-Gallate (EGCG). It is a powerful antioxidant, which includes a benzenediol ring (label A) joined to a tetrahydropyran moiety (C), a pyrogallol ring (B) and a galloyl ring (D) (Figure 36).

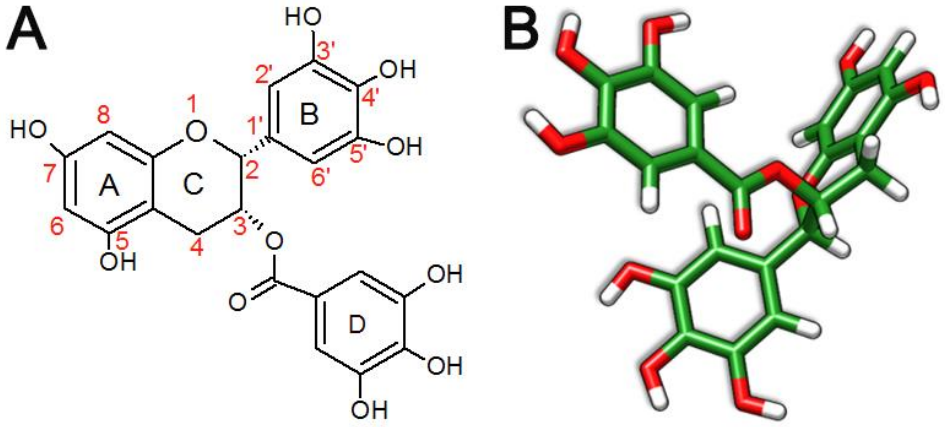

Figure 36: Epigallo Catechin 3-Gallate structure.
36A shows 2D structure, 36B shows 3 D structure

EGCG is the most abundant catechin in green tea and accounts for 55 up to 79 % of the total catechin content. The radical scavenging activities of tea catechins have been examined in numerous *in vitro* experiments showing them to be efficient scavengers of singlet oxygen ($^1O_2$), superoxide radicals ($O^{\cdot-}_2$), hydroxyl and peroxyl radicals. In most of the studies, EGCG is more efficient than the other catechins. Especially on pathologies accompanied by oxidative stress like inflammation, cancer or infections, it is note that especially the galloylated catechins exhibit higher antioxidant potential than other antioxidants like ascorbic acid and tocopherol. Furthermore, EGCG is a weak acid with a pKa value of 7.99. This is an important property as deprotonation is the first step towards autoxidation to dimeric and polymeric structures. Consequently, it became object of several *in silico* and *in vivo* studies that investigate its potential health benefits.

As shown by several scientific groups, the biological effects of EGCG do not just derive from its potential to scavenge radicals and by this to reduce the oxidative stress. EGCG is capable of interacting with proteins, enzymes and DNA/RNA, for example MAP kinases, phosphatases, DNA methyltransferase, topoisomerases and many others. As consequence, it induces apoptosis of cells, arrests cell cycle and modulates cell signaling, and in this way exhibits its pharmacological effects. The list of investigated health benefits and/or pharmacological effects is long, and some of these are here reported: antibacterial [72, 73], anticancer [74, 75], anticholesterol [76, 77, 78], antineurodegenerative

[79], antitoxin [72], and antiviral [80] effects. EGCG represents the most abundant and powerful antioxidant present in green tea [78], but, due to its high solubility and reactivity, the Epigallocatechin 3-Gallate powders are easily oxidized and unstable, and hence, difficult to be used as medicine or as natural food additive [81]. For these reason, we want to create a stable and efficient system to deliver the EGCG molecules, at the aim to improve the bioavailability of molecule that reaches its specific biologic target.

First, we started with the applications of our functionalization strategy to create a lipophilic derivative of EGCG without loose of its antioxidant potential. Thus, we evaluated the possibility to functionalize this polyphenol, to reduce its high solubility and then to make it more lipophilic, but many studies present in literature prove that EGCG has itself great affinity with lipid bilayers cell membranes. In fact, EGCG, as catechins in general, interacts strongly with the bilayer, binding to the lipid head groups near the bilayer surface (adsorption). After absorption into the bilayer occurred, all catechins caused a lateral expansion in the bilayer below the phosphate groups of the lipid chains. These observations suggest that the aggregated molecules are absorbed more slowly inside the bilayer [84]. The qualitative and quantitative nature of the molecular interactions of flavonoids inside cell membranes associated to their biological activities remains, largely undefined [84, 85, 86]. Recent experimental studies have shown EGCG induced rupture of giant vesicles by binding to their membrane surface [87].

The dynamics of the interactions of the catechins with the lipid bilayers are interpreted in terms of hydrogen bonding and adsorption/absorption phenomena to the lipid bilayer, as influenced by the phenolic hydroxyl and gallate groups associated with the catechin ring structures. Two possible relevant interactions are: (a) the partitioning of the polyphenol in the non-polar core of the membrane, associated with the hydrophobic nature of the flavonoid; and (b) the interaction of the hydrophilic flavonoids and oligomers with the polar head groups of lipids at the lipid–water interface, mainly associated with the formation of hydrogen bonds. In fact, flavonoids can vary in their number and distribution of hydroxyl groups, key points of interaction between the polyphenols and the membrane surface at the water–lipid interface through the formation of hydrogen bonds. Using a phosphatidylcholine-coated HPLC column, many studies showed that the surface interaction (measured as the retention delay) between eight different flavonoids and the phospholipid was positively correlated with the number of hydroxyl groups in the compounds [88].

Both *in vitro* and *in vivo*, the polyphenols have a well-recognized antioxidant capacity. It is possible to attribute this antioxidant activity mainly to their capacity to scavenge oxygen and nitrogen active species and to chelate redox-active metals. The relevant chemical characteristics that contribute to the flavonoids' antioxidant/oxidants scavenging activity are: (a) the 30, 40 hydroxyl (catechol) groups

in the Bring, (b) the 2, 3 double bond in conjugation with a 4-oxo group in the C ring, and (c) the presence of hydroxyl groups in positions 3 and 5. The interaction of polyphenols with bilayers could be a relevant mechanism in the protection by flavonoids of membrane oxidation. For flavonoids, the partition in the non-polar region of the bilayer, and their antioxidant activity can be attributed to both their capacity to interact with free radicals and (similarly to vitamin E) to inhibit the propagation of lipid oxidation or, by increasing membrane fluidity.

These studies show clearly that has the basis of any effect began with the direct interaction with membranes. For these reason, we decided to consider the EGCG as it is with no functionalization. When a natural molecule spontaneously interacts with phospholipid system, we have a lipid carrier named phytosome. Moreover, for conventional pharmacology, the drug's interactions with lipid bilayer membranes is fundamental to optimize its ability to reach intracellular targets. Therefore, biophysical and biochemical investigations of drug–membrane interactions have always been of interest in Drug Design. The possible modes of action are not necessarily exclusive, and it is likely that some drugs have multiple concomitant effects [86]. Molecular dynamics (MD) simulations have been widely used to study drug–membrane systems: both to capture interaction details on the molecular scale, and to extract thermodynamic properties that are directly comparable to complementary analytical measurements. The MD simulations are particularly suited to study such systems owing to the ability of the method to quantify non-covalent interactions of the magnitude of thermal energy, which often determine the evolution and assembly of soft systems such as lipid bilayers. In this section, we focus on the interactions between natural plants extracts used as drugs with lipid bilayers, focusing particularly on EGCG as antioxidant molecule that has a wide range of biological activities. We remark the emphasis on the biophysics of the effects of EGCG on membranes, rather than on pharmacological properties such as improved bioavailability in the cell.

6.1 INTERACTIONS OF EGCG WITH BILAYER

Plants and plant extracts have been use in traditional medicine in various parts of the world for centuries. Plant extracts have played and still play a major role in modern medicine [90, 91]. Using our simulations protocol, before investigation the behavior of EGCG molecules within the bilayer lipids, we studied EGCG property to aggregate, catting out MD simulation of five EGCG molecules randomly disposed in a solvation box containing 7043 TIP3P water molecules. We want to observe the eventual self-association of these catechins in solution. This peculiar behavior of polyphenols is well known in the literature, and many papers can be found investigating the surface active drugs

(e.g. antibiotics, benzodiazepine, local anesthetics), their self-assembly and resulting modulation of physicochemical properties like chemical stability.

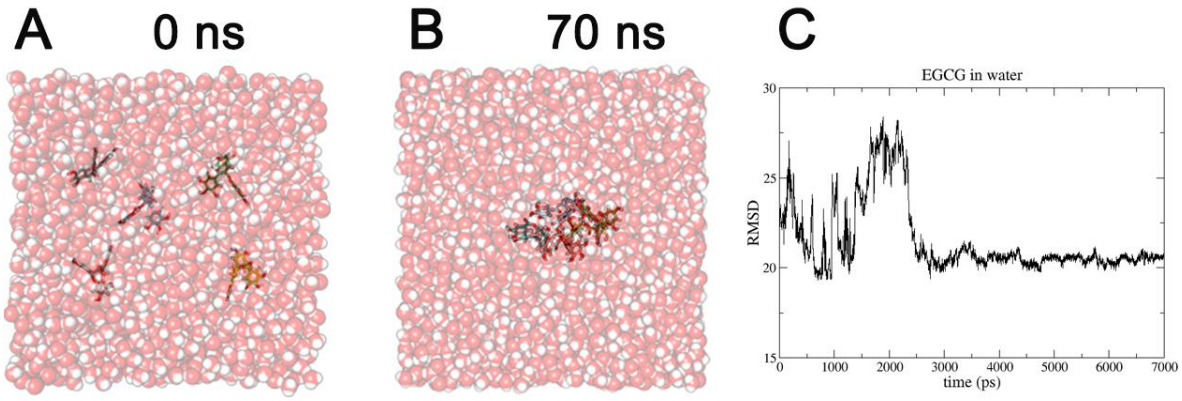

Figure 37= five EGCG molecules in a solvation box. 37A shows the EGCG disposition at the beginning of molecular dynamics; 37B is a representative structure of steady state of the model; 37C shows the root-mean-square deviation (RMSD) of EGCG atoms along molecular dynamics.

Regarding this starting model, we carried out 70 ns of MD simulations at 310 K using Periodic Boundary Conditions (PBC) and TIP3P water model; in the figure 37, we note that after only 30 ns, the catechin molecules tend to create a unique and vary stable aggregate, stabilized by strong intermolecular aromatic interactions and H-bonds between EGCG molecules that compete with the H-bonds of solvent.

Then, we carried out molecular dynamics simulations starting by a pure POPC lipid model in a box with dimensions x=5.638 nm, y=5.486 nm and z= 7.778 nm. We added TIP3P water molecules and EGCG molecules presents in aqueous phase of bilayer. In particular, we started for five EGCG molecules aggregate obtained by first MD simulation in water. The simulation model contains 80 POPC molecules and 4006 TIP3P water molecules, and EGCG aggregate in the water phase. We carried out 250 ns MD simulations, and we evaluated RMSD values of EGCGs and membrane parameters, such as *"area per lipid"* and membrane thickness. Our aim is to verify the effective capacity of EGCG molecules to interact with the bilayer and quantify the encapsulation degree of EGCG in POPC system. The parameters of membrane are necessary to verify that the EGCG presence does not influence POPC system. This is very important, because we want to create a stable and efficient lipid vector able to deliver antioxidant molecules at their biological target, and then our carrier has to retain its properties, such true fluidity and dimensions.

For purpose of comparison, we choose another natural product, to verify the specificity of interactions about different class of molecules, and we carried out MD simulation in the same conditions considering this other antioxidant compound. We have choose Morelloflavone, which is a bioactive

biflavonoid from *Garcinia dulcis*. It is a traditional herb medicine belonging to *Guttiferae* family and it has significant antioxidant, antiviral and anti-inflammatory properties [94].

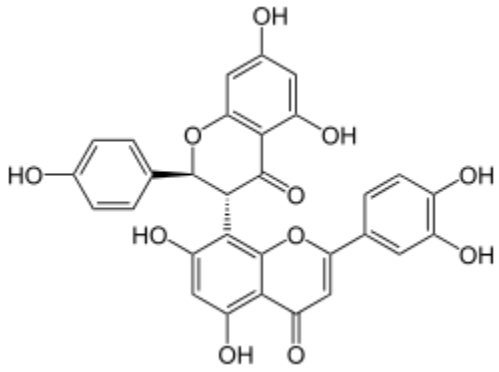

Figure 38: Morelloflavone structural formula

In literature, it results that Morelloflavone is a component of a class of flavonoids molecule that does not create phytosomes. This means that it does not interact with bilayer membrane, and rests in solution [89]. Like for EGCG simulations, we started by a previous model of five Morelloflavone molecules in a water box of simulation. We obtained an aggregate that we have used for next MD investigations considering the phospholipid system. We carried out 250 ns of molecular dynamics for both natural products, using the same simulation protocol (80 POPC and 4006 TIP3P water molecules) i. e. (first phases of equilibration in NVT and 250 ns of MD simulations in NPT at 310 K). We monitored the structures of both systems along MD trajectories, to observe the behavior of natural products and the variations of membrane parameters.

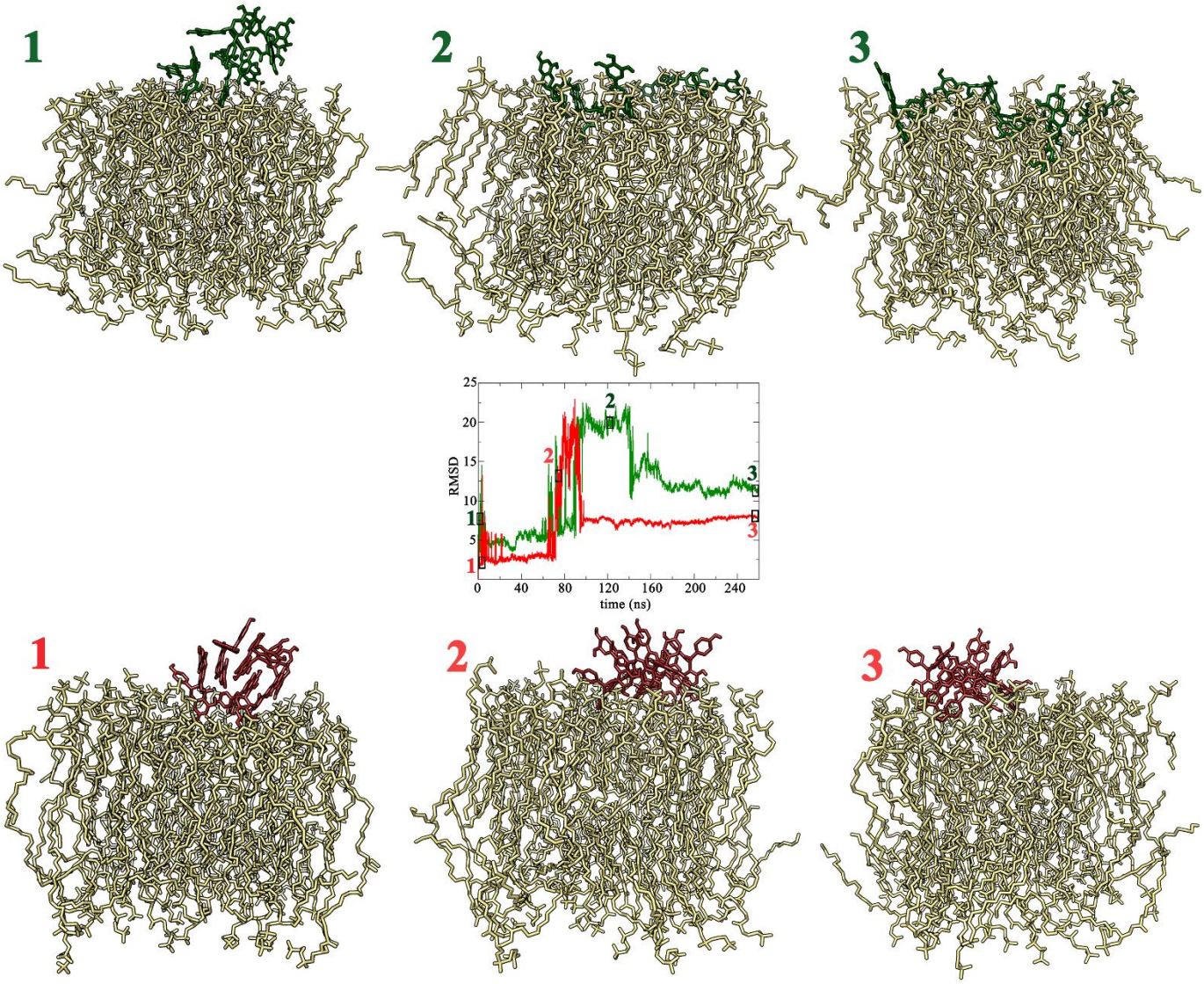

Figure 39: Comparison data between Epigallocatecin 3-Gallate and Morelloflavone behaviors. We report root-mean-square deviation values of skeletons of EGCG (in green) and Morelloflavone (in red), and the proceeding of MD simulations for the POPC/EGCG systems and for POPC/Morelloflavone systems. We reported POPC molecules in yellow, EGCG molecules in green and Morelloflavone compounds in red.

After bilayer equilibration, (figure 39-1 green and red) we analyzed the natural compounds' aggregates in water phase. At middle of MD trajectories, we observed a reorienting phenomenon for the EGCG molecules (figure 39-2 green) that break the aggregate and dispose themselves on the interface of the lipid phase. For Morelloflavone, we note the initial aggregate remains the same through all the simulation (figure 39-2 red). Reached the MD steady states, confirmed by the monitoring of RMSD values, we observe that finally EGCG molecules strongly interact with the polar phosphate groups of POPC molecules (figure 39-3 green), confirming the behavior of this catechin to create phytosomes. This is not observed for Morelloflavone, which keeps on in its starting aggregate form, strongly stabilized by intermolecular interactions between molecules (figure 39-3

red). This behavior is in line with the literature data, which confirm that Morelloflavone does not create stable systems with phospholipids.

We want to improve encapsulation efficiency of EGCG molecules in lipid system, increasing bioavailability of antioxidant that reaches its biological target. Then, we evaluated the encapsulation efficiency of Epigallocatechin 3-Gallate in lipid matrix using different kinds and concentrations of salts. The aim is to observe if there is any salt effect on the EGCG incorporation in membrane. In particular, we carried out 250 ns of MD simulations on eight different models (0.15M NaCl, KCl, $CaCl_2$, $MgCl_2$, and 0.25 M NaCl, KCl, $CaCl_2$, $MgCl_2$), and we observed the reaching of steady state for the all studied models.

We verified the effective stability of lipid bilayers observing the RMSD values monitoring EGCG and lipids skeletons. We carried out membrane parameters analysis and the investigations of EGCG interaction with the lipid leaflets at the steady states; we considered membrane parameters as the "area per lipid value" and the "membrane thickness". We checked out if also the EGCG presence influence physical-chemical properties of the membrane, such fluidity and density, and then maintaining the necessary characteristics to use these lipid systems as carriers of antioxidant molecules.

6.1.1 MODELS WITH KCl

From the analysis of the KCl 0.15 M model, we noted that these salt did not influence EGCG behavior, and then we observed that the catechin molecule makes aggregate in water phase through aromatic interactions between rings of different EGCG molecules.

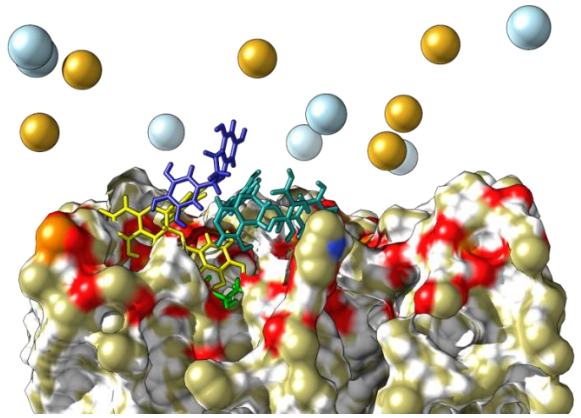

Figure 40: EGCG aggregate close to polar head groups of POPC system. We highlight hydrophobic surface of phospholipids, EGCG molecules (in yellow, green, blue and light blue). We also evidence K^+ ions in light blue and Cl^- ions in yellow

Increasing KCl concentration to 0.25 M, we observed variations on EGCG distribution; in fact, we did not observe the same aggregates that were present in the first simulated model. We evaluated the stability of systems observing the fluctuations of EGCG molecules, and we found that increasing KCl concentration, we have a different stabilization pathway.

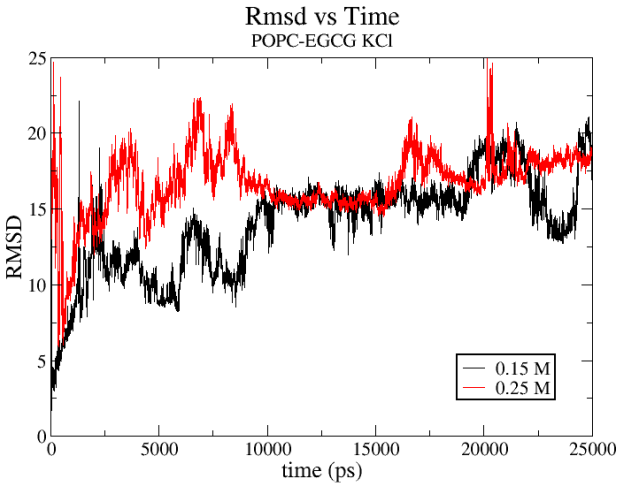

Figure 41: root-mean square deviations for EGCG molecules in system with 0.15 M KCl (in black) and 0.25 M KCl (in red)

Beside, we found very little variations on membrane parameters due to the salt increase. In fact, area per lipid values are 0.60 nm^2 for 0.15 M KCl model and 0.61 nm^2 after increasing salt concentration. The membrane thickness does not vary, but we noted a little decrease on the order degree of phosphate groups increasing the KCl concentration.

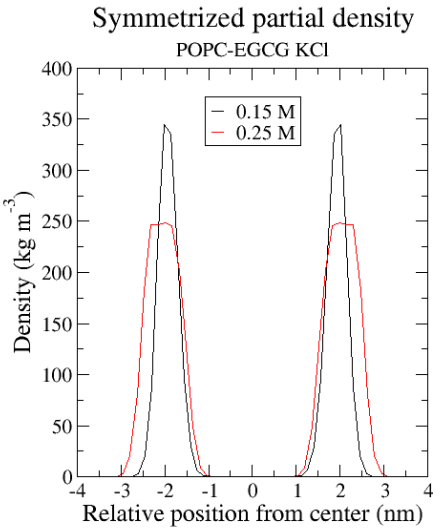

Figure 42: membrane thickness of system with 0.15 M KCl (in black) and 0.25 M KCl (in red)

However, the number of antioxidant encapsulated molecules is the same in both system with KCl, and this means that K^+ cations did not improve the EGCG molecules penetration inside the mmbrane, on the contrary seem to decrease this phenomenon (figure 43).

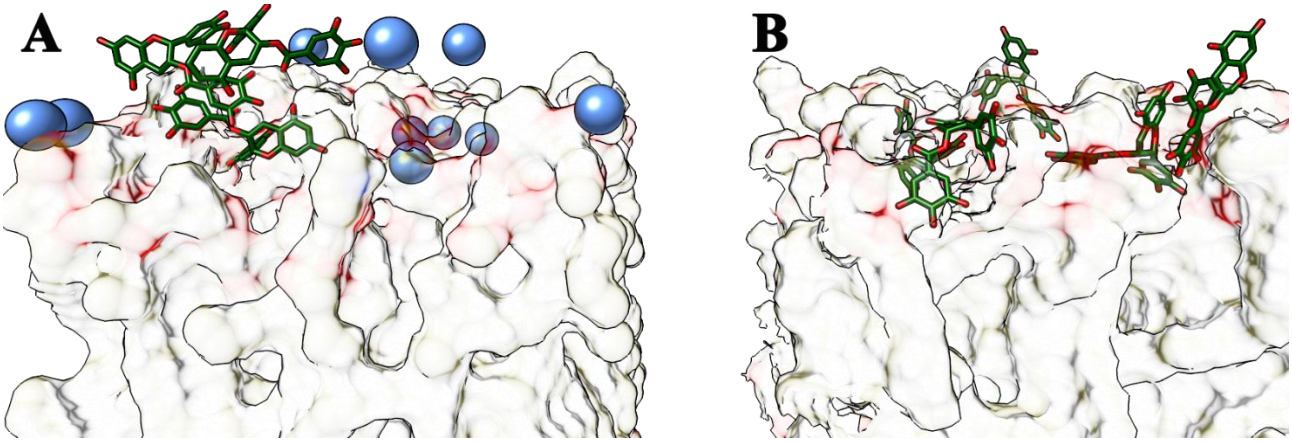

Figure 43: comparison between EGCG behaviors in presence of K+ cations (37A) and without salts (37B)

6.1.2 MODELS WITH NaCl

The NaCl models show different stabilization pathways with respect KCl, but after 200 ns of MD simulations we reached the same steady state, as we note by RMSD values.

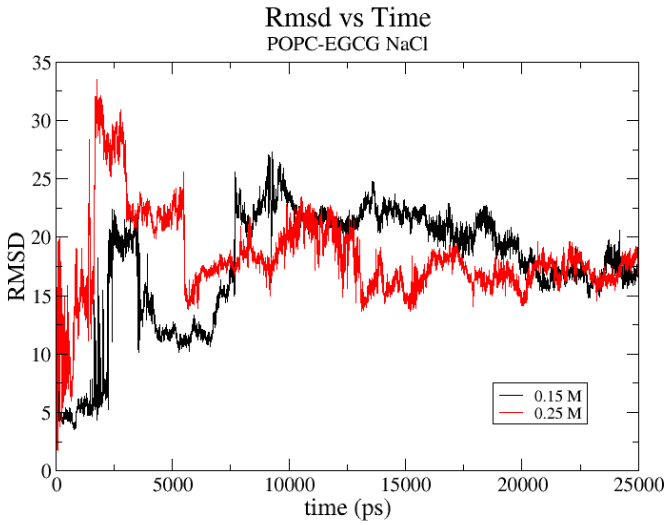

Figure 44: root-mean square deviations for EGCG molecules in system with 0.15 M NaCl (in black) and 0.25 M NaCl (in red)

At 0.15 M NaCl, we observed a lesser degree of aggregation in water phase and a corresponding major encapsulation of EGCG molecules; this means that NaCl is could to promote encapsulation, as confirmed by the mass density profiles of EGCG molecules. The *Area per lipid* values, which are 0.66 nm^2 and 0.63 nm^2 respectively for 0.15 M and 0.25 M NaCl models.

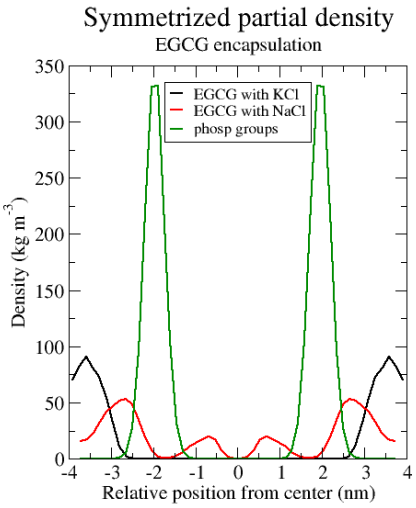

Figure 45: mass density profile of EGCG molecules in system with KCl (in black) and NaCl (in red). We report position of phosphate groups (in green) to give an idea of the effective position of the EGCG molecules in both systems.

However, we noted that increasing NaCl concentration, EGCG molecules tend to aggregate again, and the encapsulation degree is lower, as confirmed by the decreasing of *Area per lipid*. It seems that 0.15 M NaCl is the optimale concentration for this salt to improve EGCG encapsulation.

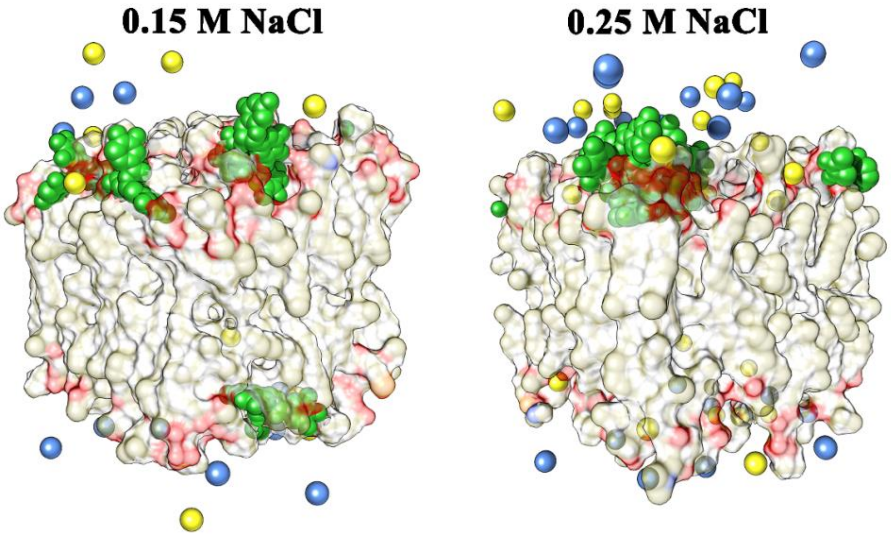

Figure 46: EGCG molecules close to polar head groups of POPC in 0.15 M (first) and 0.25 M (second) NaCl system. We highlight hydrophobic surface of phospholipids, EGCG molecules (in green). We also evidence Na^+ ions in blue and Cl^- ions in yellow

6.1.3 MODELS WITH $MgCl_2$

For the model with $MgCl_2$, we observed two different stabilization trends for 0.15 M and 0.25 M, and this is due to the increasing of salt. This is the only case where we observed different stabilization pathways within the two salt concentrations.

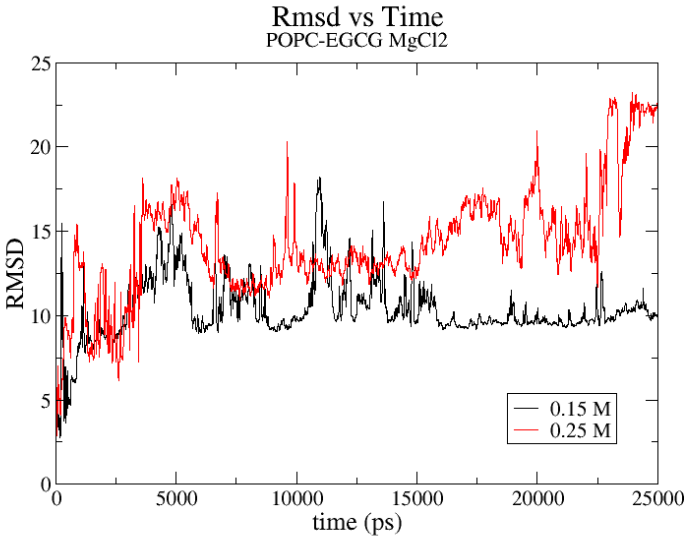

Figure 47: root-mean square deviations for EGCG molecules in system with 0.15 M $MgCl_2$ (in black) and 0.25 M $MgCl_2$ (in red)

Analyzing the 0.15 M $MgCl_2$ model, we found out a very stable system, where EGCG molecules are encapsulated like in 0.15 M NaCl model, although we found a different pathway for reaching the steady state.

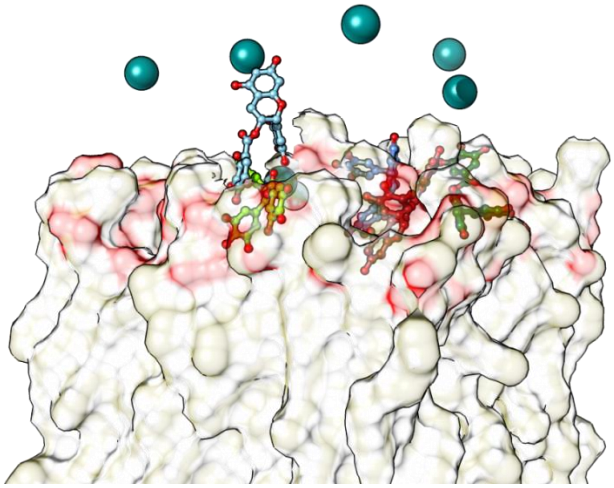

Figure 48: EGCG molecules (in blue, light blue, green and light green) are encapsulated in POPC systems (in hydrophobic surface). We report in cyan Mg++ ions.

The *Area per lipid* value of this system (0.64 nm^2) is very close that of 0.15 M NaCl model (0.65 nm^2), and this means that also $MgCl_2$ seems to enhance the EGCG encapsulation in lipid medium. At higher concentration, we observed very interesting data: we found an increase of the EGCG encapsulation when we add more $MgCl_2$.

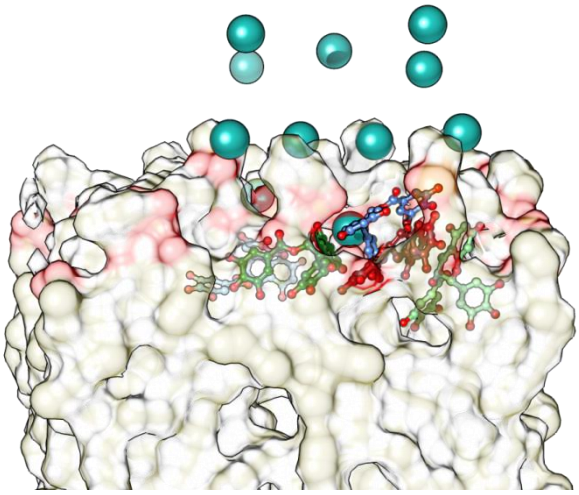

Figure 49: EGCG molecules (in blue, light blue, green and light green) are more encapsulated in POPC systems (in hydrophobic surface), respect to previous system. We report in cyan Mg++ ions.

Analyzing a representative structure of the steady state, we found that Mg^{++} cations are in solution, but there is a gradient due to the condensation of divalent cations. In fact Mg^{++} cations seem to promote the EGCG encapsulation indirectly, by interacting itself with phosphate groups of POPC lipids, and resting in solution. In fact, due to its length solvation energy, magnesium stays in aqueous medium. The POPC phosphate groups are however attracted by these cations, and as consequence, they slightly stretch the membrane leaflets along the z axis (figure 50).

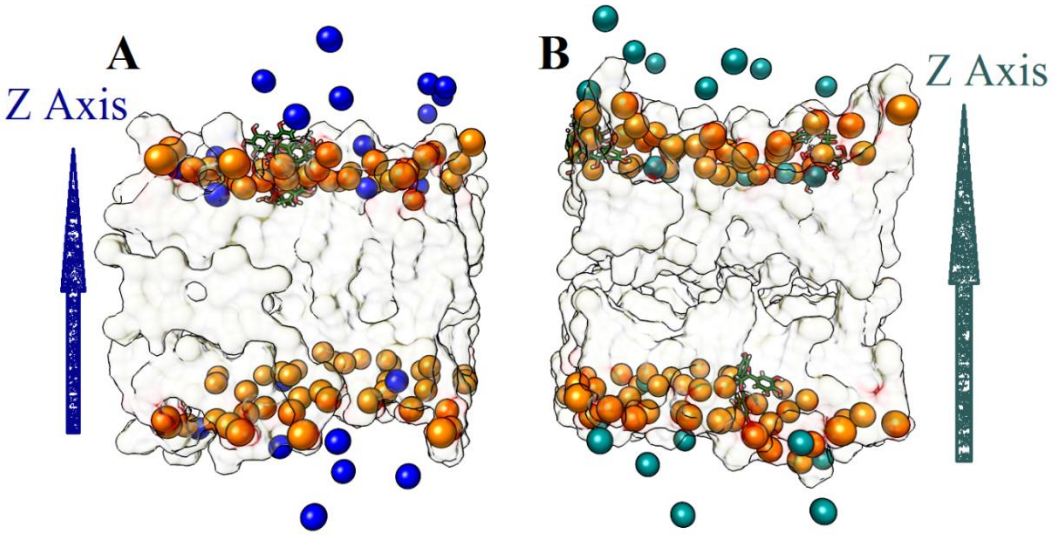

Figure 50: comparison between system with Na+ cations (50A, ions in blue), and system with Mg++ cations (50B, ions in cyan). Note the stretch along z axis due to Mg++ ions

The membrane thickness values confirm our hypothesis; in fact, while in 0.15 M $MgCl_2$ model the phosphate groups are ordered at a certain distance from box center; in the model with 0.25 M $MgCl_2$ these groups are arranged on two different planes, and this is evident by observing the two different peaks for each leaflet of membrane.

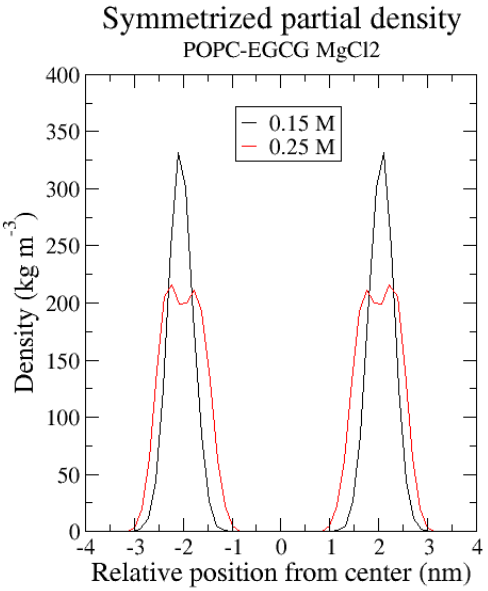

Figure 51: membrane thickness of system with 0.15 M $MgCl_2$ (in black) and 0.25 M $MgCl_2$ (in red)

6.1.4 MODELS WITH $CaCl_2$

Analyzing the systems with $CaCl_2$, we obtained very similar stabilization pathways for both models (figure 52), as observed for the NaCl and KCl models previously described.

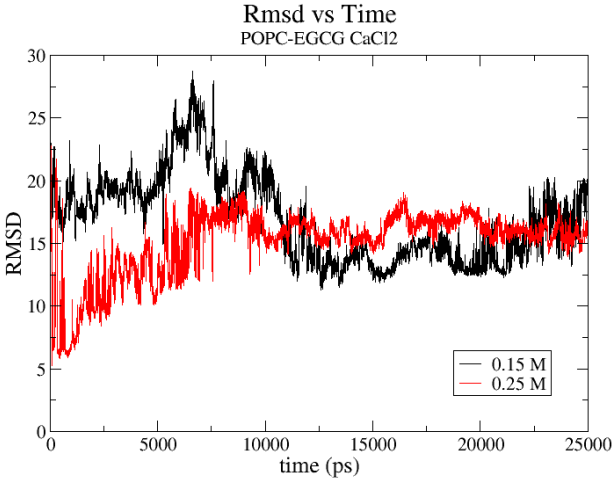

Figure 52: root-mean square deviations for EGCG molecules in system with 0.15 M $CaCl_2$ (in black) and 0.25 M $CaCl_2$ (in red)

More in details, at 0.15 M concentration we did not find aggregates, and every EGCG molecule interacted with polar heads of phospholipids. Analyzing representative structure of 0.15 M $CaCl_2$ system, we found that the Ca^{++} ions pose themselves very close to the polar groups of POPC lipids, but only in the areas where EGCG molecules are not present.

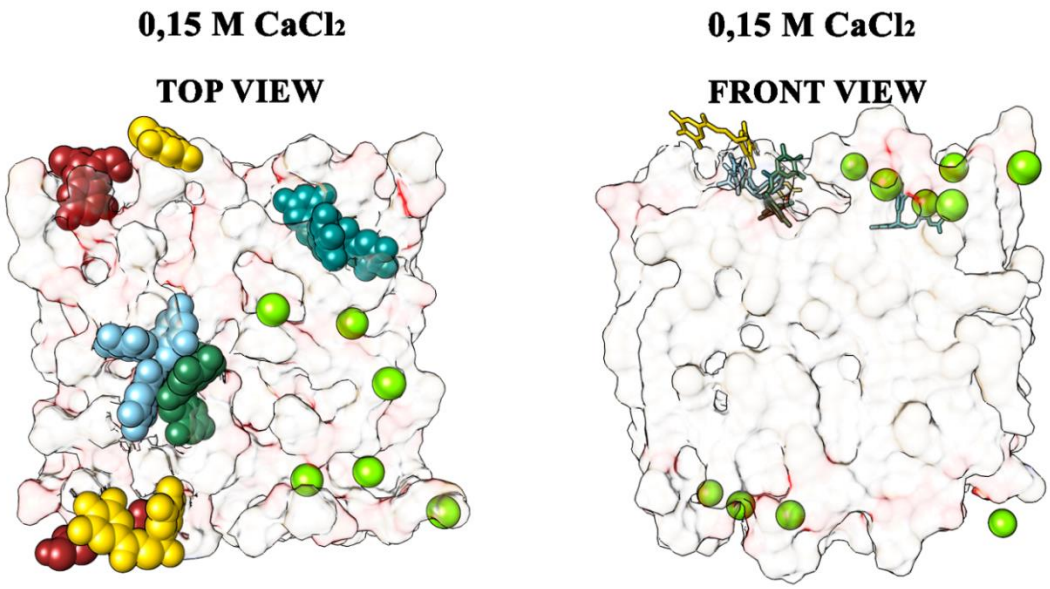

Figure 53: POPC-EGCG models with 0.15 M $CaCl_2$. Fig 53A shows model in top view. Fig 53B shows model in front view.

In fact, calcium ions break the shell of solvation and create ionic interactions with phosphate groups of lipids, and this phenomenon is very important, because Ca^{++} ions compete with EGCG molecules in the interactions with phosphate groups, decreasing encapsulation degree of epigallocatechin-gallate.

This effect is more evident if we increase $CaCl_2$ concentration, because the EGCG encapsulation is smaller than the previous system and the antioxidant molecules are arrange in the areas where the Ca^{++} cations are not presents.

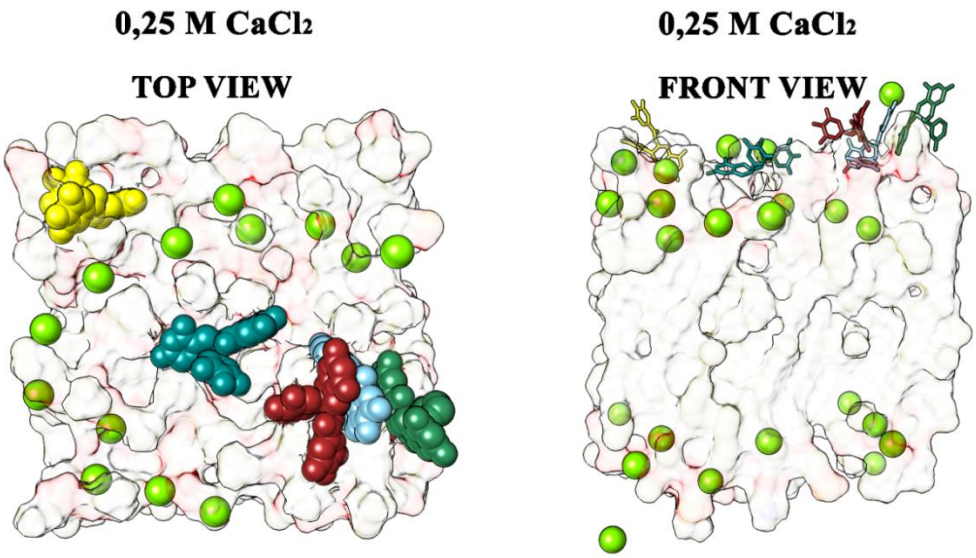

Figure 54: POPC-EGCG models with 0.25 M $CaCl_2$. Fig 54A shows model in top view. Fig 54B shows model in front view.

$CaCl_2$ is the salt that has major effects on the simulated lipid system, because of the strong interactions between calcium divalent cations and the lipids' phosphate groups. This is clear observing thicknesses membranes at 0.15 M and 0.25 M $CaCl_2$, where we observed a high change of the phosphate groups' disposition during the increase of the salt concentration.

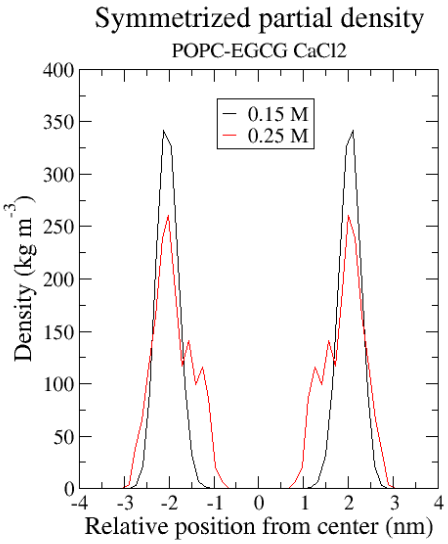

Figure 55: membrane thickness of system with 0.15 M $CaCl_2$ (in black) and 0.25 M $CaCl_2$ (in red).

In conclusions, despite the fact that the Ca^{++} ions strongly interacts with POPC membranes, it seems not to be the best choice in the strategy to increase EGCG encapsulation; on the contrary, $MgCl_2$ is the best salt to use, because the Mg^{++} cations lie in solution and determine a little stretch of membrane,

that increase the amount of EGCG in lipid medium. It is very evident observing the mass density profiles of epigallocatechin-3-gallate molecules in the presence of four tested salts and in relation to the phosphate groups' positions.

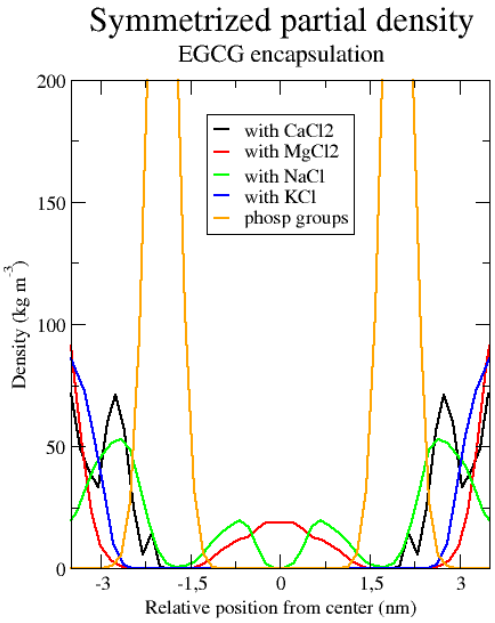

Figure 56: mass density profile of EGCG molecules in system with $CaCl_2$ (in black) and $MgCl_2$ (in red), NaCl (in green) and KCl (in blue). We report phosphate groups positions (in orange) to give an idea of the effective position of the EGCG molecules in both systems.

6.2 INFLUENCE OF LIPID MATRIX AND SALT CONCENTRATION ON EGCG ENCAPSULATION

As described in the previous section (6.1), we confirmed that Epigallocatechin 3-Gallate interacts with phospholipids to create phytosomes. More, we observed that the measure of the salt that we introduce in water phase plays a crucial role on the behavior of EGCG molecules. All studies described in section 6.1 are carried out in bilayers composed by only one type of natural phospholipids (POPC or DOPC). Now, we want to remark the effects of mixed membrane composition systems on the EGCG encapsulation. The carrier that we have chosen, is an anionic one, and it contains POPC, DOPE and CHEMS in molar ratio 1:1:1. We used DOPE because it has a fusogenic nature, and then it facilities the fusion of liposomal carrier on the membranes of target site. It is already used to create vectors for drug and gene delivery systems **[95, 96]**.

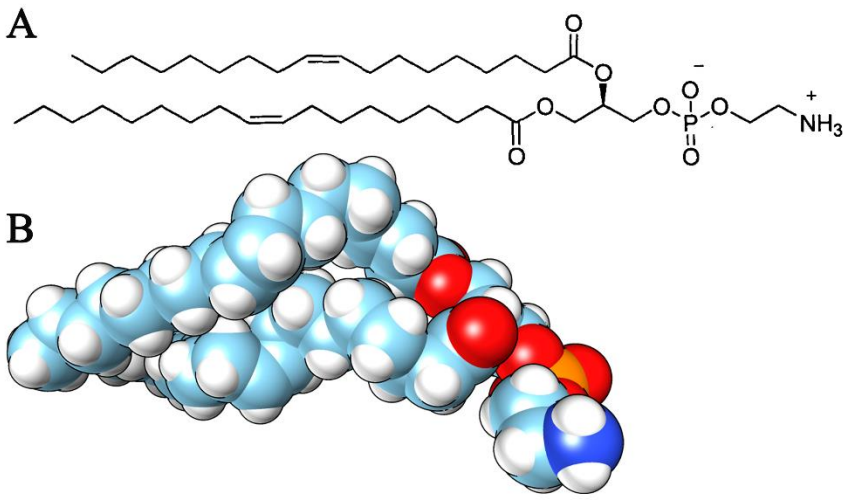

Figure 57: DOPE phospholipid
51A shows the 2D structure
51B shows the 3D structure

Lipids in a fluid bilayer are highly dynamic. Many movements on different timescales take place: rotation around chemical bonds and trans/ gauche isomerization (picoseconds), rotation (axial diffusion) around the lipid axis (nanoseconds), wobbling (nanoseconds), lateral diffusion (microseconds), flip-flop across the bilayer (milliseconds–seconds) and undulating movements of the membrane (milliseconds–seconds) [97]. Most of these movements influence the order parameters of the acyl chains, and the type of acyl chains that are present in a lipid system is very important to determine the features of liposomal carrier. Generally, the bilayers are constituted of different lipids have different properties. Changes in lipid compositions, such as differing acyl chain lengths [98] or the inclusion of unsaturated chain lipid species [99], are reported to modulate membrane properties. Over the phospholipids POPC and DOPE, we added a cholesterol derivate that has a negative net charge, to obtain an anionic liposomal vector, Cholesteril-emisuccinate (CHEMS). It is composed by a cholesteryl skeleton having a succinate residue at the head (figure 58).

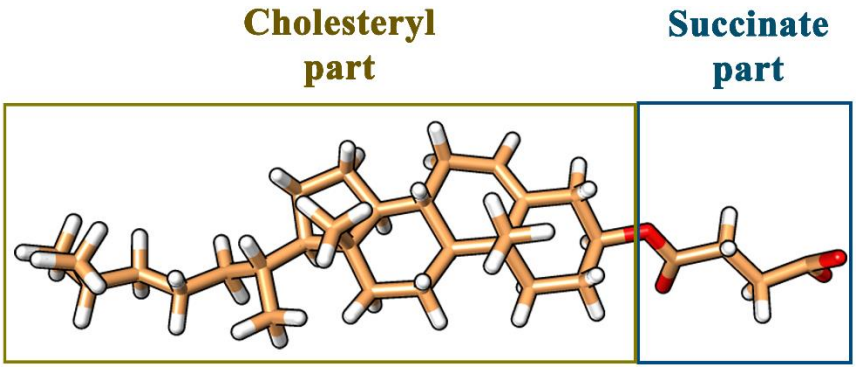

Figure 58:
CHEMS MOLECULE. We evidence the cholesteryl moiety and the succinate moiety

It is well known that Cholesterol increases the order in Lα phase bilayers. The amount of additional ordering induced by cholesterol, differs depending on the type of lipids. The MD simulations are used

to provide atomic detail on the cholesterol–lipid interactions, and, in according with molecular dynamics results, cholesterol and its derivatives in general increase the ordering in both the sn-1 and the sn-2 chain of phospholipids; more, the α and β face of cholesterol have a preferential interaction with saturated and unsaturated chains, respectively. Considering all these properties, we added CHEMS not only to give a negative net charge to our lipid system, but also to increase the package degree after EGCG encapsulation.

Once again, we added thirty EGCG molecules in the water phase in a simulation box containing lipids described above, and we have set up different simulation systems in which we add different concentration of $MgCl_2$; our aim is to investigate the influence of an increasing salt concentration. Indeed, we obtained different encapsulation degree of the same molecule (EGCG).

The aim of this part of study is to find an optimal formulation ratio between the EGCG concentration and salt in our mixed lipid system, to improve the encapsulation degree of this catechin. For each model, we carried out 100 ns of MD simulations, and we monitored the stability of systems observing the root-mean square deviation (RMSD) of EGCG skeleton. We took in considerations the representative structures of the steady states, observing at atomistic level the positions of every single EGCG molecule, to evaluate the encapsulation degree. We also considered the membrane parameters, such area per lipid and mass density membrane values calculated on last 20 ns for every MD simulation. The aim is to find a correlation between variations of membrane parameters and encapsulation degree, and also to confirm the integrity of the anionic lipid vector formed.

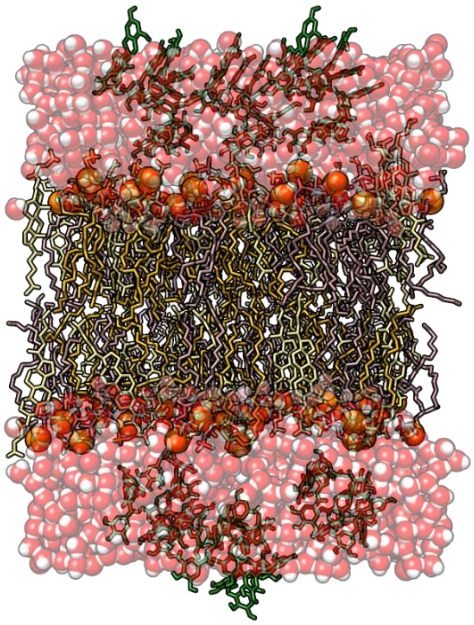

Figure 59: starting structure of MD simulations. We highlighted EGCG (green), water (sphere), phosphate groups (orange), CHEMS (khaki), DOPE (dark khaki) and POPC molecules (yellow)

The first simulation model that we have investigated presents the physiological conditions, thus we added 0,15 M NaCl without $MgCl_2$; then, we applied our previously described simulation protocol.

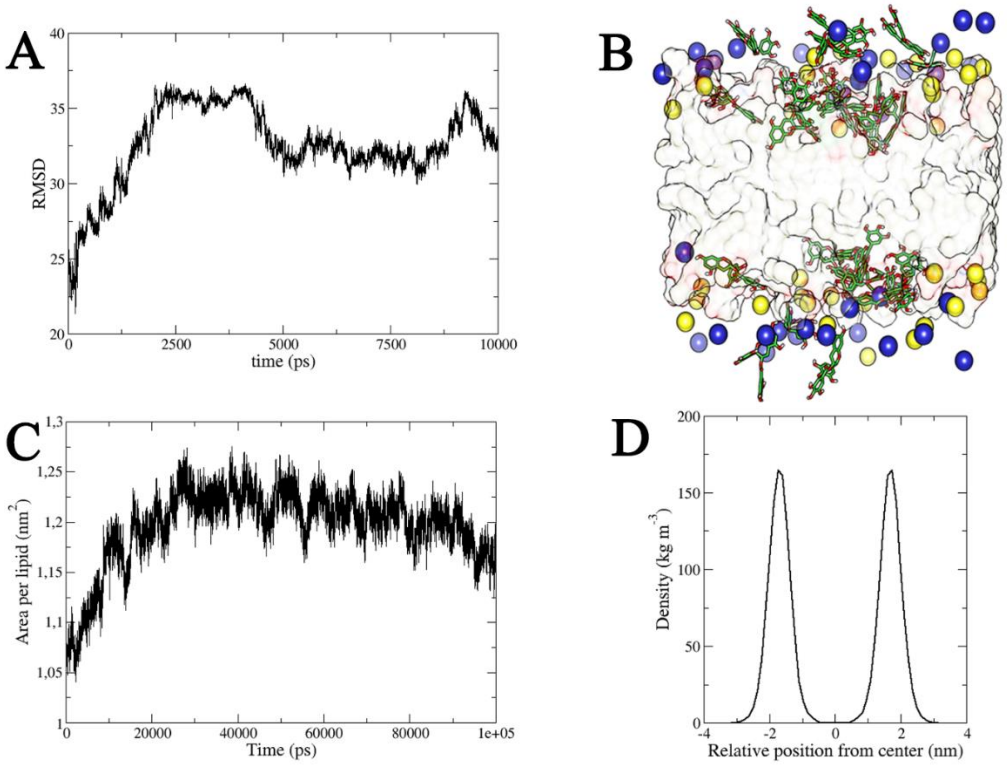

Figure 60: anionic mixed lipid system with 0.15 M NaCl and EGCG molecules.
60A shows root-mean square deviation, 60B shows representative structure of steady state, blue spheres are Na^+ ions, yellow sphere are Cl^- ions
60C shows area per lipid values, 60D shows the membrane mass density

Analyzing RMSD table (Fig 60A) the system reach stability after 50 ns of MD simulation. Observing the representative structure of steady state (Fig 60B), we note that the EGCG molecules reorient themselves close to lipid layers. We have no more aggregates, and some molecules lie in water phase. This means that not all the EGCG molecules are encapsulated in lipid system. Indeed, the experimental data show that the encapsulation percentage of EGCG molecules is 78 ± 0.3 %. We calculated *Area per lipid* value (Fig 60C), and at last 20 ns of MD simulations this parameter is 0.85 ± 0.03 nm^2.

For the second simulation model, we added $MgCl_2$ in a molar ratio 1:1 with respect to EGCG.

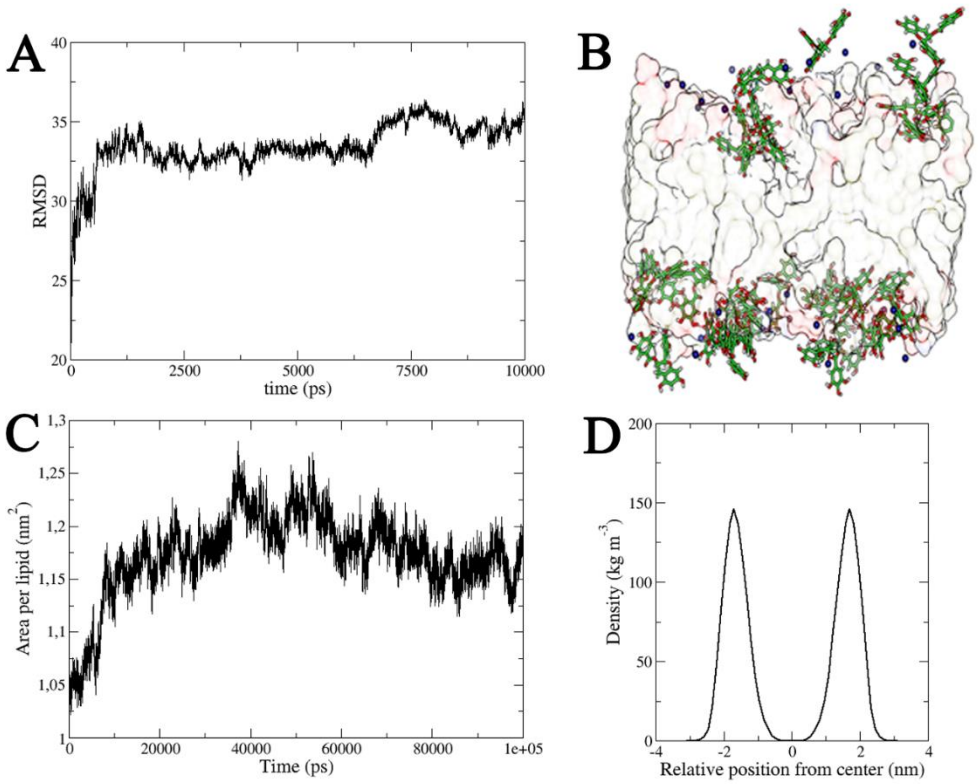

Figure 61: anionic mixed lipid system with $MgCl_2$ and EGCG molecules (1:1).
61A shows root-mean square deviation, 61B shows representative structure of steady state,
Blue spheres are Mg^{++} ions
61C shows area per lipid values, 61D shows the membrane mass density

Analyzing RMSD table (Fig 61A), the system reaches stability after 20 ns of MD simulations. This means that Mg^{++} ions stabilize the EGCG molecules. As reported in figure 61B, we noted that also in this case the EGCG molecules reorient themselves close to lipid layers. The starting aggregate disappears, and the molecules interact strongly with lipids. Experimental data show that the encapsulation percentage of EGCG molecules is 79 ± 0.6 %, very close to the value of the first model investigated. In fact, comparing the structures of steady states, we did not observe so much differences between the two systems. In addition, Area per lipid value (Fig 61C) averaged for the last 20 ns of MD simulations is not so different from the calculated value for the first model (0.91 ± 0.02 nm^2).
For the third simulation model, we added $MgCl_2$ in a molar ratio 3:1 in relation to EGCG molecules.

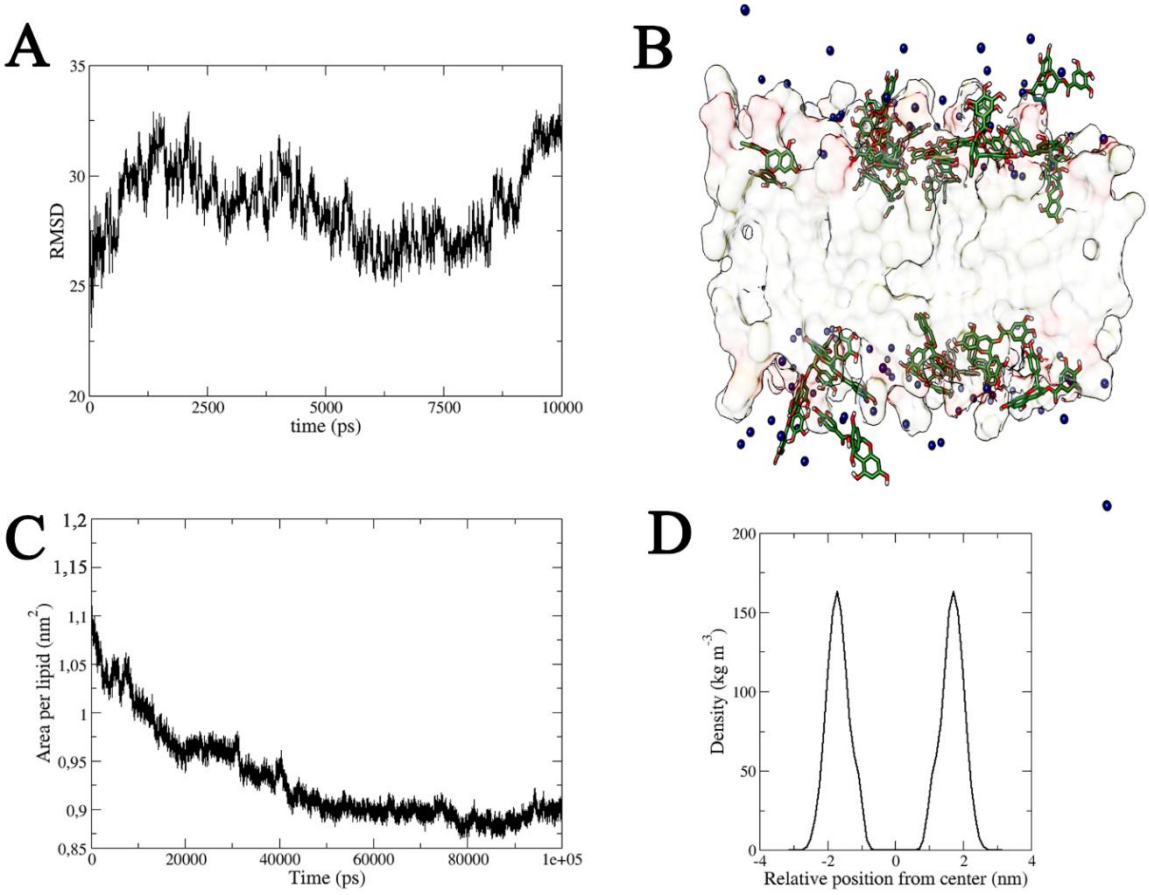

Figure 62: anionic mixed lipid system with $MgCl_2$ and EGCG molecules (3:1).
62A shows root-mean square deviation, 62B shows representative structure of steady state,
Blue spheres are Mg^{++} ions
62C shows area per lipid values, 62D shows the membrane mass density

As reported in figure 62, we obtained a system that is structurally very similar to the previous model, but EGCG molecules do not reach stability so fast, maybe in relation to the increase of Mg^{++} concentrations. However, comparing both systems at 1:1 and 3:1 molar ratios, we observe a very similar disposition of EGCG molecules (figure 62B), so we did not expect great differences about the encapsulation degree. In fact, this percentage, experimentally derived, is about 80 ± 0.4 %, this means that the same quantitative of our antioxidant compound is encapsulated. More, membrane parameters did not vary, because *"Area per lipid"* value (figure 62C) is 0.91 ± 0.03 nm^2, and membrane thickness has always the same value (figure 62D).

Then, we increased $MgCl_2$ concentration to reach a molar ratio 5:1 respect to EGCG molecules.

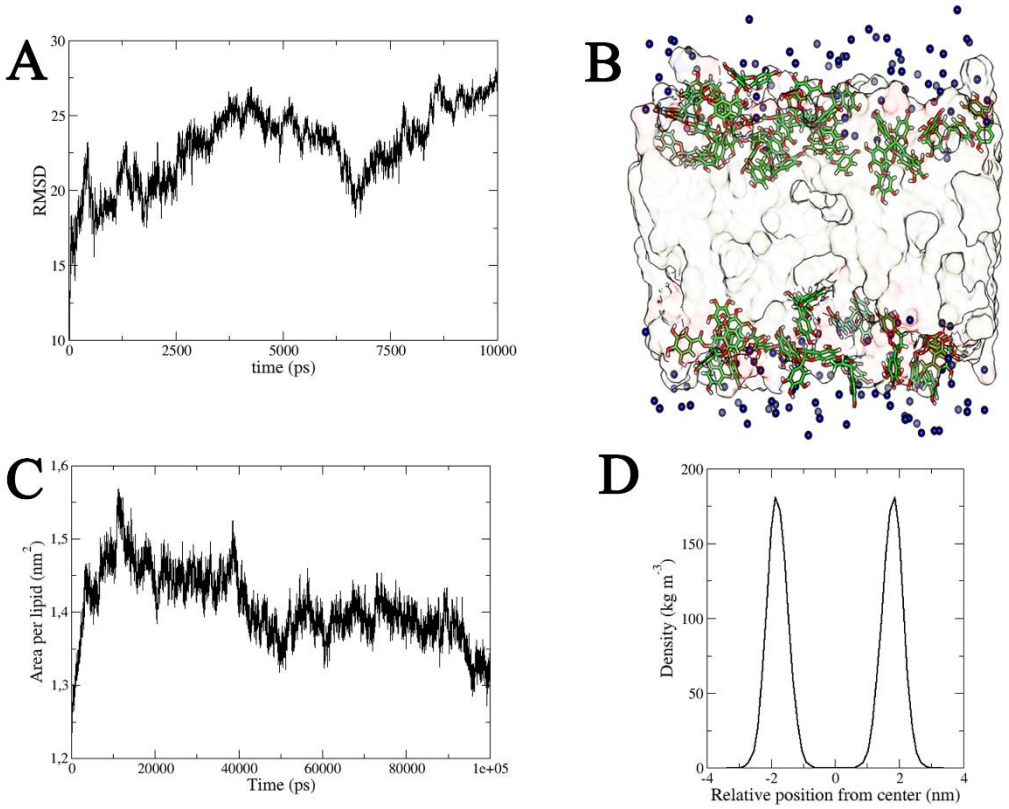

Figure 63: anionic mixed lipid system with $MgCl_2$ and EGCG molecules (5:1).
63A shows root-mean square deviation, 63B shows representative structure of steady state,
Blue spheres are Mg^{++} ions
63C shows area per lipid values, 63D shows the membrane mass density

Analyzing RMSD values (63A), we noted a total different trend of stabilization if compared to the other systems observed before; it seems that EGCG molecules have a peculiar behavior, and it is evident observing the representative structure of steady state (63B). In fact, all EGCG molecules interact with lipid medium, and no catechin molecules remain in water phase. From the computational data, it's clear that all EGCG molecules are encapsulated, and we compute this behavior analyzing "area per lipid values" (figure 63 C), that is 1.16 ± 0.03 nm on last 20 ns of MD simulation. This increased value is relative to a major concentration of encapsulated EGCC, while membrane thickness parameters did not vary respect to previous systems (figure 63D), meaning that the lipid system retain its stability. Experimental data obtained in our laboratories show that for this model there is 98 ± 0.6 percentage of EGCG encapsulation, confirming the reliability of our computational data.
Even if we reached the maximum encapsulation degree of EGCG, we evaluated the possibility of increasing $MgCl_2$ concentration to evaluate every different behaviors. For these reason, we added more divalent salt, reaching a 6:1 molar ratio between Mg^{++} cations and EGCG molecules.

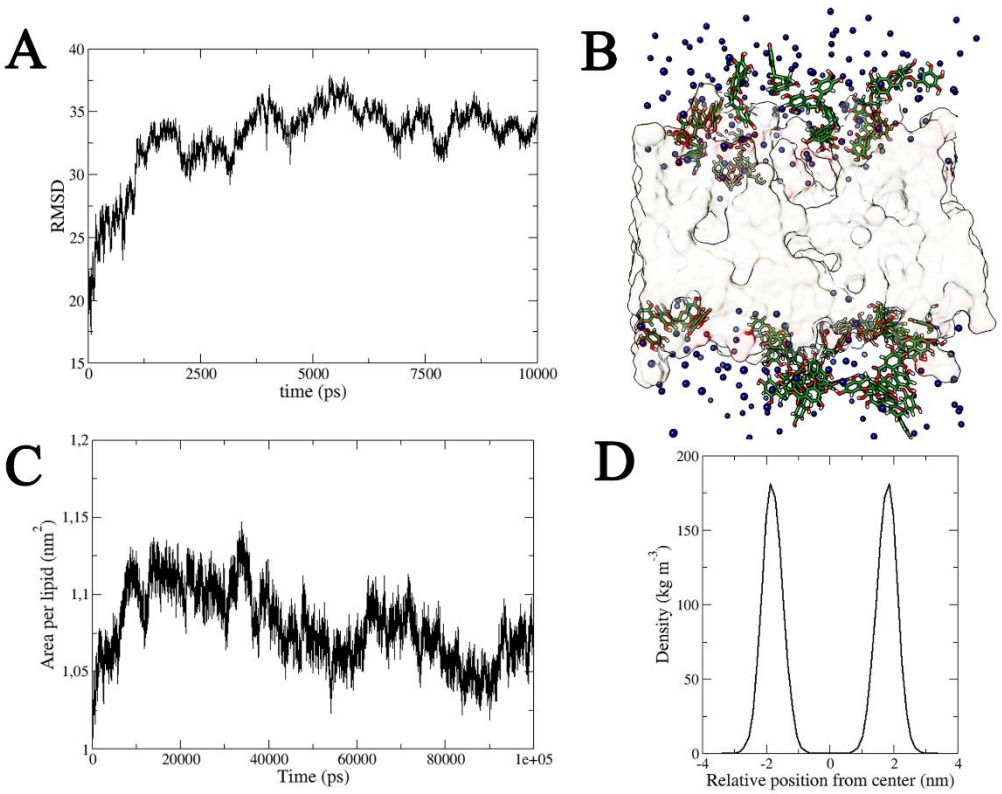

Figure 64: anionic mixed lipid system with $MgCl_2$ and EGCG molecules (6:1).
64A shows root-mean square deviation, 64B shows representative structure of steady state,
Blue spheres are Mg^{++} ions
64C shows area per lipid values, 64D shows the membrane mass density

The root-mean square deviations (figure 64A) show a very stable system, with values very similar to models with 0.15 M NaCl and Mg^{++} in 1:1 molar ratio with EGCG compounds. From the representative structure of steady state (figure 64B), we note that some aggregate again appears, and this means that we observe a decrease of the encapsulation degree. *"Area per lipid"* value (figure 64C) at last 20 ns of MD simulation is 0.85 ± 0.03 nm^2, so we report a decrease of this value due to a minor amount of encapsulated EGCG molecules. Experimental data confirm this trend, because we obtain 76 ± 0.2 % of Encapsulation degree. Also in this case, we observe that the membrane thickness (figure 64D) retains the same values respect previous systems.

Beside, in order to rationalize the behavior of EGCG molecules using MD simulations, we compared encapsulation percentage determined in our laboratories with the time to obtain the steady states and the Δ root-mean square deviation values calculated on EGCG trajectories along MD simulations (Figure 65), we show a linear trend between the two approaches.

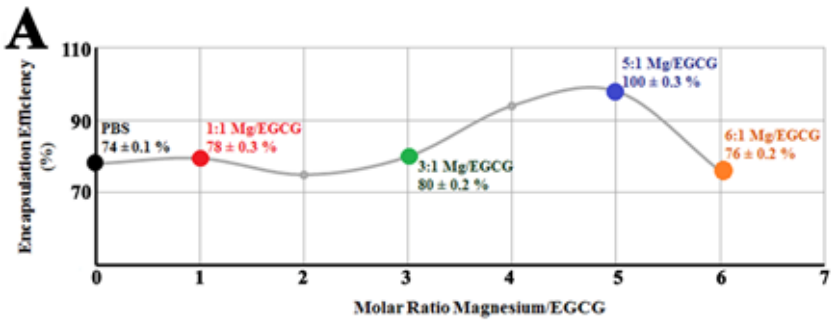

B

SYSTEM	*Time to reach the Steady State*	*ΔRMSD*
PBS	20 ns	9.7086 Å
1:1	18 ns	9.9874 Å
3:1	40 ns	12.7519 Å
5:1	83 ns	19.4201 Å
6:1	22 ns	9.8264 Å

Figure 65: comparison between experimental and computational data. Fig 65A shows encapsulation percentage of all systems studied. Fig 65B shows the time necessary to reach the steady state and ΔRMSD.
We highlighted model with 0.15 M NaCl (black), 1:1 (red), 3:1 (green), 5:1 (blue), 6:1 (orange) in molar ratio

7. CONCLUSIONS

My PhD work was aimed to create stable liposomal vectors with antioxidant properties able to insert in the lacrimal tear film and to deliver the active principle in the eye with high bioavailability and high stability. The final product will be innovative artificial tear, to prevent damages of retina and cornea. With our study, we setted up an efficient MD protocol that allow us to simulate membrane models for different purposes, including a great variety of lipids and containing antioxidant compounds and other molecules able to solve different functions (for example Gene Delivery). Using our protocol, we tested different type and concentration of antioxidant molecules, salts and lipid, and we evaluated the possibility to functionalize these compounds to increase specific characteristics preserving its antioxidant capacity.

We have chosen Edaravone for a functionalization strategy, and we obtained an efficient derivate that is stable in liposomal vector. Through MD simulations, we found the optimal concentration of EDR-C18 in lipid medium, at the aim to obtain a major bioavailability of antioxidant compound without influencing the fluidity and stability of liposomal carrier. We tested different salts to influence EDR-C18 behaviors and dispositions in POPC matrix, and we found that in presence of $CaCl_2$, the Edaravone derivative exposes the aromatic heads toward the solvent medium, and then it exerts its

antioxidant activity like a shield in the lipid layer of lacrimal film. EDR-C18 shows a great stability in liposomal vector, moving itself between the two leaflets of membrane, so it can be more efficent . During our studies, we demonstrated that the choice of liposome environment around an antioxidant molecule plays a crucial role to increase the bioavailability of active principle. We have demonstrated that Epigallocatechin 3-Gallate interacts with phospholipid system, creating very stable systems named phytosomes. For these reason, we did not chose a functionalization strategy for this compound. The type and the concentration of salts can improve this natural behavior, and this means that we observed changes on membrane parameters and stabilization pathways, and could be very different between them. More in details, the chemical-physical properties of used lipid matrix is also important. In fact, net charge, the presence of unsaturated chains and of cholesterol can alter membrane parameters. Thus, the lipid matrix plays a crucial role for an efficient encapsulation of antioxidant compound. We demonstrated that modulating opportunely the mixed lipid matrix used and the type and concentration of salt, it is possible to reach the maximum encapsulation degree of antioxidant compounds, increasing the bioavailability of drug or active natural product. For our studies, we have choose a mixed negative lipid matrix composed by POPC, DOPE, and CHEMS compounds, and we opportunely added $MgCl_2$. At the end of molecular dynamics simulations, we observed so many different behaviors for Epigallocatechin 3-Gallate molecules. Computational data show that increasing the salt concentration to reach a molar ratio 5:1 with EGCG, we observed a growing of antioxidant encapsulation in lipid bilayer. When added more salt, to obtain a model with 6:1 molar ratio with our green tea extract and we observe a net decrease on EGCG encapsulation.

We combined computational approach with experimental field to create very interesting systems for the development of artificial tears. Our formulations are still in progress and seem to be very promising for an ophthalmic use.

8. REFERENCES

1. *Ohashi Y, Dogru M, Tsubota K, Clinica Chimica Acta 369 (2006) 17 – 28*
2. *Rantamäki A, Telenius J, Koivuniemi A, Vattulainen I, Holopainen J M, Progress in Retinal and Eye Research 30 (2011) 204-215*
3. *Rantamäki A H; Javanainen M; Vattulainen I; Holopainen J M, Investigative Ophthalmology & Visual Science 53 (2012) 6442-6447*
4. *Telenius J, Koivuniemi A, Kulovesi P, Holopainen J M, Vattulainen I, Langmuir 28 (2012) 17092−17100*
5. *Agarwal R, Iezhitsa I, Agarwal P, Nasir A N A, Razali N, Alyautdin R, and Ismail N M, Drug Delivery (2014) 1071-7544*
6. *Vanommeslaeghe K, Guvench O, MacKerell Jr A D; Curr. Farm. Des. 2014; 20 (20) 3281-3292*
7. *Lange O F, van der Spoel D, de Groot B L; Biophysical Journal 99 (2010), 647-655*
8. *Gurtovenko A A, Vattulainen I, J. Phys. Chem. B 112 (2008) 1953-1962*
9. *Molina A M, Rodrıguez-Beas C, Faraudo J, Biophysical Journal Volume 102 (2012) 2095–2103*
10. *Galeazzi R, Laudadio E, Massaccesi L, Frontiers in Computational Chemistry, 2 (2015) 326-388*
11. *Weiner S J, Kollman P A, Case D A, Singh U , Ghio C, Alagona G, Profeta S Jr, Weiner P, J. Am. Chem. Soc. 106 (1984) 765-784*
12. *Pearlman, David A, Case, David A, Caldwell J W R, Wilson S, Cheatham, Thomas E. III; DeBolt S, Ferguson D, Seibel G, Kollman P. Computer Physics Communications, Volume91.*
13. *Hagler A T, Huler E, Lifson S, J. Am. Chem. Soc., (1974) 96 (17), 5319–5327*
14. *William L, Jorgensen J. Am. Chem. Soc. (1981) 103 (2), 335–340*
15. *Tomimoto M , Go N, J. Phys. Chem., (1995), 99 (2), 563–577*
16. *Cornell W D, PiotrCieplak , Bayly C I, Gould I R, Merz K M , Ferguson D M, Spellmeyer D C, Fox T, Caldwell J W, Kollman P A J. Am. Chem. Soc., (1995) 117 (19), 5179–5197.*
17. *Kollman P A, Dixon R, Cornell W, Fox T, Chipot C, Pohorille A. Computer Simulation of Biomolecular System (1997)*
18. *Wang J, PiotrCieplak, Kollman P A Journal of Computational Chemistry (2000), 21 (12), 774–787*
19. *Damm W, van Gunsteren W F Journal of Computational Chemistry (2000), 21 (9) 774–787*
20. *Ponder J W, Case D A Advances in Protein Chemistry (2003), 66, 27–85*
21. *Hornak V, Abel R, Okur A, Strockbine B, Roitberg A, Simmerling C Proteins: Structure, Function, and Bioinformatics (2006),65 (3), 712–725*
22. *Salomon-Ferrer R, Case D A, Walker R C Computational Molecular Science (2013), 3 (2), 198–210*
23. *Case D A, Babin V, Berryman J T, Betz R M, Cai Q, Cerutti D S, Cheatham III T E, Darden T A, Duke RE, Gohlke, H, Goetz AW, Gusarov S, Homeyer N, Janowski P, Kaus J, Kolossváry I, Kovalenko A, Lee T S, LeGrand S, Luchko T, Luo R, Madej B, Merz K M, Paesani F, Roe D R, Roitberg A, Sagui, C, Salomon-Ferrer R, Seabra G, Simmerling C L, Smith W, Swails J, Walker R C, Wang J, Wolf R M, Wu X, Kollman P A, The AMBER molecular modeling package AMBER 14, University of California, San Francisco 2014*
24. *Dickson C J, Madej B D, Skjevik Å A, Betz R M, Teigen K, Gould I R, Walker R C Lipid14: the Amber Lipid Force Field, J. Chem. Theory Comput., 2014, 10 (2), 865-879*
25. *McCammon JA, Gelin BR, Karplus M. Nature. 1977; 267(5612):585–590*

26. *Brooks BR, Brooks CL 3rd, Mackerell AD Jr, Nilsson L, Petrella RJ, et al. J Comput Chem. 2009; 30(10):1545–1614*
27. *Alder BJWTE. J Chem Phys. 1957; 27(1208)*
28. *MacKerell AD, Bashford D, Bellott M, Dunbrack RL, Evanseck JD, et al. J Phys Chem B. 1998; 102(18):3586–3616*
29. *Jorgensen WL, Tirado-Rives J. Journalof the American Chemical Society. 1988; 110(6):1657–1666*
30. *Klauda JB, Brooks BR, MacKerell AD Jr, Venable RM, Pastor RW. J Phys Chem B. 2005; 109(11):5300–5311.*
31. *Jo S, Rui HA, Lim JB, Klauda JB, Im W. Journal of Physical Chemistry B. 2010; 114(42):13342–13348*
32. *Rui HA, Im W. Journal of Computational Chemistry. 2010; 31(16):2859–2867*
33. *Broemstrup T, Reuter N. Phys Chem Chem Phys. 2010; 12(27):7487–7496*
34. *Klauda JB, Venable RM, Freites JA, O'Connor JW, Tobias DJ, et al. J Phys Chem B. 2010; 114(23): 7830–7843*
35. *Halgren TA. MMFF VII. J Comp Chem. 1999; 20:730–748*
36. *Wang J, Wolf RM, Caldwell JW, Kollman PA, Case DA. J Comput Chem. 2004; 25(9):1157–1174*
37. *Ewig CS, Berry R, Dinur U, Hill J-R, Hwang M-J, et al. Derivation of Class II Force Fields. VIII. J Comp Chem. 2001; 22:1782–1800*
38. *Sun H. J Phys Chem B. 1998; 102:7338–7364*
39. *Momany FA, Rone R. Journal of Computational Chemistry. 1992; 13(7):888–900*
40. *Hopfinger AJ, Wang S, Tokarski JS, Jin BQ, Albuquerque M, et al. Journal of the American Chemical Society. 1997; 119(43):10509–10524*
41. *Bernard D, Coop A, MacKerell AD Jr. J Am Chem Soc. 2003; 125(10):3101–3107*
42. *Reddy, MR.; Erion, MD. Springer –Verlag*
43. *Price MLP, Ostrovsky D, Jorgensen WL. Journal of Computational Chemistry. 2001; 22(13):1340–1352*
44. *McDonald NA, Jorgensen WL. The Journal of Physical Chemistry B. 1998; 102(41):8049–8059*
45. *Shashi K, Satinder K, Bharat P. International Research Journal of Pharmacy, 2012 3 (7).*
46. *Berendsen H J C, Postma J P M, DiNola A, Haak J. R. J. Chem. Phys. 1984(81),3684–3690*
47. *Nosé, S. Mol.Phys. 52:255–268, 1984*
48. *Hoover WG Phys. Rev. A31:1695–1697, 1985*
49. *Bussi G, Donadio D, Parrinello M. J.Chem. Phys. 126:014101, 2007*
50. *Parrinello M, Rahman A. J. Appl. Phys. 1981 (52) 7182–7190*
51. *Nosé S, Klein M. L. Mol.Phys. 1983 (50) 1055–1076*
52. *Budin I, Devaraj Neal K. (2011). Journal of the American Chemical Society (2012)134 (2): 751–753*
53. *Budin I, Devaraj Neal K. Journal of the American Chemical Society (2012) 134 (2): 751*
54. *Lodish H, Berk A, Zipursky LS, et al. New York: Scientific American Books. 2004 0-7167-3136-3.*
55. *Doherty, Annette M. (2002). Annual Reports in Medicinal Chemistry, Volume 37 (Annual Reports in Medicinal Chemistry)*
56. *Watanabe T, Tanaka M, Watanabe K, Takamatsu Y, Tobe A (March 2004) Research and development of the free radical scavenger edaravone as a neuroprotectant 124 (3): 99–111*
57. *Galeazzi R, Bruni P, Crucianelli M, Laudadio E, Marini M, Massaccessi L, Mobbili G, Pisani M; RCS Advanced (2015) 5, 54070-54078*

58. *Higashi Y, Jitsuiki D, Chayama K, Yoshizumi M (January 2006). Recent Patents on Cardiovascular Drug Discovery 1 (1): 85–93*
59. *Yoshida H, Yanai H, Namiki Y, Fukatsu-Sasaki K, Furutani N, Tada N. CNS Drug Reviews 12 (1): 9–20*
60. *Yuan WJ, Yasuhara T, Shingo T, et al. BMC Neuroscience. (2008) 9: 75*
61. *Kawasaki T, Ishihara K, Ago Y, et al European Journal of Pharmacology (2008) 542 (1-3): 92–9*
62. *Kawasaki T, Ishihara K, Ago Y, Baba A, Matsuda T The Journal of Pharmacology and Experimental Therapeutics (2007) 322 (1): 274–81*
63. *Yokoyama H, Takagi S, Watanabe Y, Kato H, Araki T Journal of Neural Transmission (1996) 115 (6): 831–42*
64. *Yokoyama H, Yano R, Aoki E, Kato H, Araki T Metabolic Brain Disease. (2008) 23 (3): 335–49*
65. *Shimazaki H, Hiromaka K, Fujisawa T, Tsuruma K, Tozuka Y, Shimazawa M, Takeuchi H, Hara H, Investigative Ophthalmology and Visual Science. (2011) 52 (10)*
66. *Horia I. Petrache, Steven W. Dodd, Michael F. Brown, Biophysical Journal Volume 79, Issue 6, December 2000, 3172–3192*
67. *Norbert Kučerka a,b, Mu-Ping Nieh c, John Katsaras Biochimica et Biophysica Acta 1808 (2011) 2761–2771*
68. *Murube J, Peterson A, Murube E; Advances in Experimental Medicine and Biology (1998) 438, 693-704*
69. *Masood A, Chowhan A, Huagang C; US006620797B2 (2003)*
70. *Molina M A, Beas C R, Faraudo J; Biophysical Journal (2012), 102, 2095-2103*
71. *Hummer G, Pratt L R, Garcia A E; J. Phys. Chem. (1996), 100, 1206-1215*
72. *Friedman, M. Mol. Nutr. Food Res. 2007, 51, 116–134.*
73. *Sharangi, A. B. Food Res. Int. 2009, in press.*
74. *Friedman, M.; Mackey, B. E.; Kim, H. J.; Lee, I. S.; Lee, K. R.; Lee,S. U.; Kozukue, E.; Kozukue, N. J. Agric. Food Chem. 2007, 55, 243–253.*
75. *Shimizu, M.; Fukutomi, Y.; Ninomiya, M.; Nagura, K.; Kato, T.;Araki, H.; Suganuma, M.; Fujiki, H.; Moriwaki, H. Cancer Epidemiol. Biomarkers Prev. 2008, 17, 3020–3025.*
76. *He, R.-R.; Chen, L.; Lin, B.-H.; Matsui, Y.; Yao, X.-S.; Kurihara, H. Chin. J. Integr. Med. 2009, 15, 34–41.*
77. *Pearson, D. A.; Frankel, E. N.; Aeschbach, R.; German, J. B. J. Agric. Food Chem. 1998, 46, 1445–1449.*
78. *Frankel, E. N.; Huang, S.-W.; Aeschbach, R. J. Am. Oil Chem. Soc. 1997, 74, 1309–1315.*
79. *Mandel, S. A.; Amit, T.; Weinreb, O.; Reznichenko, L.; Youdim, M. B. H. CNS Neurosci. Ther. 2008, 14, 352–365.*
80. *Isaacs, C. E.; Wen, G. Y.; Xu, W.; Jun, H. J.; Rohan, L.; Corbo, C.; Di Maggio, V.; Jenkins, E. C. Jr.; Hillier, S. Antimicrob. Agents Chemother. 2008, 52, 962–970.*
81. *Friedman, M.; Kim, S.-Y.; Lee, S.-J.; Han, G.-P.; Han, J.-S.; Lee, R.-K.; Kozukue, N. J. Food Sci. 2005, 70, C550–559.*
82. *Friedman, M.; Levin, C. E.; Lee, S.-U.; Kozukue, N. J. Food Sci. 2009, 74, H47–H51.*
83. *Timothy W, S, Eugene F B, Mendel F, Amadu K S; J. Agric. Food Chem. 2009, 57, 6720–6728*
84. *Chen, L.; Yang, X.; Jiao, H.; Zhao, B. Toxicol. Sci. 2002, 69, 149–156.*
85. *Kajiya, K.; Kumazawa, S.; Nakayama, T. Biosci., Biotechnol., Biochem. 2001, 65, 2638–2643.*
86. *Kumazawa, S.; Kajiya, K.; Naito, A.; Saito, H.; Tuzi, S.; Tanio, M.; Suzuki, M.; Nanjo, F.; Suzuki, E.; Nakayama, T. Biosci., Biotechnol., Biochem. 2004, 68, 1743–1747*
87. *Tamba, Y.; Ohba, S.; Kubota, M.; Yoshioka, H.; Yoshioka, H.;Yamazaki, M. Biophys.J. 2007, 92, 3178–3194*

88. *Oteiza P I, Erlejman A J, Verstraeten S V, Keen C L, Fraga C G; Clinical & Developmental Immunology, March 2005; 12(1): 19–25*
89. *Wojciech K, Telenius J,and Himanshu K; FEBS Journal, 10-4-2013*
90. *Tapsell LC, Hemphill I, Cobiac L, Patch CS, Sullivan DR, Fenech M, Roodenrys S, Keogh JB, Clifton PM, Williams PG et al. (2006) Med J Aust 185, S4–S24.*
91. *Lai PK & Roy J (2004) Curr Med Chem 11, 1451–1460.*
92. *Karewicz A, Bielska D, Gzyl-Malcher B, Kepczynski M, Lach R & Nowakowska M (2011) Colloids Surf B Biointerfaces 88, 231–239.*
93. *Barry J, Fritz M, Brender JR, Smith PES, Lee D-K & Ramamoorthy A (2009). J Am Chem Soc 131, 4490–4498.*
94. *Pang X, Yi T, Yi Z, Cho SG, Qu W, Pinkeaw D, Fujise K, Liu M; Cancer Res (2009), 69 (2); 518-525.*
95. *Kearns M D, Patel Y N, Savva M; Chem Phys Lipids 163 (2010), 8 755-764*
96. *Muller J P E, Aytar B S, Kondo Y, Lynn D M, Abbott N L; Soft Matter (2012) 8 (24): 2608-2619*
97. *Vermeer L S, de Groot B L, Réat V, Milon A, Czaplicki J; Eur Biophys J (2007) 36:919–931*
98. *Silvius J R, Gagne J; Biochemistry 1984, 23, 3241*
99. *Sanchez-Migallon M P, Aranda F J, Gomez-Fernandez J C; Biophys. J. 1995, 68, 558*
100. *Stendardo E, Pedone A, Cimino P, Menziani M, Crescenzi O, Barone V. PhysChemChemPhys. 2010, 12(37):11697-709*
101. *Nakagawa H., Ohyama R., Kimata A., Suzuki T., Miyata N. Bioorg. Med. Chem. Lett. 2006;16:5939–5942*
102. *Yoshihara E, Nakae T; Biochim Biophys Acta 19856, 854 (1), 93-101*
103. *Duzgunes N, Nir S; Advanced Drug Delivery Reviews 40 (1999) 3-18*
104. *Allen TM; Biochim Biophys Acta 1981,640 (2)*
105. *Lipowsky R; Current Opinio in Structural Biology 1995, 5; 531-540*
106. *Wojewodzka J, Pazdzior G, Langner M; Chemistry and Physics of lipids 135 (2005) 181-187*
107. *Rathod S, Desphande SG; Indian J Farm Sci 2010 72(2), 155-60*
108. *Law SL, Huang KJ, Chiang CH; Journal of Controlled Release 63 (2000) 135-140*
109. *Felt O, Furrer P, Mayer J M, Plazonnet B, Buri P, Gurny R; Int J Pharm 180, 185-193*
110. *Lee VH, Carson LV; J Ocul Pharmacol 1986 (4): 353-64*
111. *Monem A S, Ali FM, Ismail MW; Int J Pharm 2000, 198 (1): 29-38*
112. *Fitzgerald P, Hadgraft J, Wilson C G; Journal of Pharmacy and Pharmacology; 1987, 39 (6): 487-490*
113. *Kitagawa K, Fukuda M, Sasaki K; Lens Eye Toxic Res 1989, 6 (1-2): 365-73*
114. *Fresta M, Panico A M, Bucolo C, Giannavola C, Puglisi G; Journal of Pharmacy and Pharmacology; 1999, 51 (5): 565-576*
115. *Budai L, Hajdu M, Budai M, Grof P, Beni S, Noszai B, Klebovich I, Antal I; Int J Pharm; 2007, 242 (1-2): 34-40*
116. *Jain R L, Shastri J P; Internat Journ of Pharm Investigations 2011, 1 (1)*
117. *Abdelbary G, Pharm Develop and Tecnhology; 2011 (16): 44-56*
118. *Taha E I, El-Anazi M H, Ibrahim M, El-Bagory, Bayomi M A; Saudi Pharmaceutical Journal; 2014, 22, 231-239*
119. *Agraval AK, Gupta CM; Adv Drug Deliver Rev ; 2000, 41 (2): 135-46*
120. *Milani J K, Pleyer U, Duke A, Chou H J, Lutz S, Ruckert D, Schmidt K-H, Mondino B J; Ophtalmology , 1993, 100 (6): 890-896*